Investigations of the reactivity of palladium and platinum complexes with molecular oxygen and characterization of a gold(III)-alkene complex

Margaret Louise Scheuermann

A dissertation

submitted in partial fulfillment of the

requirements for the degree of

Doctor of Philosophy

University of Washington

2013

Reading Committee:

Karen I. Goldberg, Chair

D. Michael Heinekey

James M. Mayer

Program Authorized to Offer Degree:

Chemistry

University of Washington

Abstract

Investigations of the reactivity of Pd and Pt complexes with molecular oxygen and characterization of a gold(III)-alkene complex

Margaret Louise Scheuermann

Chair of the Supervisory Committee:

Professor Karen I. Goldberg

Department of Chemistry

Understanding the reactivity of metal complexes with molecular oxygen will facilitate the development of catalysts that can enable the widespread use of molecular oxygen as an oxidant for organic synthesis. This thesis presents two new classes of reactions between metal complexes and molecular oxygen. Neutral five-coordinate Pt complexes were tested for reactivity in the presence of molecular oxygen. In arene solution, the complexes ($^{t\text{BuMe2}}$nacnac)PtMe$_3$ (**1**, $^{t\text{BuMe2}}$nacnac$^-$ = [((4-*t*Bu-2,6-Me$_2$C$_6$H$_2$)NC(CH$_3$))$_2$CH]$^-$), ($^{\text{Me3}}$Me-nacnac)PtMe$_3$ (**2**, $^{\text{Me3}}$Me-nacnac$^-$ = [((2,4,6-Me$_3$C$_6$H$_2$)NC(CH$_3$))$_2$CCH$_3$]$^-$), and ($^{t\text{Bu2}}$PyPyr)PtMe$_3$ (**3**, $^{t\text{Bu2}}$PyPyr$^-$ = 3,5-di-*tert*-butyl-2-(2-pyridyl)pyrrolide) reacted immediately with oxygen to form peroxo species in which two oxygen atoms bridge between the metal center and a carbon atom in the ligand backbone. In contrast, no reaction between ($^{\text{iPr2}}$AnIm)PtMe$_3$ (**4a**, $^{\text{iPr2}}$AnIm$^-$ = [*o*-C$_6$H$_4$-

{N($C_6H_3{}^iPr_2$)}(CH=N$C_6H_3{}^iPr_2$)]$^-$) or (^{Me3}AnIm)PtMe_3 (**4b**, ^{Me3}AnIm$^-$ = [*o*-C_6H_4-{N($C_6H_2Me_3$)}(CH=N$C_6H_2Me_3$)]$^-$) and oxygen was observed. As activation of oxygen by five-coordinate Pt^{IV} species was found to involve cooperation between the metal center and the ligand, the ability of the ligand to participate in the oxygen binding appears to be a vital component. Oxygen atom transfer reactions of the novel peroxo species are also presented. In a separate study, an unusual reaction involving the activation of both molecular oxygen and a C–H bond at the same metal center was investigated. Pd(P(Ar)(*t*Bu)$_2$)$_2$ (**15**, Ar = naphthyl) was found to react with molecular oxygen at room temperature in arene solvent to form a hydroxide dimer in which one equivalent of phosphine per Pd was lost and the remaining phosphine was cyclometalated through the naphthyl ring. At low temperature, two intermediates were observed. The nature of these intermediates suggests a mechanism involving initial reaction of Pd(P(Ar)(*t*Bu)$_2$)$_2$ with O_2 followed by the C–H activation step. In a final chapter unrelated to oxygen reactivity, the generation and characterization of a gold^{III}-alkene complex by NMR and X-ray crystallography is presented. Such species have been proposed as intermediates in catalytic reactions but until recently none had been observed.

Table of Contents

Table of Contents ..... **i**

List of Figures ..... **iv**

List of Tables ..... **viii**

Glossary ..... **ix**

Numbering Scheme ..... **xi**

Acknowledgements ..... **xiii**

Chapter 1: Reactions of Pd and Pt complexes with molecular oxygen **1**

Aerobic oxidation of organic substrates *1*
Oxidase catalysis *2*
Oxygenase catalysis *3*
Stoichiometric reactions of Pd^0 with O_2 ..... *4*
Oxygen binding and oxidation 5
Stoichiometric reaction of a Pd^I dimer with O_2 ..... *10*
Stoichiometric reactions of Pd^{II} with O_2 ..... *11*
Formal insertion of O_2 into a Pd^{II} −H bond 11
Oxidation of Pd^{II} complexes by O_2 15
Stoichiometric reactions of Pt^0 with O_2 ..... *16*
Oxygen binding and oxidation 16
Addition across a metal–metalloid bond 17
Stoichiometric reactions of Pt^{II} with O_2 ..... *18*
Aerobic oxidation of Pt^{II} complexes to Pt^{IV} 18
Addition across a Pt–Pt bond 21
Insertion into a Platinacycle 22
Insertion into Pt^{II}–Me bond 22
Insertion into a Pt^{II}–H bond 23
Stoichiometric reaction of Pt^{IV} with O_2 ..... *24*
Insertion into a Pt^{IV}–H bond 24
Perspective *25*
Notes to Chapter 1 ..... *25*

Chapter 2: Reactions of five-coordinate Pt^{IV} complexes with molecular oxygen **30**

Introduction *30*
Results and discussion *32*
Reactions of five-coordinate Pt complexes with molecular oxygen 32
Reactivity of the Pt^{IV}-peroxo complexes 44
Summary *45*
Experimental *46*
General Considerations 46
Synthesis of (^{Me3}Me-nacnac)$PtMe_3$ (**2**) 47
Reaction between ($^{t\text{BuMe2}}$nacnac)$PtMe_3$ (**1**) and dioxygen to form **5** 47

Synthesis of **6** from **1** and CO 48
Synthesis of **7** from **1** and *tert*-butylisonitrile 49
Synthesis of **8** from **1** and ethylene 49
Synthesis of **9** from **1** and 3,3-dimethylbutyne 50
Formation of **10** from **5** 50
Reaction of **2** with air to form **11** 51
Generation of **12** from **3** and O_2 52
Crystallization of **13** 52
Typical procedure for testing **4a** and **4b** for reaction with O_2 53
Generation of **14** by oxygen-atom transfer from **11** 53
Generation of **14** using CO 54
Crystallographic characterization of **9** 54
Crystallographic details for compound **10** 56
Crystallographic details for compound **11** 57
Crystallographic details for compound **12** 59
Crystallographic details for compound **13** 62
Crystallographic details for compound **14** 65
Coauthor contributions 66
Notes to chapter 2 ..... *67*

Chapter 3: Oxygen-promoted C–H bond cleavage at Pd 70

Introduction *70*
Results and discussion *71*
Preparation and characterization of $Pd(P(Ar)(tBu)_2)_2$ (Ar = naphthyl) 71
Reaction of **15** with O_2 73
Characterization of two intermediates at low temperature 76
Kinetic study of Intermediates **A** and **B** 83
Mechanistic consideration 85
Summary *88*
Experimental *89*
General considerations 89
Synthesis of 1-napthtyl-di-*tert*-butylphosphine 90
Synthesis of $Pd(P(Ar)(tBu)_2)_2$ (**15**, Ar = naphthyl) 90
Generation of intermediate **A** 91
Generation of intermediate **B** 91
Synthesis of **16a** and **16b** from **15** 92
Spectroscopic characterization of mixtures containing **16a** and **16b** 93
Independent synthesis of **16a** and **16b** 93
Crystallographic characterization of **15** 94
Crystallographic characterization of **16a** 96
Simulated NMR spectra 97
General computational methods 99
Coauthor contributions 99
Notes to Chapter 3 ..... *99*

Chapter 4: Generation and Structural Characterization of a Gold^{III} Alkene Complex 104

Introduction *104*
Results and Discussion *105*
Spectroscopic and structural characterization of Au^{III} species 105
Summary *110*
Experimental *110*
General experimental methods 110
In situ generation of (2-(*p*-tolyl)pyridine)$AuMe_2$(OTf) (**18**) 111
In situ generation of [(1,5-cyclooctadiene)$AuMe_2$]$^+$[OTf]$^-$ (**19**-OTf) 111
In situ generation of [(1,5-cyclooctadiene)$AuMe_2$]$^+$[BArf]$^-$ (**19**-BArf) 111
Independent generation of [(2-(*p*-tolyl)pyridine)$_2$$AuMe_2^+$][OTf$^-$] (**20**-OTf) 112
Crystallographic characterization of **19**-BArf 112
Crystallographic characterization of **17**-OTf 114
Coauthor contributions 117
Notes to Chapter 4 ..... *117*

List of Figures

Figure 1.1. Generic catalytic cycle of oxidase type catalysis. 3

Figure 1.2. Optimized conditions for conversion of alkenes to diols using a Pd catalyst and O_2. 3

Figure 1.3. Hydroxylation reported by Ritter and coworkers. 4

Figure 1.4. Hydroxylation of benzoic acid derivatives. 4

Figure 1.5. Hyrdoxylation of phenyl pyridine 4

Figure 1.6. Generic representation of the reactions of Pd^0 complexes with oxygen. 6

Figure 1.7. Ligands for which LL'Pd(η^2O_2) complexes have been reported. 6

Figure 1.8. Anionic Pd peroxo complex. 8

Figure 1.9. Summary of computational work on the binding of O_2 to Pd. 9

Figure 1.10. Pd^{II} bis-superoxo complex. 10

Figure 1.11. Reaction of $[(^{F}PNP)Pd]_2$ dimer with molecular oxygen. 10

Figure 1.12. Reaction of $(^{tBu}PCP)Pd–H$ with O_2 11

Figure 1.13. Formal oxygen insertion into a Pd−H bond by a mechanism involving reductive elimination. 12

Figure 1.14. Mechanism for formal insertion by protonation of a Pd^{I} superoxo. 13

Figure 1.15. Mechanism for the formal insertion of O_2 into a Pd−Me bond. 14

Figure 1.16. Reaction involving the insertion of an oxygen atom into a Pd-phenoyl bond. 15

Figure 1.17. Trapping experiment supporting the involvement of a Pd^{III} superoxo intermediate. 15

Figure 1.18. Oxidative Me group transfer reported by Mirica and coworkers. 16

Figure 1.19. Addition of oxygen across a M–Ge bond. 18

Figure 1.20. Oxidations of dmps ligated Pt^{II} complexe. 19

Figure 1.21. Reaction of (dmdpb)$PtMe_2$ complexes with O_2 in alcoholic solvents..... 19

Figure 1.22. Reaction sequence for (NN)$PtMe_2$ complexes reaction with oxygen. 20

Figure 1.23. Proposed mechanism for the formation of $[Pt_2Cl_2\text{-}(\mu_2\text{-}O_2)_2([9]aneN_3)_2]Cl_2$ 21

Figure 1.24. Reaction of a bimetallic matalloborane complex with O_2 21

Figure 1.25. Reaction with oxygen accompanied by alkene inversion..... 22

Figure 1.26. Reaction of (PN)$PtMe_2$ with O_2..... 23

Figure 1.27. Insertion of oxygen into a Pt–Me bond reported by Britovsek 23

Figure 1.28. Insertion of O_2 into a Pd^{IV}–H bond. 24

Figure 2.1. Five-coordinate Pt^{IV} complexes studied in our laboratory 31

Figure 2.2. Reaction of **1** to form **5** and **10**. 33

Figure 2.3. $^1J_{C-H}$ values for a series of Pt complexes with sp^2 or sp^3 hybridized carbon atoms in the ligand backbone. 34

Figure 2.4. Formation of complexes **8** and **9** by reaction of **1** with ethylene and 3,3-dimethylbutyne respectively. 35

Figure 2.5. POV-Ray rendition of the ORTEP of **9** at the 50% probability level 35

Figure 2.6. POV-Ray rendition of the ORTEP of **10** at the 50 % probability 36

Figure 2.7. Reaction of **2** with O_2 to form **11**. 37

Figure 2.8. POV-Ray rendition of the ORTEP of **11** at the 50 % probability 38

Figure 2.9. Previously reported Ir–peroxo complex with an O–O bond length of 1.466(7) Å.... 38

Figure 2.10. Reaction of **3** with O_2 to form **12** and **13**..... 40

Figure 2.11. POV-Ray rendition of the ORTEP of **12** at the 50 % probability level of the two independent molecules of **12** 41

Figure 2.12. POV-Ray rendition of the ORTEP of **13** at the 50 % probability 42

Figure 2.13. Reaction of **11** with oxygen atom acceptors to form **14.** 45

Figure 2.14. POV-Ray rendition of the ORTEP of **14** at the 50 % probability 45

Figure 2.15. Crystal with signs of twinning, seen in (from left to right) transmission, birefringence, and extinction. 60

Figure 3.1. POV-Ray rendition of the ORTEP of **15** at the 50% probability 72

Figure 3.2. POV-Ray rendition of the ORTEP for the growth fragment of **16a** at the 50% probability level 74

Figure 3.3. Structures of **16a** and its isomer **16b**. 75

Figure 3.4. IR spectra of intermediate **B**. 79

Figure 3.5. Proposed structure for intermediate **B**. 80

Figure 3.6. Resonance Raman spectra of solution resulting from treatment of **15** with O_2 in THF at -80 °C (λ_{ex}: 406.7 nm, 77 K). 82

Figure 3.7. First order plot for the appearance of intermediate **B**. 83

Figure 3.8. First order plot for the disappearance of intermediate **B**. 84

Figure 3.9. Eyring plot for the disappearance of intermediate **B** 84

Figure 3.10. Addition of a C–H bond across an Ir–O bond. 86

Figure 3.11. Addition of an O–H bond to a Pt-peroxo. 86

Figure 3.12. Addition of a C–H bond across a Pd–O bond after phosphine loss. 87

Figure 3.13. Addition of a C–H bond across a Pd–O bond concurrent with phosphine loss..... 87

Figure 3.14. BP86 calculated transition state for the addition of a C–H bond across a Pd–O bond..... 88

Figure 3.15. Experimental and simulated spectra for the *t*Bu resonance of **15**. 98

Figure 3.16. Experimental and simulated spectra for the aromatic proton in close proximity to the metal center. 98

Figure 4.1. Protonation of (tpy)$AuMe_2$ **17** at low temperature followed by addition of cod to generate $[(cod)AuMe_2]^+[X]^-$ (**19**-X; X=OTf or BArf)..... 105

Figure 4.2. POV-Ray rendition of the ORTEP of (**17**-OTf) at the 50% probability level..... 108

Figure 4.3. POV-Ray rendition of the ORTEP of **19**-BArf with 50% probability ellipsoids.... 109

List of Tables

Table 1.1. Key crystallographic and spectroscopic data for LL'Pd(η^2O_2) complexes..... 7

Table 1.2. Spectroscopic and crystallographic data for Pt(η^2-O_2) complexes. 17

Table 2.1. Crystallographic data for **9**..... 55

Table 2.2. Crystallographic data for **10.**..... 57

Table 2.3. Crystallographic data for **11**..... 59

Table 2.4. Crystallographic data for **12**..... 62

Table 2.5. Crystallographic data for **13**..... 64

Table 2.6. Crystallographic data for **14**..... 66

Table 3.1. Crystallographic data for **15**..... 95

Table 3.2. Crystallographic data for **2a**..... 97

Table 3.3. Spin system for the simulated *t*Bu resonance of **15**. 98

Table 3.4. Spin system the aromatic proton in close proximity to the metal center in **15**. 99

Table 4.1. Structural parameters for **19**-BArf 114

Table 4.2. Structural parameters for **17**-OTf..... 116

Glossary

[9]aneN_3:	1,4,7-triazacyclononane
AIBN:	azobisisobutyronitrile
^{iPr2}AnIm$^-$:	[*o*-C_6H_4-{N($C_6H_3{}^iPr_2$)}(CH=N$C_6H_3{}^iPr_2$)]$^-$
^{Me3}AnIm$^-$:	[*o*-C_6H_4-{N($C_6H_2Me_3$)}(CH=N$C_6H_2Me_3$)]$^-$
BArf:	tetrakis[3,5-bis(trifluoromethyl)phenyl]borate
Bc:	2,9-dimethyl-4,7-diphenyl-1,10-phenanthroline
BHT:	4-methyl-2,6-di-*tert*-butylphenol
Bpy:	2,2'-bipyridine
cod:	1,5-cyclooctadiene
dach:	*cis*-1,3-diaminocyclohexane
dba:	dibenzylideneacetone
dipp:	2,6-$(iPr)_2C_6H_3$)
dmdpb:	di(methyl)di(2-pyridyl)borate
DMPO:	5,5-dimethyl-1-pyrroline-N-oxide
dmps:	di(2-pyridyl)methanesulfonate
DMSO:	dimethylsulfoxide
dpdpb:	di(phenyl)di(2-pyridyl)borate
dpp:	N,N′-di-tert-butyl-2,11-diaza[3.3](2,6)pyridinophane
dppbp:	2,11-bis(diphenylphosphinomethyl)benzo[c]phenanthrolene
dppe:	1,2-bis(diphenylphosphino)ethane
HOTf:	triflic acid
IMes:	1,3-di(2,4,6-trimethylphenyl)imidazoline-2-ylidene

ITmt:	1,3-bis(2,2″,6,6″- tetramethyl-m-terphenyl-5′-yl)imidazol-2-ylidene)
^{Me3}Me-nacnac^{-}:	$[((2,4,6\text{-}Me_3C_6H_2)NC(CH_3))_2CCH_3]^-$
Me_3tacn:	N,N′,N″-trimethyl-1,4,7-triazacyclononane
$^{t\text{BuMe2}}$nacnac^{-}:	$[((4\text{-}t\text{Bu-}2,6\text{-}Me_2C_6H_2)NC(CH_3))_2CH]^-$
NHPI:	*N*-hydroxy-phthalimide
OTf:	triflate
$^{t\text{Bu2}}$PC:	aryl-cyclometallated naphthyl-di-*tert*-butylphosphine
$^{t\text{Bu}}$PCP^{-}:	$2,6\text{-bis}(CH_2Pt\text{Bu}_2)C_6H_3^-$
PN:	2-((di-*tert*-butylphosphino)methyl)pyridine
^{F}PNP:	bis(2-iPr_2P(4-flouro-phenyl)amido)
$^{t\text{Bu2}}$PyPyr^{-}:	3,5-di-*tert*-butyl-2-(2-pyridyl)pyrrolide
pz:	pyrazolyl
tach:	*cis,cis*-1,3,5-triaminocyclohexane
terpy:	terpyridine
$^{(NH2)2}$terpy:	6,6’-diaminoterpyridine
THF:	tetrahydrofuran
tmeda:	N,N,N,N-tetramethylethylenediamine
^{Me2}Tp:	hydridotris(3,5-dimethylpyrazolyl)borate
tpyH:	2-tolylpyridine
ttpp:	1,3,5,7-tetramethyl-2,4,8-trioxa-6-phenyl-6-phosphaadamantane
tz:	triazolyl

Numbering Scheme

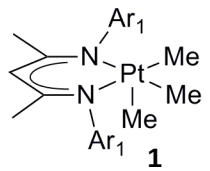

1

Ar_1 = 4-*t*butyl-2,6-dimethylphenyl

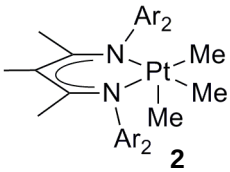

2

Ar_2 = 2,4,6-trimethylphenyl

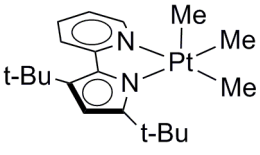

3

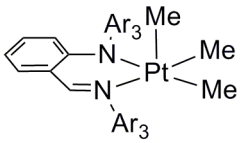

4a

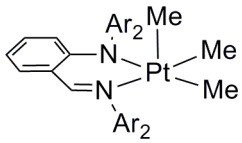

4b

Ar_2 = 2,4,6-trimethylphenyl
Ar_3 = 2,6-diisopropylphenyl

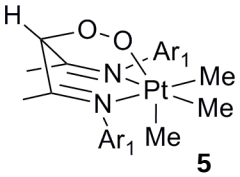

5

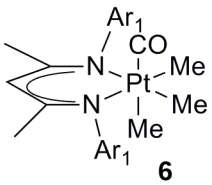

6

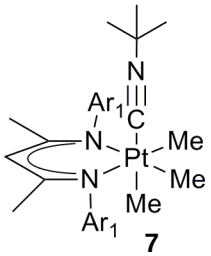

7

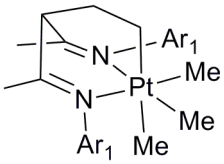

8

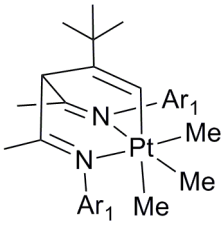

9

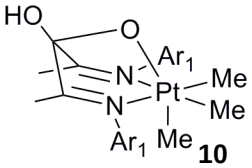

10

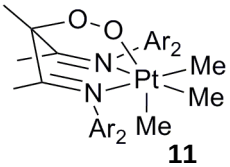

11

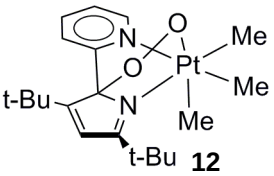

12

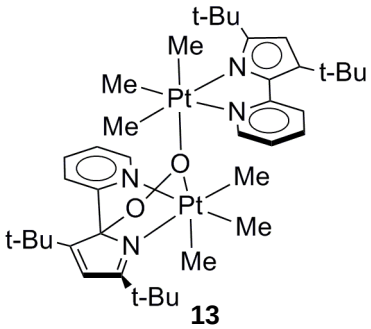

13

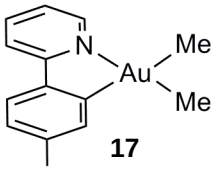

17

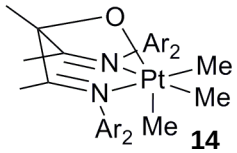

14

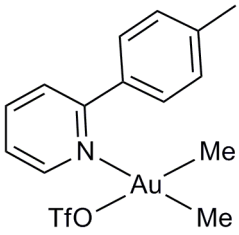

18

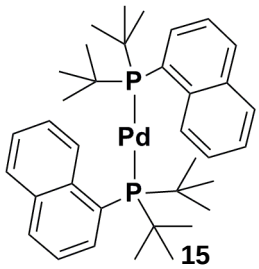

15

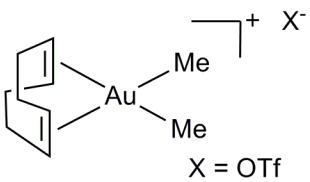

X = OTf
or BArf

19

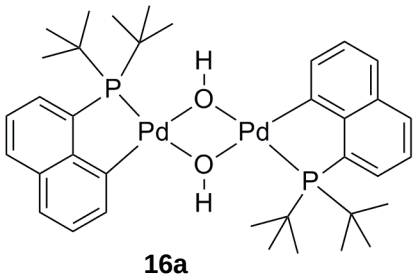

16a

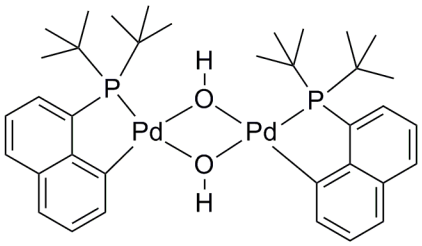

16b

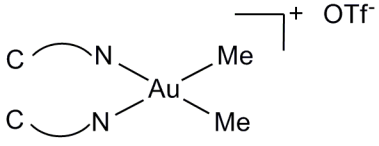

20

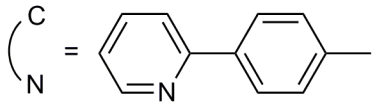

Acknowledgements

I am grateful to Karen for helping me to identify and pursue opportunities in which to grow both personally and professionally during graduate school. Karen made sure she was the advisor I needed and I am coming to appreciate this even more with the benefit of hindsight. I also thank Jim Mayer, Mike Heinekey, Mats Tilset, and Ole Swang for their significant contributions to my graduate education.

In the course of my graduate research I have worked with many excellent collaborators. Their contributions are noted in the appropriate chapters and I am grateful for their work. In addition, this work would have been impossible without the efforts of the technical, administrative, and support staff at the University of Washington and the University of Oslo, and my colleagues at both institutions.

This work was supported by the National Science Foundation under grant nos. CHE-00719372, CHE-1012045, and DGE-0718124, the Research Council of Norway, under grant nos. 185513/I30 and 212030/F11, the ARCS foundation, and the University of Washington. I am grateful to the donors and taxpayers who made these awards possible.

Finally I want to thank my family and friends for their love and support.

Chapter 1: Reactions of Pd and Pt complexes with molecular oxygen

Aerobic oxidation of organic substrates

Advances in organometallic chemistry have enabled many new transformations of organic substrates. Homogeneous catalysts have been developed and optimized for a wide range of reactions including hydrogenations, carbonylations, olefin metathesis, hydroformylations, cross couplings, and numerous others.[1] Recently, significant effort has been focused on developing C−H functionalization reactions mediated by transition metal catalysts. Transition metal complexes have shown high selectivity in the activation of C−H bonds[2-5] and considerable progress has been made on C−H bond functionalizations using a variety of oxidants. However, in terms of catalyzing oxidations on large scale, it is clear that inexpensive, benign and readily available oxidants are and will continue to be required. Along these lines, the aerobic oxidation of C−H bonds in organic substrates is most desirable as both molecular oxygen and the potential byproducts of such reactions (H_2O and H_2O_2) are environmentally benign.[6-9] Catalysis using molecular oxygen for oxidations can be classified into two types in analogy with biological oxidations: oxidase-type, in which molecular oxygen serves as the oxidant without being incorporated into the product, or oxygenase-type in which molecular oxygen is employed as the stoichiometric oxidant and oxygen atom source.[10]

Late transition metals have several properties that make them potentially amenable to aerobic C−H functionalization. In general, electron-rich late metal centers are only mildly oxophilic meaning that in the right coordination environment they can react with molecular oxygen and then undergo further reaction to break a metal−oxygen bond. This is in contrast to the highly oxophilic early transition metals which in many cases react rapidly with molecular

oxygen, however, the resulting oxides are often unreactive toward oxygen-atom transfer. Even more significant, decades of research have demonstrated the ability of late metal centers to break C−H bonds, and in many cases, the mechanisms of these reactions are well understood.[2-5]

Oxidase catalysis

Using Pd in particular, good progress has been made on discovering catalysts that can oxidize existing functional groups using molecular oxygen. Most of these catalytic cycles can be described as being oxidase-type (Figure 1.1).[6, 9,11] In these processes an existing functional group is oxidized with oxygen serving as the oxidant and proton acceptor, thus generating water or hydrogen peroxide as byproducts. Although C−H bonds are broken in some cases, the bond cleavage event is dependent on the presence of a functional group and will not occur in an analogous unfunctionalized substrate. The most prominent example of Pd oxidase catalysis is the Wacker oxidation in which ethylene can be converted into acetaldehyde using $PdCl_2$ with $CuCl_2$ serving as a co-catalyst.[12-14] Similar systems have been shown to oxidize a wide range of alkenes and alkynes.[14,15] Although in these systems an oxygen atom is incorporated into the product, it has been shown that this oxygen atom comes from water and that the role of the molecular oxygen is simply to reoxidize the catalyst. Molecular oxygen has also been used as the oxidant and hydrogen acceptor for selective oxidations of alcohols to ketones.[9,16,17] The Stahl group reported the use of molecular oxygen as terminal oxidant and proton acceptor in the conversion of cyclohexanones to phenols.[18] In cross coupling chemistry molecular oxygen has seen use as the terminal oxidant in reactions to couple aromatic C–H bonds to alkenes and other arenes.[9,15,19]

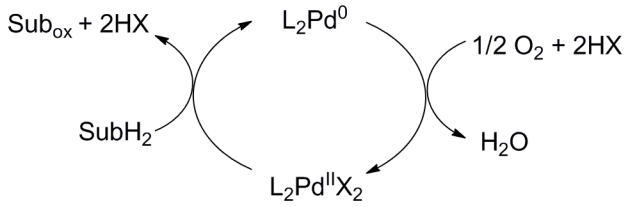

Figure 1.1. Generic catalytic cycle of oxidase type catalysis.

Oxygenase catalysis

In oxygenase-type catalysis molecular oxygen serves as the oxidant and is also incorporated into the final product, however only a handful of Pd-oxygenase reactions involving molecular oxygen have been reported. Loh and Jiang recently developed Pd-catalyzed methods for the oxygenation of alkenes using O_2 as the oxidant and oxygen atom source (Figure 1.2).[20]

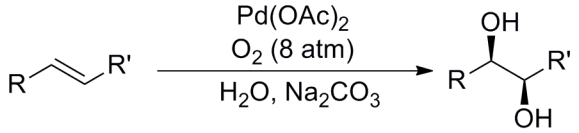

Figure 1.2. Optimized conditions for conversion of alkenes to diols using a Pd catalyst and O_2.[20]

The remaining examples of Pd-catalyzed oxygenase catalysis fall into the tantalizing arena of functionalization of arenes and alkyl C−H bonds. Benzene and biphenyl have been hydroxylated with O_2 using Pd catalysts and CO but the yields and selectivities are modest.[21,22] Using a catalyst proposed to involve the Pd^{II} and Pd^{III} oxidation states, Ritter and coworkers affected the α-hydroxylation of ketones (Figure 1.3).[23] Yu and coworkers reported the hydroxylation of substituted benzoic acids using $Pd(OAc)_2$ with air or O_2 as the oxidant and oxygen atom source (Figure 1.4). ^{18}O labeling studies confirmed that the oxygen atoms in the product are from molecular oxygen, however the mechanism of this reaction is not well understood.[24] Phenyl-pyridine derivatives have been hydroxylated in the presence of Pd and NHPI (Figure 1.5, NHPI = *N*-hydroxy- phthalimide) with toluene solvent serving as a co-

reductant thus generating benzaldehyde and benzoic acid along with the hydroxylated phenyl-pyridine product.[25] It is proposed that an $^{\bullet}OH$ radical generated in the decomposition of a $^{\bullet}OOCH_2C_6H_5$ radical is the species that serves as the active oxidant.

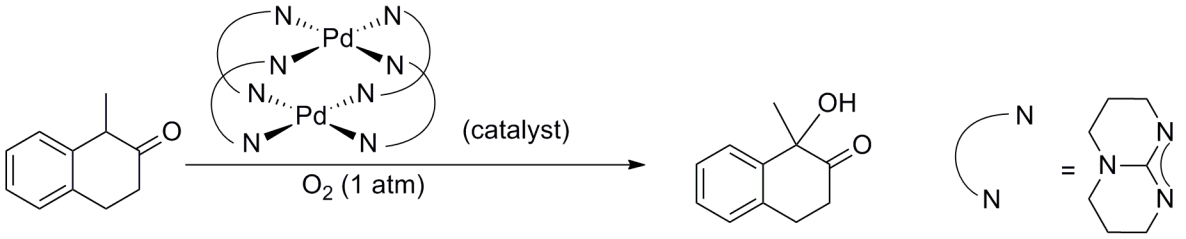

Figure 1.3. Hydroxylation reported by Ritter and coworkers.[23]

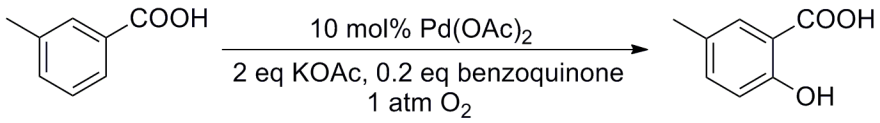

Figure 1.4. Hydroxylation of benzoic acid derivatives.[24]

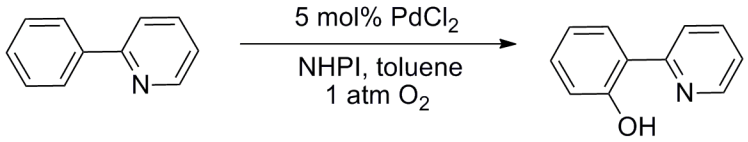

Figure 1.5. Hyrdoxylation of phenyl pyridine.[25]

To facilitate the discovery of new processes for C−H functionalization using molecular oxygen as a stoichiometric oxidant and oxygen atom source in catalytic transformations, there has been significant effort aimed at discovering how oxygen reacts with transition metal complexes. Of particular relevance to the Pd-catalyzed oxidase and oxygenase chemistry presented above, are the stoichiometric reactions involving oxygen and model Pd or Pt complexes that have been studied. Our nascent understanding of how oxygen interacts with palladium and platinum complexes is primarily based on the examples reviewed below.

Stoichiometric reactions of Pd^0 with O_2

Oxygen binding and oxidation

The most commonly observed reaction of neutral Pd^0 complexes with oxygen is oxygen binding and oxidation to form LL'Pd(η^2-O_2) peroxo complexes (Figure 1.6). Along with the formation of the peroxo moiety, the "L" ligands distort from the trans configuration characteristic of the LL'Pd^0 starting complexes. Similarities between the binding of dioxygen and isoelectronic olefins to Pd[26,27] and Pt[28] centers have been noted. The formation of LL'Pd(η^2-O_2) complexes has been seen with L = L' = phosphine for a range of phosphines including PPh_3,[29,30] $PPh(t\text{Bu})_2$,[31-34] $P(p\text{-tolyl})_3$,[35] $P(n\text{Bu})(\text{Ad})_2$,[36] $P(n\text{Bu})(t\text{Bu})_2$,[36] $P(c\text{-}C_6H_{11})_3$,[32] and 1,3,5,7-tetramethyl-2,4,8-trioxa-6-phenyl-6-phosphaadamantane (ttpp) (Figure 1.7).[37] Notably, Pd^0 complexes bearing $PPh(t\text{Bu})_2$,[31] and $P(n\text{Bu})(t\text{Bu})_2$,[36] react with air even in the solid state. In contrast, $Pd(P(t\text{Bu})_3)_2$ does not appear to react with O_2, perhaps because of the large cone angle of the phosphine.[33] Chelating phosphines such as 1,2-$(CH_2Pt\text{Bu}_2)_2C_6H_4$[38] and TRANSDIP, a cyclodextrin-derived diphosphine,[39] have also been used. LL'Pd(η^2-O_2) complexes can be formed in which L = phosphine, L' = carbene.[40,41] LL'Pd^{II}(η^2- O_2) complexes in which L and L' are carbenes have been characterized for L = L' = 1,3-di(2,4,6-trimethylphenyl)imidazoline-2-ylidene (IMes)[42] and 1,3-bis(2,2″,6,6″- tetramethyl-m-terphenyl-5′-yl)imidazol-2-ylidene) (ITmt).[43] The Pd^0 isonitrile adducts, $Pd(t\text{BuNC})_2$ and $Pd(\text{CNAr}^{\text{Dipp2}})_2$ (Dipp = 2,6-$(i\text{Pr})_2C_6H_3$), have been reported to react with O_2 resulting in the formation of $(t\text{BuNC})_2Pd(O_2)$[44] and $(\text{CNAr}^{\text{Dipp2}})_2Pd(O_2)$.[45] When a solution of Pd(bc)(dba) (bc = 2,9-dimethyl- 4,7-diphenyl-1,10-phenanthroline, dba = dibenzylideneacetone) was exposed to dioxygen, the dba was displaced by an O_2 fragment generating Pd(bc)(η^2-O_2) which was crystallographically characterized.[46] Key spectroscopic and crystallographic data for LL'Pd(η^2-O_2) complexes are summarized in Table 1.1. The O–O stretching frequencies, which at other metals have been shown to correlate well

with O–O bond length and the degree of charge transfer from the metal center to the bound O_2 moiety,[47] are consistent with assignment as a η^2-peroxo complex.

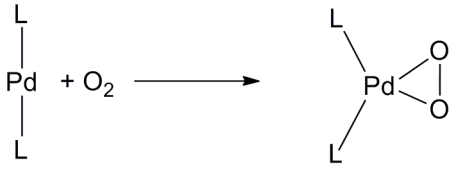

Figure 1.6. Generic representation of the reactions of Pd^0 complexes with oxygen.

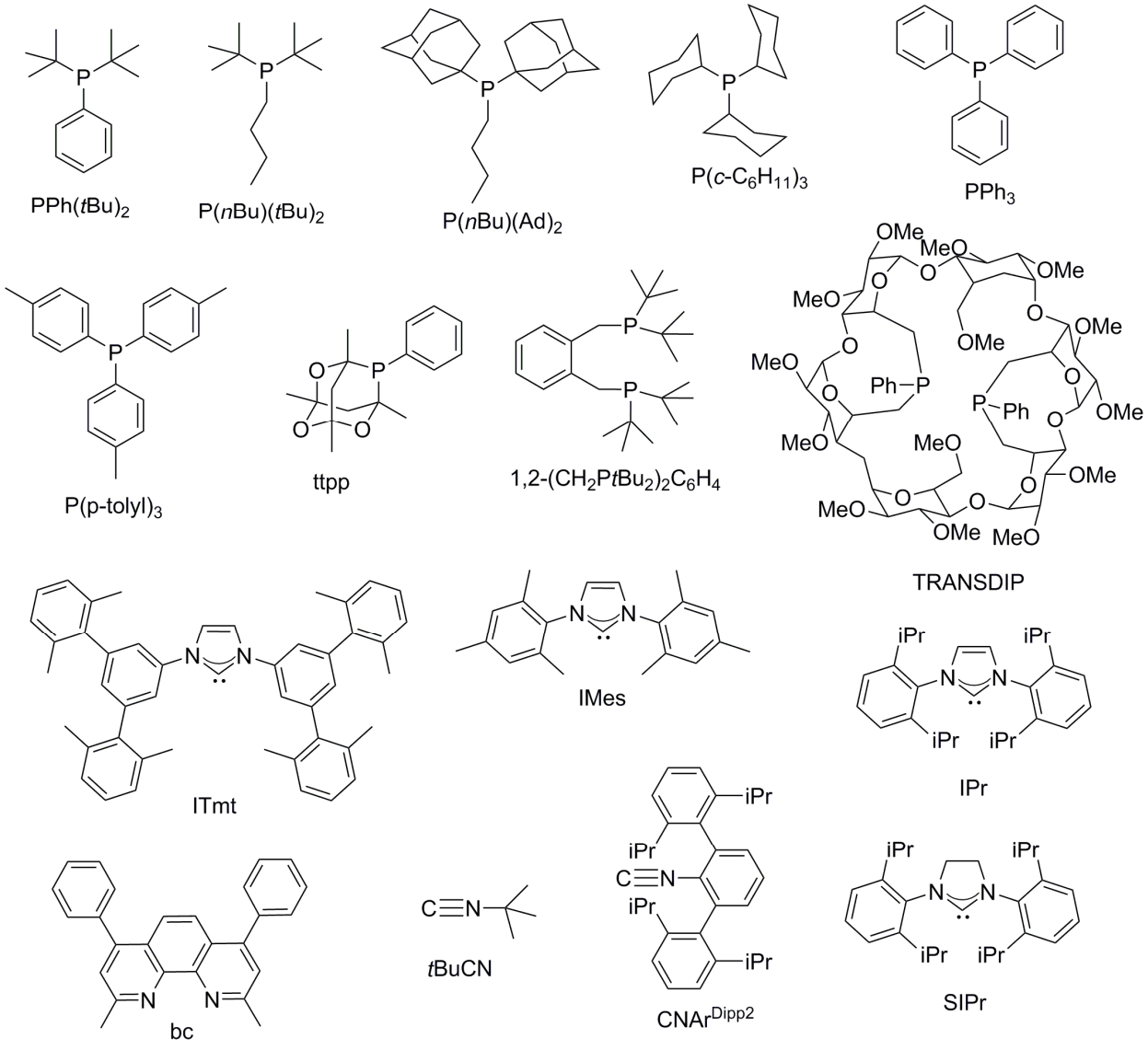

Figure 1.7. Ligands for which LL'Pd(η^2O_2) complexes have been reported.

Table 1.1. Key crystallographic and spectroscopic data for LL'Pd(η^2O_2) complexes.

complex	**υ_{O-O} (cm^{-1})**	**O–O (Å)**	**Pd–O (Å)**	**^{31}P (ppm)**
$(PPh(tBu)_2)_2Pd(O_2)$	915[a]	1.37(2)[b]	2.06(1), 2.05(1)[b]	–
(TRANSDIP)Pd(O_2)	–	1.409(5), 1.454(6)[c]	1.993(3), 2.005(3)[c]	28.8 (C_6D_6)[d]
$(P(c\text{-}C_6H_{11})_3)_2Pd(O_2)$	900[a]	–	–	–
$(PPh_3)Pd(O_2)$	828[e,f]	1.422(3)[g]	1.999(2), 2.013(2)[g]	34.2(THF)[h]
$(P(p\text{-tolyl})_3)Pd(O_2)$	882[i]	–	–	31.7 ($CDCl_3$)[i]
$(P(nBu)(Ad)_2)_2Pd(O_2)$	–	1.395(4)[j]	2.0070(19)[k]	60.32 ($CDCl_3$)[l]
$(P(nBu)(tBu)_2)_2Pd(O_2)$	–	–	–	64.04 (C_6D_6)[l]
$(ttpp)_2Pd(O_2)$	–	1.412(3)[m]	2.0118(13) [m]	–
$(1,2\text{-}(CH_2PtBu_2)_2C_6H_4)$-Pd($O_2$)	–	1.443(3)[n]	2.0130(16), 2.0187(16) [o]	60.1 (tol)[n]
$(IMes)_2$ Pd(O_2)	867[p]	1.443(2)[q]	2.0104(11), 2.0104(12)[p]	n/a
$(ITmt)_2$ Pd(O_2)	–	1.479[r]	2.004, 2.015[r]	n/a
$(tBuNC)_2Pd(O_2)$	893[s]	–	–	n/a
$(CNAr^{Dipp2})_2Pd(O_2)$	805 or 1056[t]	1.415(4)[u]	1.978(3), 1.987(3)[u]	n/a
(bc)Pd (O_2)	891[v]	1.415(15), 1.407(18)[w]	1.944(12), 1.954(11), 1.959(13), 2.000(13)[w]	n/a
$(IPr)(PPh_3)Pd(O_2)$	–	1.430(2) 1.4399(18)[x]	1.9912(16), 1.9975(15) 2.0023(14) 2.0138(15)[x]	36.45(C_6D_6)[y]
$(SIPr)(PPh_3)Pd(O_2)$	–	1.621(9)[z]	2.006(6), 2.058(7)[z]	30.7[aa]
$(SIPr)(PCy_3)Pd(O_2)$	–	1.448(5)[bb]	2.004(4), 2.015(4)[bb]	49.9[aa]

[a] ref 26. [b]ref 25. [c] CCDC-746930. [d] ref 39. [e] $^{18}O_2$. [f] ref 30 supporting information. [g] CCDC-235181. (THF)[h] ref 30. [i] ref 35. [j] ref 36. [k] ref 36 supporting information, CIF. [l] ref 36 supporting information. [m]CCDC-233088. [n] ref 38. [o] CCDC-181821. [p] ref 42 supporting information. [q] ref 42. [r] ref 43 supporting information, CIF [s] ref 44. [t] ref 45 supporting information; IR data was reported but the vibrations were not assigned. [u] ref 45 supporting information, CIF. [v] ref 46. [w] ref 46 supporting information. [x] CCDC-682048. [y] ref 40.[z] CCDC-799173, some ellipsoids are distorted. [aa] ref 41. [bb] CCDC-799172.

There is one example of an anionic Pd^{II} peroxo formed by reaction with O_2, $[(PPh_3)Pd(\eta^2\text{-}O_2)CN]^-$.[48] For $[(PPh_3)Pd(\eta^2\text{-}O_2)CN]^-$ an O–O bond length of 1.441(4) Å and Pd−O bond lengths of 1.990(3) and 2.016(3) Å were measured crystallographically. These values

fall within the range of O–O and Pd−O bond lengths observed in neutral Pd(η^2-O_2) complexes (Table 1.1). In the crystal the K^+ (ligated by a crown ether) is situated in close proximity to the η^2-O_2 moiety(K---O = 2.784 and 2.698 Å).

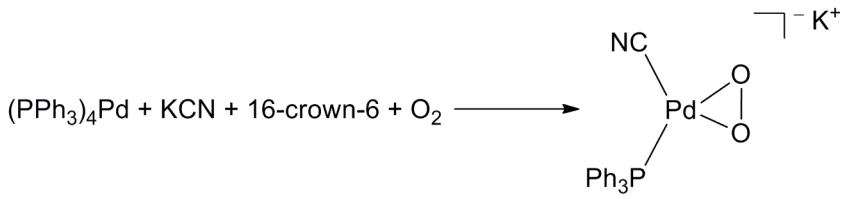

Figure 1.8. Anionic Pd peroxo complex.

Given the large number of Pd^0 complexes that have been found to react with oxygen to generate Pd^{II}-peroxo complexes and the likely involvement of such complexes in various oxidase-type catalytic cycles, there has been significant computational effort to investigate the mechanism by which the molecular oxygen binds.[49-51] Calculations suggest a mechanism for the reaction between LL'Pd^0 complexes and oxygen involving initial end-on coordination of molecular oxygen in its triplet ground state to form an open shell triplet species that may be best described as a Pd^I-superoxo complex (Figure 1.9). In this geometric configuration, with the O_2 moiety bound η^1 and the two L ligands still nearly trans to one another, the open shell and closed shell singlet species are substantially higher in energy. For the triplet species, formation of a second Pd−O bond is a spin forbidden process. However as the superoxo moves from an η^1 toward an η^2 binding mode the singlet energy surface lowers in energy and in fact dips below that of the triplet surface when the second Pd−O distance reaches ~2.3 Å. Once this spin crossover has occurred the formation of the second Pd−O bond is a barrier-less process.

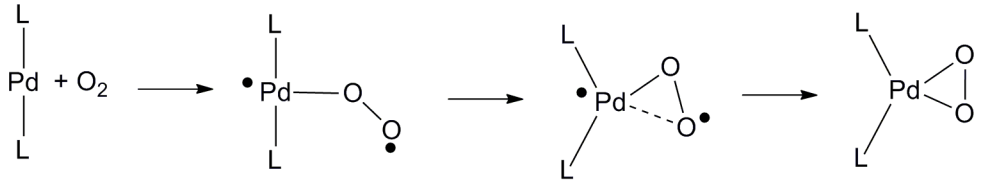

Figure 1.9. Summary of computational work on the binding of O_2 to Pd.

In addition to computational efforts, experimental work has been performed to probe the mechanism of the reaction of LL'Pd^0 with oxygen. Roth and coworkers measured kinetic isotope effects for the reaction between $Pd(PPh_3)_3$ and O_2 to form $(PPh_3)_2Pd$ (η^2-O_2) and found a $k_{16,16}/k_{16,18}$ value of 1.0093(29).[52] Based on comparison of this value to isotope effects observed in the binding of molecular oxygen to other transition metals they suggested that the reaction of Pd^0 with dioxygen occurs by a concerted transfer of two electrons to the O_2 fragment. Subsequent calculations by Stahl and coworkers indicate that the kinetic isotope effect observed by Roth could also be consistent with a stepwise mechanism.[50]

In one recent report a bis-carbene-Pd^0 complex with sterically hindered 1,3-bis(diisopropyl)phenylimidazol-2-yli-dene ligands was found to react with O_2 at low temperature to generate a bis superoxo complex rather than the more commonly observed Pd^{II}-η^2-peroxo (Figure 1.10).[53] The bis superoxo complex was characterized crystallographically and the O–O bond distances were found to be 1.314(11) and 1.340(11) Å. The O–O bond lengths are shorter than those reported for the peroxo complexes in Table 1.1 consistent with the superoxo description. A broad NMR spectrum was presented and magnetic susceptibility studies measured 1.8 unpaired electrons but resonance Raman and EPR data were not reported.

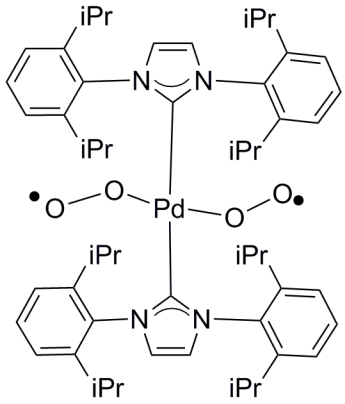

Figure 1.10. Pd^{II} bis-superoxo complex.[53]

Stoichiometric reaction of a Pd^{I} dimer with O_2

Ozerov and coworkers investigated the reactivity of a $[(^{F}PNP)Pd]_2$ dimer (^{F}PNP = bis(2-iPr_2P(4-flouro-phenyl)amido)) with molecular oxygen (Figure 1.11).[54] If greater than 10 equivalents of O_2 were added the product $(^{F}PNP)Pd(O_2)$, a crystallographically-characterized Pd^{II} η^1-superoxo complex, formed in high yield. However if less oxygen was used or if the superoxo complex was subsequently exposed to vacuum or treated with additional starting material, the peroxo dimer complex $[(^{F}PNP)PdO-]_2$ was generated. Based on crystallographic data, this complex is best described as a μ-κ^1:κ^1-peroxo bridging two Pd^{II} centers. The O−O bond length of the peroxo in $[(^{F}PNP)PdO-]_2$ was found to be 1.47(2) Å. In contrast, the O−O bond for the superoxo in $(^{F}PNP)Pd(O_2)$ was found to be only 1.293(2) Å.

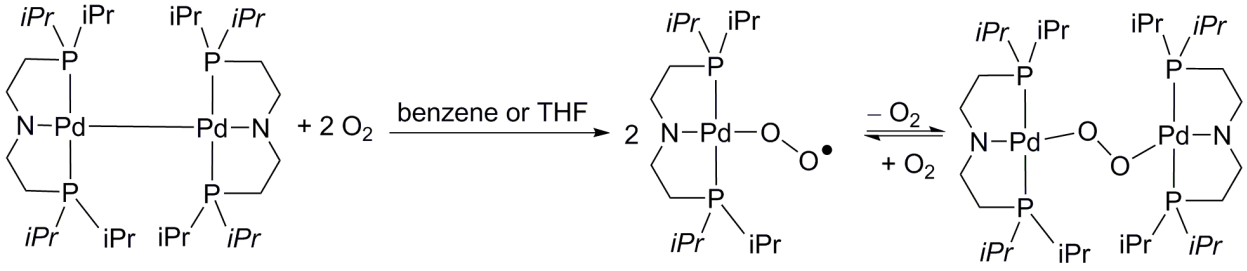

Figure 1.11. Reaction of $[(^{F}PNP)Pd]_2$ dimer with molecular oxygen.[54]

Stoichiometric reactions of Pd^{II} with O_2

Formal insertion of O_2 into a Pd^{II} −H bond

The reactions in this section are referred to as formal insertions of O_2 into Pd–H bonds as the end result is formation of a Pd−OOH moiety. Notably several mechanisms for this reaction have been identified. The mechanisms are distinctly different than those established for carbonyl and olefin insertion reactions.[1]

The first example of a directly observed insertion of molecular oxygen into a Pd–H bond was reported in 2006.[55] In this reaction insertion of O_2 into the Pd–H bond of ($^{t\text{Bu}}$PCP)Pd–H ($^{t\text{Bu}}$PCP = 2,6-bis(CH_2P*t*Bu_2)C_6H_3) yielded the Pd^{II}-hydroperoxide complex ($^{t\text{Bu}}$PCP)PdOOH (Figure 1.12). The corresponding hydroxide complex ($^{t\text{Bu}}$PCP)PdOH was observed as a minor product in the reaction. ($^{t\text{Bu}}$PCP)PdOOH was crystallographically characterized and found to have an O−O bond length of 1.470(4) Å. The insertion of oxygen into the Pd−H bond followed a second-order rate law (first order in both oxygen and Pd−H). The rate of the reaction was not significantly impacted by light or radical initiators and a k_H/k_D value of 5.8(5) was determined. Computational studies suggested a mechanism involving initial H-atom abstraction by O_2 to generate a ($^{t\text{Bu}}$PCP)Pd^{I} fragment and an $^{\bullet}$OOH radical which rapidly recombine to generate the observed ($^{t\text{Bu}}$PCP)PdOOH.[56,57] ($^{t\text{Bu}}$PCP)PdOOH undergoes further reaction to form the ($^{t\text{Bu}}$PCP)PdOH species.

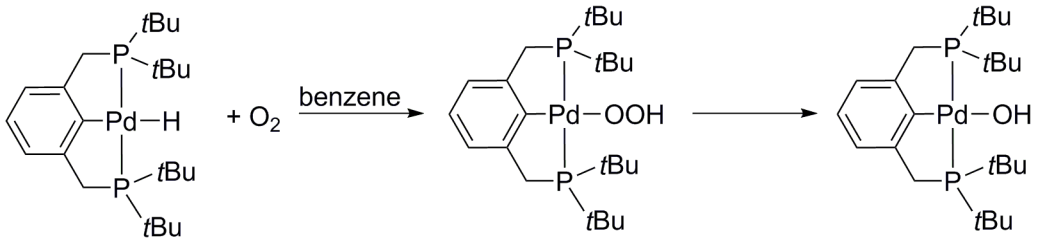

Figure 1.12. Reaction of ($^{t\text{Bu}}$PCP)Pd–H with O_2.[55]

Mechanistic studies of the insertion of O_2 into a Pd^{II}−H bond in non-pincer ligated systems revealed a different mechanism for the reaction. Initial reductive elimination of HX from the Pd^{II} hydride complex to generate a Pd^0 species is followed by reaction of the Pd^0 complex with molecular oxygen to form an η^2-peroxo complex (Figure 1.13). The mechanism of formation for the η^2-peroxo complex from Pd^0 species would be analogous to those described above in the Pd^0 section. The Pd^{II} η^2-peroxo then undergoes protonation to generate the observed Pd−OOH product.[58-60] It has been noted that some formal oxygen insertion reactions are facilitated by benzoquinone. [27,61,62] The role of the benzoquinone is likely to help stabilize Pd^0 intermediates prior to the binding of oxygen when the reductive elimination pathway is operative.

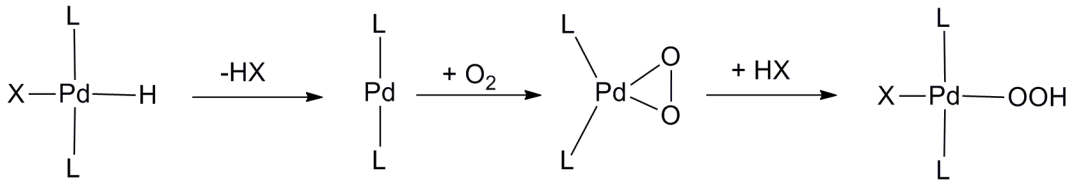

Figure 1.13. Formal oxygen insertion into a Pd−H bond by a mechanism involving reductive elimination.

Computational studies have also recognized a variation in which the O_2 fragment stays η^1 rather than forming an η^2-peroxo prior to the protonation event (Figure 1.14).[63] Hydrogen bonding between the Pd center and the coordinated acid helps stabilize the Pd^0 species prior to the reaction with oxygen. Oxygen then binds to form a superoxo structure, which is protonated by the bound acid. The intersystem crossing then involves the transfer of an electron from the Pd center to the OOH fragment.

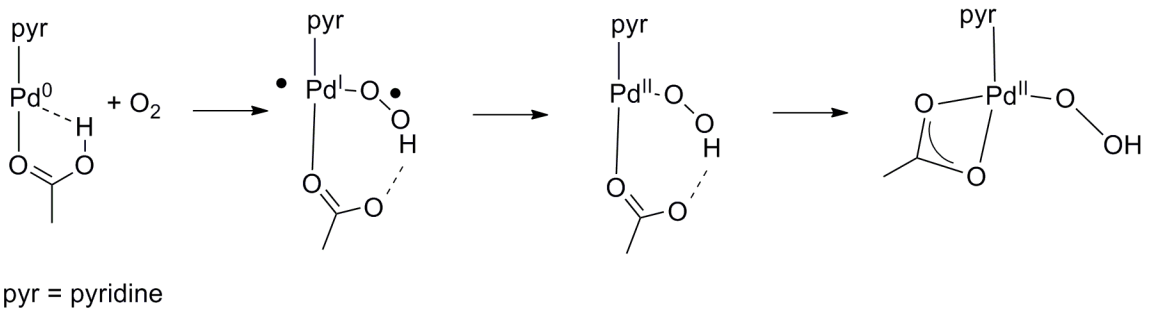

Figure 1.14. Mechanism for formal insertion by protonation of a Pd^{I} superoxo.

In agreement with a suggestion in the literature that the reductive elimination and H-atom abstraction pathways might be competitive,[64] computational studies found that the reductive elimination pathway and the H-atom abstraction pathway have similar activation energies for the reaction of some complexes with oxgyen.[51,62, 63,65] Recently, a combined experimental and computational study involving a series of L_2PdHX complexes (L = NHC, X = para substituted benzoic acids) was undertaken to investigate the interplay between the reductive elimination and H-atom abstraction mechanisms.[66] A Hammett study revealed that for benzoic acids with Me, H, Cl, or N_2O as the para substituent, the rate of the reaction increased with increasing σ_p. However when the substituent was OMe, the rate of the reaction was faster than would have been predicted by the Hammett correlation. Further study of the *p*-OMe substituted benzoic acid case led to a two term rate law (equation 1) in which one term is first order in $[O_2]$ and the other term is zero order in $[O_2]$.

$$\text{Rate} = k_1[\text{Pd}-\text{H}] + k_2[\text{Pd}-\text{H}][O_2] \qquad (1)$$

This rate law is consistent with competition between the reductive elimination pathway (zero order in $[O_2]$) and the H-atom abstraction pathway which is first order in $[O_2]$. Further computational study revealed that at more electron poor metal centers the reductive elimination pathway is favored whereas the hydrogen atom abstraction pathway predominates at more electron rich metal centers.

Detailed mechanistic studies on the insertion of molecular oxygen into a Pd–Me bond in (bpy)$PdMe_2$ (bpy = 2,2'-bipyridine) have been performed.[67] In order to achieve reproducible rates of reaction, the experiments were performed in the presence of the radical initiator AIBN (AIBN = azobisisobutyronitrile). Under these conditions, kinetic studies support a radical chain mechanism (Figure 1.15) with a five-coordinate Pd^{III} complex, (bpy)$PdMe_2$(OOMe), serving as a key intermediate.

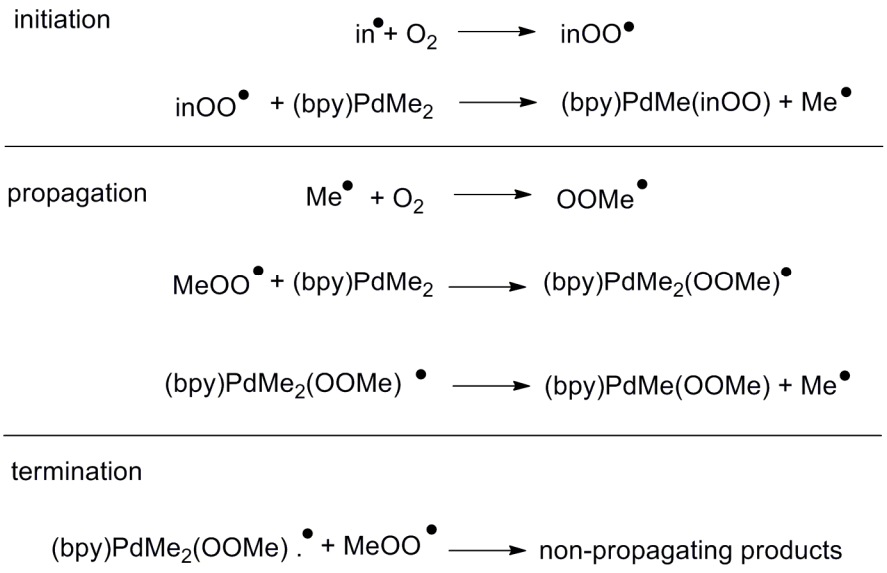

Figure 1.15. Mechanism for the formal insertion of O_2 into a Pd−Me bond.[67]

The groups of Vicente and Abad have shown several examples of the oxidation of Pd-phenoyl fragments to the corresponding Pd-phenolate fragments using O_2 (Figure 1.16).[68] They propose a reaction preceding through an unobserved Pd-perbenzoate intermediate generated by the insertion of O_2 into a Pd–C_{sp2} bond. No mechanistic proposals for this insertion of O_2 into the Pd−C bond were offered.

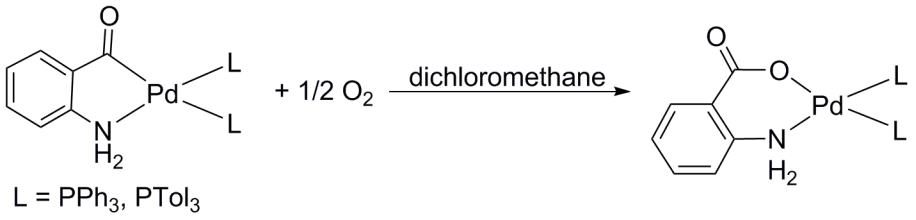

Figure 1.16. Reaction involving the insertion of an oxygen atom into a Pd-phenoyl bond.[68]

Oxidation of Pd^{II} complexes by O_2

Mirica and coworkers have reported examples of Pd^{II} complexes undergoing oxidation by molecular oxygen to generate Pd^{IV} species. When a (κ^2-dpp)$PdMe_2$ complex where dpp is the potentially tetradentate ligand N,N′-di-tert-butyl-2,11-diaza[3.3](2,6)pyridinophane was exposed to molecular oxygen in a mixture of benzene and methanol at room temperature, the observed products were ethane and (κ^2-dpp)PdMe(OH).[69] The authors proposed a mechanism involving initial end-on coordination of molecular oxygen to generate the Pd^{III} superoxo complex, [(κ^3-dpp)$PdMe_2(O_2)$]. Supporting the involvement of a Pd^{III} superoxo intermediate, the reaction was tested in the presence of 5,5-dimethyl-1-pyrroline-N-oxide (DMPO), and the observed EPR spectrum was consistent with Pd^{III}-peroxo-DMPO adduct (Figure 1.17).

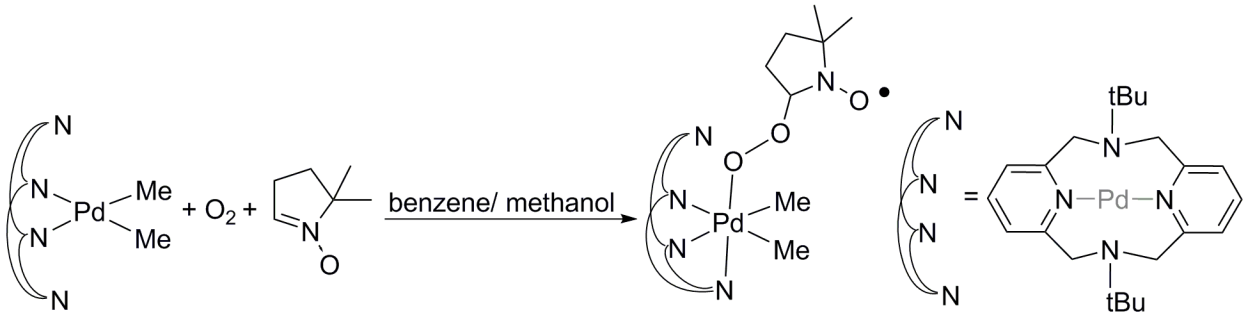

Figure 1.17. Trapping experiment supporting the involvement of a Pd^{III} superoxo intermediate.[69]

In a further study, (κ^2-Me_3tacn)$PdMe_2$ (Me_3tacn = N,N′,N″-trimethyl-1,4,7-triazacyclononane), a Pd^{II} complex bearing a potentially tridentate ligand, was treated with molecular oxygen in acetonitrile to produce a Pd^{IV} complex [(κ^3-Me_3tacn)$PdMe_3$]$^+$ and a Pd^{II}

species (κ^2-Me_3tacn)PdMeX (X = OOH or OH) (Figure 1.18).[70] Observation of the reaction mixture by mass spectrometry at early reaction times reveals a compound with *m/z* = 340.1208 consistent with a Pd^{IV} hydroperoxide complex $[(\kappa^3\text{-}Me_3tacn)PdMe_2(OOH)]^+$. When the reaction was performed at −70 °C in EtCN a UV-vis absorbance of λ_{max} = 407 nm, $\varepsilon \geq 11\ 000\ M^{-1}\ cm^{-1}$ was observed, which the authors postulate would be consistent with a peroxo or a superoxo species.

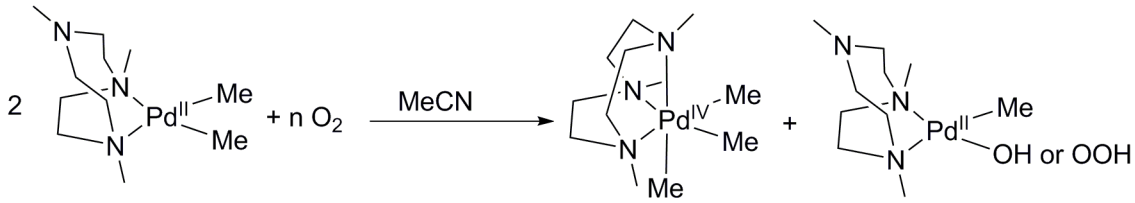

Figure 1.18. Oxidative Me group transfer reported by Mirica and coworkers.[70]

Stoichiometric reactions of Pt^0 with O_2

Oxygen binding and oxidation

As with Pd^0 (above), the most common reaction of molecular oxygen with Pt^0 complexes is the binding of oxygen and oxidation of the Pt center forming Pt^{II} η^2-peroxo complexes. $L_2Pt(\eta^2\text{-}O_2)$ complexes in which L represents the monodentate phosphines PPh_3,[29,35,71,72] P(*c*-$C_6H_{11})_3$,[32, 73] $PPhMe_2$,[73] PEt_3,[73] and P*t*Bu_2Ph[32] have all been reported. A similar $L_2Pt(\eta^2\text{-}O_2)$ complex where L_2 is the bidentate ligand 2,11-bis(diphenylphosphinomethyl)benzo[c]phenanthrolene (dppbp) is also known.[71] Hwang also reports a low temperature IR spectrum of a thermally unstable complex $(C_2H_4)_2Pt(O_2)$.[73] Selected spectroscopic and crystallographic data are reported in Table 1.2.

Table 1.2. Spectroscopic and crystallographic data for Pt(η^2-O_2) complexes.

complex	**υ_{O-O} (cm^{-1})**	**O–O (Å)**	**Pt–O (Å)**	**^{31}P (ppm)**
$Pt(O_2)(C_2H_4)_2$	814[a]	–	–	n/a
$(PEt_3)_2Pt(O_2)$	824[a]	–	–	–
$(PPhMe_2)_2Pt(O_2)$	825[a]	–	–	–
$(PPh_3)_2Pt(O_2)$	828[a]	1.45(4)[e]	2.01(2), 2.01(3)[e]	14.8[c]
$(P(c\text{-}C_6H_{11})_3)_2$-$Pt(O_2)$	818[a], 820[b]	–	–	–
$(PPht\text{Bu}_2)_2Pt(O_2)$	835[b]	1.43(2)[d]	2.02(1)[d]	–
(dppbp) $Pt(O_2)$	–	–	–	8.4[c]

[a] ref 73. [b] ref 32. [c] ref 72. [d] ref 31. [e] ref 71.

The ^{17}O NMR spectrum of $(PPh_3)_2Pt(O_2)$ has been recorded and the chemical shift for the peroxo group was found to be 385 ppm (from H_2O).[74] This shift is comparable to the 325 ppm observed for $Ir(CO)Cl(O_2)(PPh_3)_2$ and the 350 ppm observed for $Ir(CO)I(O_2)(PPh_3)_2$.

Addition across a metal–metalloid bond

The bis phosphine platinum germanium complex, $(Et_3P)_2PtGe(N(SiMe_3)_2)_2$, was found to react with molecular oxygen to form a complex containing a four membered Pt–O–O–Ge ring (Figure 1.19).[75] The Pt-peroxo complex was crystallographically characterized and found to have an O–O bond length of 1.503(11) Å and a Pt–Ge bond length of 2.2486(13) Å. This peroxo species undergoes photochemical reaction resulting in O–O bond cleavage to form $(Et_3P)_2Pt(\mu\text{-}O)_2Ge(N(SiMe_3)_2)_2$. A preliminary report noted that similar reactivity was seen with Pd−Ge complexes bearing monodentate or chelating phosphines, however the corresponding Pd species were less stable and were not isolated.[76]

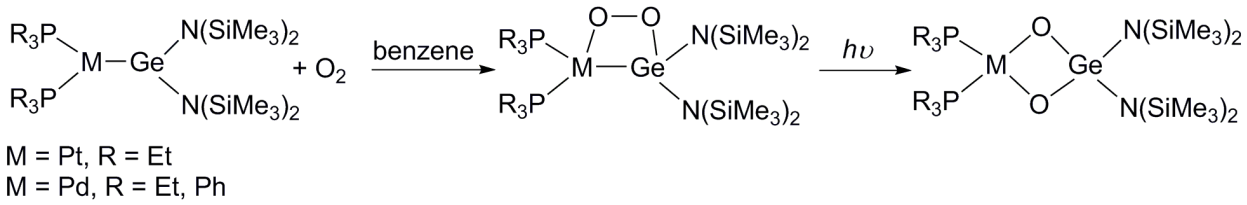

Figure 1.19. Addition of oxygen across a M–Ge bond.[75,76]

Stoichiometric reactions of Pt^{II} with O_2

Aerobic oxidation of Pt^{II} complexes to Pt^{IV}

In 1977 it was reported that (bpy)$PtCl_2$ reacted with *cis*,*cis*-1,3,5-triaminocyclohexane (tach) in air to form (κ^3-$tach^{-2}$)Pt(bpy)$(H_2O)^{2+}$ ($tach^{-2}$ =twice deprotonated *cis*,*cis*-1,3,5-triaminocyclohexane).[77] In contrast a reaction of (bpy)$PtCl_2$ with *cis*-1,3-diaminocyclohexane (dach) under the same conditions yielded the Pt^{II} complex, (κ^2-dach)Pt(bpy) $^{2+}$. This result suggested that a facially coordinating ligand might help promote aerobic oxidation of Pt^{II} centers.

Using similar nitrogen donor ligands, the groups of Wieghardt[78] and Puddephatt[79] offered examples of ligands switching from κ^2 to κ^3 binding modes upon reaction of their Pt^{II} complexes with air. (κ^2-[9]aneN_3)$_2Pt^{2+}$ ([9]aneN_3 =1,4,7-triazacyclononane) was found to react with O_2 to generate (κ^3-[9]aneN_3)$_2Pt^{4+}$ and (κ^2-[9]aneN_3)$PtMe_2$ reacted with O_2 to form (κ^3-[9]aneN_3)$PtMe_2OH$.

More recently Pt^{II} complexes with ligands specifically designed for their κ^2 to facial-κ^3 hemilability have been tested for aerobic oxidation. Using a di(2-pyridyl)methanesulfonate (dmps) ligand with a hemilabile sulfonate group Vedernikov reported several examples of well-defined square planar Pt^{II} complexes undergoing oxidation by O_2 to generate octahedral Pt^{IV} complexes with concommitant binding of the hemilabile ligand arm. Clean oxidations have been reported for (κ^2-dmps)$PtMe_2$ and (κ^2-dmps)$PtMe(H_2O)$,[80] and (κ^2-dmps)$Pt(CH_2CH_2OH)X$ (X =

Cl or OH) (Figure 1.20).[81] For each of these reactions, the products are octahedral Pt^{IV} complexes in which the dmps is bound κ^3.

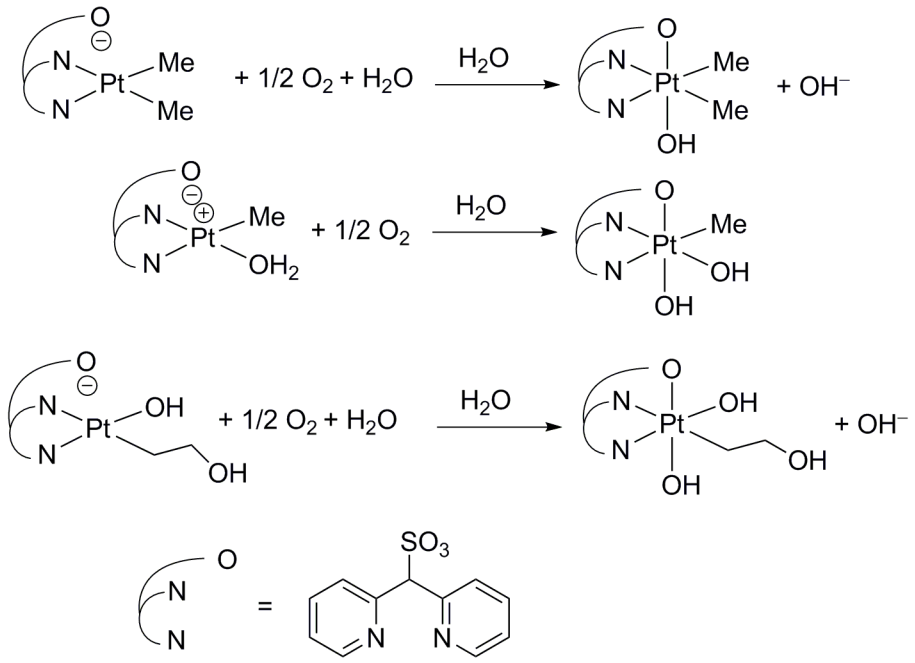

Figure 1.20. Oxidations of dmps ligated Pt^{II} complexe.[80,81]

In addition, the Vedernikov group has reported O_2 oxidation of Pt complexes bearing di(hydrocarbyl)di(2-pyridyl)borate (dmdpb and dpdpb) ligands (Figure 1.21).[82] These reactions involve migration of an "R" group (R = Me or Ph) from the boron in the ligand backbone to the Pt center.

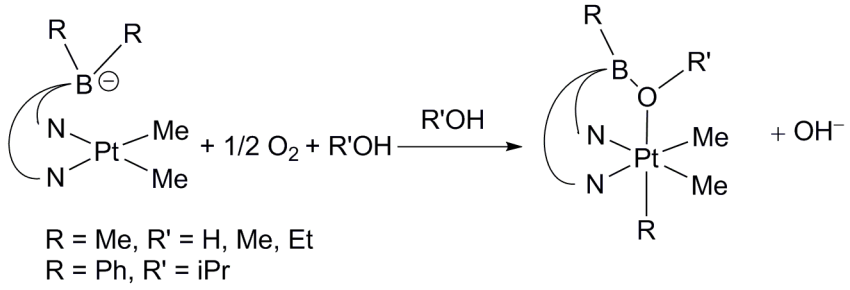

Figure 1.21. Reaction of $(dmdpb)PtMe_2$ complexes with O_2 in alcoholic solvents [82]

Bercaw and Goldberg found that a series of $(NN)PtMe_2$ complexes (NN = 2,2′-bipyridyl, 1,10-phenanthroline, N,N,N′,N′-tetramethylethylenediamine) could be oxidized to the

corresponding Pt^{IV}-methoxide-hydroxide species in methanol and further studies by Bercaw found that these reactions involve a Pt^{IV} hydroperoxo intermediate (Figure 1.22).[83] The reaction sequence was found to involve initial reaction of $(NN)PtMe_2$ with oxygen and methanol to form $(NN)PtMe_2(OOH)(OMe)$ species which could be characterized. $(NN)PtMe_2(OOH)(OMe)$ can also react with a second equivalent of starting material to form two equivalents of $(NN)PtMe_2(OH)(OMe)$. Over time the $(NN)PtMe_2(OOH)(OMe)$ converts to $(NN)PtMe_2(OH)(OMe)$ and ½ O_2. The evolved gas was measured with a Toepler pump and identified by mass spectrometry.

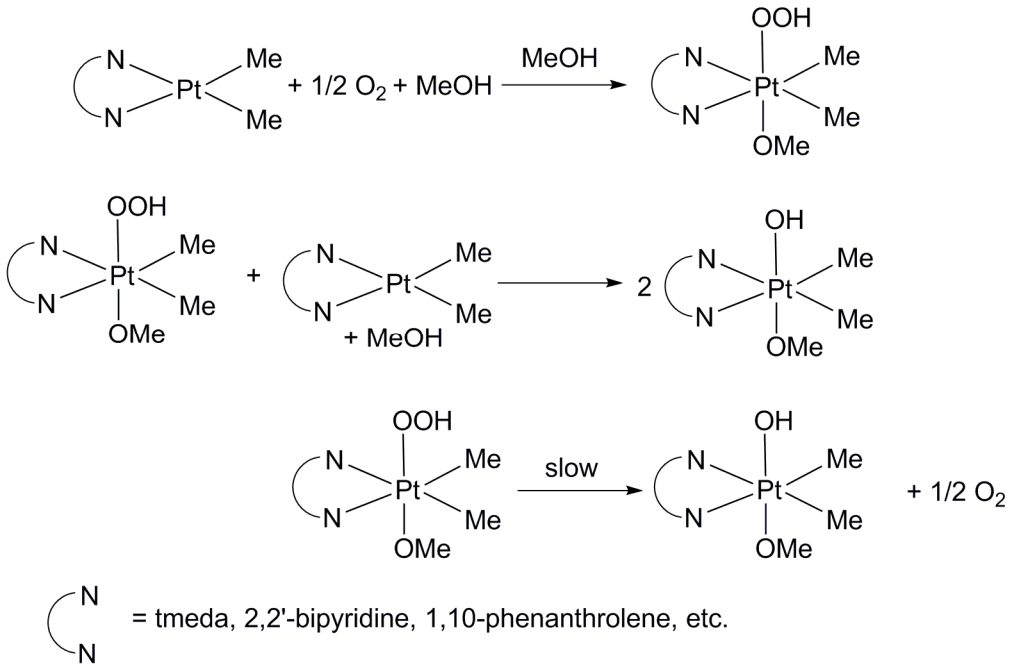

Figure 1.22. Reaction sequence for $(NN)PtMe_2$ complexes reaction with oxygen.[83]

An observation by Davies and Hambley provides additional insight into the mechanism of the oxidation of Pt^{II} by O_2. They report that the reaction of $PtCl_2(DMSO)_2$ with 1,4,7-triazacyclononane ([9]aneN_3) in the presence of O_2 gives $[Pt_2Cl_2\text{-}(\mu_2\text{-}O_2)_2([9]aneN_3)_2]Cl_2$ (Figure 1.23) in 42 % yield.[84] The authors suggest a mechanism involving initial formation of $([9]aneN_3)PtCl(O_2)(DMSO)^+$ featuring an η^1 peroxo or superoxo moiety, which then dimerizes

by displacement of the DMSO ligand. $[Pt_2Cl_2\text{-}(\mu_2\text{-}O_2)_2([9]aneN_3)_2]Cl_2$ was crystallographically characterized and found to have O–O bond lengths of 1.39(1) Å.

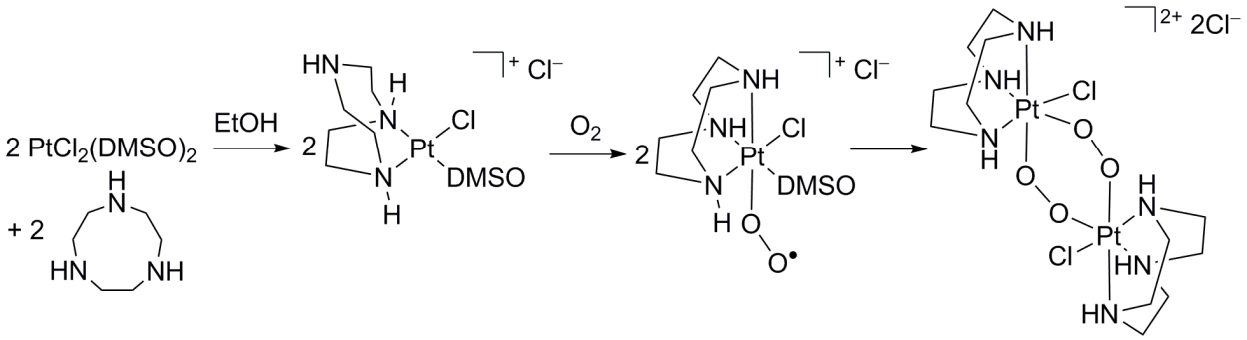

Figure 1.23. Proposed mechanism for the formation of $[Pt_2Cl_2\text{-}(\mu_2\text{-}O_2)_2([9]aneN_3)_2]Cl_2$.[84]

Addition across a Pt–Pt bond

The bimetallic metalloborane complex $[(PMe_2Ph)_4Pt_2B_{10}H_{10}]$ complex reacts with O_2 reversibly to form $[(PMe_2Ph)_4(O_2)Pt_2B_{10}H_{10}]$ in which the oxygen has added to the Pt–Pt linkage forming a four-membered Pt–Pt–O–O ring structure (Figure 1.24).[85] The crystallographically-measured O–O bond length is 1.434(6) Å and the Pt–O–O–Pt torsion angle is 15.8° suggesting a hydrogen peroxide-like structure. The reaction is accompanied by a shortening of the Pt–Pt distance from 2.9865(1) Å to 2.7143(3) Å. The reaction can be reversed with gentle heating or by purging the sample with nitrogen or argon.

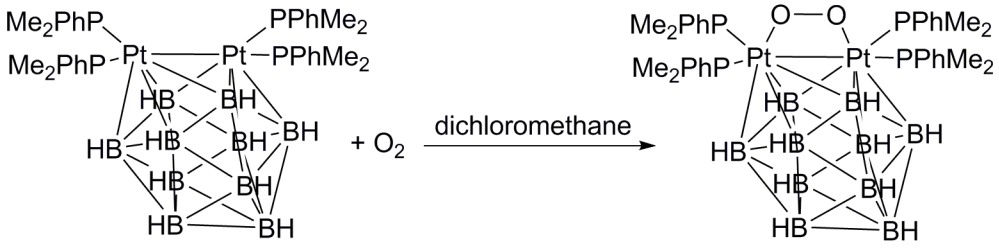

Figure 1.24. Reaction of a bimetallic matalloborane complex with O_2.[85]

Insertion into a Platinacycle

Platinacyclopentane complexes ligated by diazadiene (Figure 1.25) were found to react with oxygen accompanied by inversion of an allene group.[86] The products were isolated as green solids in 95% yield after several hours at room temperature. The material where R = 2,6-dimethylphenyl was characterized crystallographically and an O–O bond length of 1.49(1) Å was measured. The authors propose that a mechanism related to the metallo-ene reaction,[87] with molecular oxygen serving the role normally played by an isoelectronic olefin, would explain the observed regiochemistry. The observed product is inconsistent with direct insertion of O_2 into a Pt−C bond.

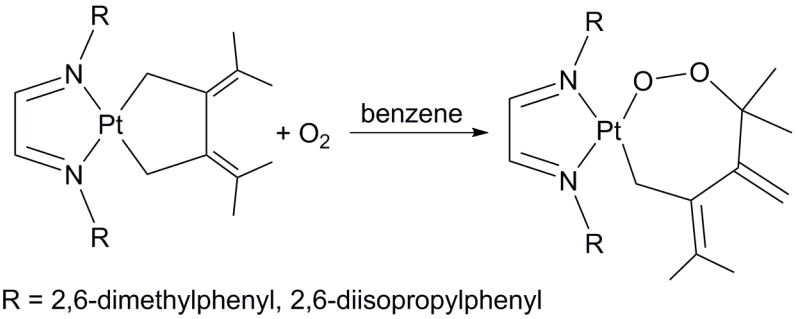

R = 2,6-dimethylphenyl, 2,6-diisopropylphenyl

Figure 1.25. Reaction with oxygen accompanied by alkene inversion.[86]

Insertion into Pt^{II}–Me bond

Exposure of (PN)$PtMe_2$ (PN = 2-((di-*tert*-butylphosphino)methyl)pyridine) to 5 atm O_2 resulted in the formation of a methylperoxo complex. The product, (PN)PtMe(OOMe) was characterized by X-ray crystallography which established that the methylperoxo moiety occupied a site trans to the phosphine arm of the bidentate ligand (Figure 1.26).[88] The O–O bond length in the product was 1.502(8) Å. The reaction was accelerated by light, and inhibited by the radical trap BHT (4-methyl-2,6-di-*tert*-butylphenol) leading the authors to suggest a radical mechanism, perhaps analogous to that proposed for the reaction of (bpy)$PdMe_2$ (above).[67]

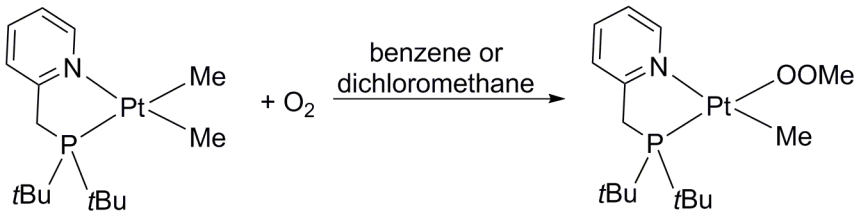

Figure 1.26. Reaction of (PN)$PtMe_2$ with O_2.[88]

Britovsek and coworkers reported the insertion of molecular oxygen into the Pt–Me bond of a cationic, amino-substituted terpyridine complex, ($^{(NH2)2}$terpy)$PtMe^+SbF_6^-$ ($^{(NH2)2}$terpy = 6,6'-diaminoterpyridine, Figure 1.27) to form ($^{(NH2)2}$terpy)$PtOOMe^+SbF_6^-$ which was crystallographically characterized.[89] Notably the reaction did not proceed when a complex with an unsubstituted terpyridine ligand, (terpy)$PtMe^+SbF_6^-$, was used. Supported by electronic spectra and luminescence properties, the authors suggested that ($^{(NH2)2}$terpy)$PtMe^+SbF_6^-$ is a singlet oxygen sensitizer while (terpy)$PtMe^+SbF_6^-$ is not. This reasoning led to their proposal that a non-radical pathway involving $^1O_2$ insertion into the Pt–Me bond is operative. The product, ($^{(NH2)2}$terpy)$PtOOMe^+SbF_6^-$, reacts further to generate ($^{(NH2)2}$terpy)$PtOH^+SbF_6^-$ and formaldehyde.

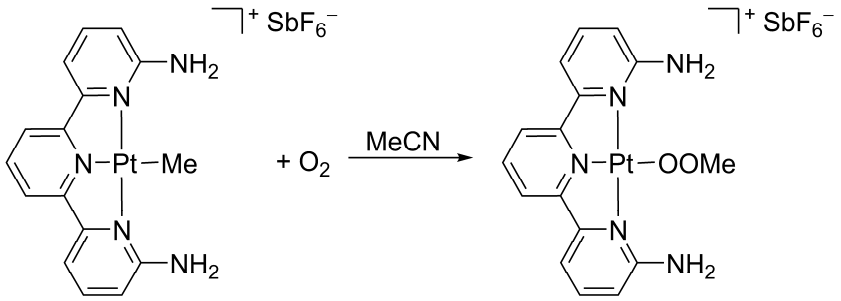

Figure 1.27. Insertion of oxygen into a Pt–Me bond reported by Britovsek.[89]

Insertion into a Pt^{II}–H bond

Wenzel reported the insertion of molecular oxygen into the Pt–H bond of (dppe)$PtHCF_3$ (dppe = 1,2-bis(diphenylphosphino)ethane) under both thermal and photochemical conditions.

Under thermal conditions, the yield of (dppe)Pt(OOH)CF_3 was 11% which could be increased to 25% in the presence of Vazo 64 or Vazo 52 initiator. However, in both cases the selectivity for (dppe)Pt(OOH)CF_3 was limited and other species including (dppe)Pt(OH) CF_3 were observed.[90] Under photochemical conditions (dppe)Pt(OH)CF_3 was observed as the major product.

Stoichiometric reaction of Pt^{IV} with O_2

Insertion into a Pt^{IV}–H bond

Insertion of molecular oxygen in the Pt–H bond of (^{Me2}Tp)PtR_2H (^{Me2}Tp = hydridotris(3,5-dimethylpyrazolyl)borate, R = Me, Ph) to form (^{Me2}Tp)PtR_2OOH has been observed and detailed mechanistic studies were carried out (Figure 1.28).[91] Initial experiments showed variable rates of reaction but investigations in the presence of the radical initiator AIBN resulted in reproducible kinetics. A radical chain mechanism involving H-atom abstraction was proposed. The proposed mechanism bears many similarities to the mechanisms generally proposed for organic autoxidation reactions. However of note is that the (^{Me2}Tp)PtR_2OOH product was also found to promote the reaction thus rendering the platinum reaction autocatalytic. The (^{Me2}Tp)PtMe_2OOH product was crystallographically characterized and found to have an O−O bond length of 2.698(5) Å. Upon heating (^{Me2}Tp)PtMe_2OOH undergoes further reaction to generate (^{Me2}Tp)PtMe_2OH.

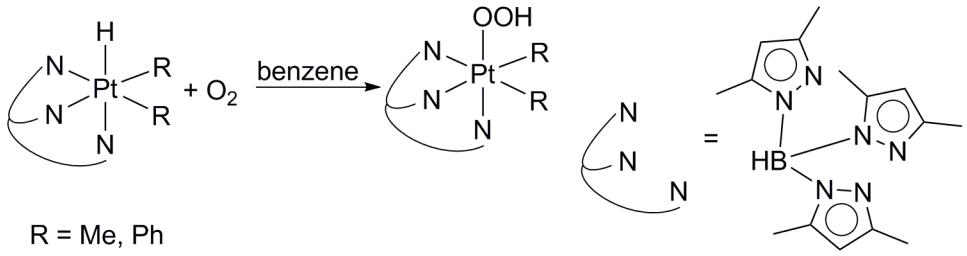

Figure 1.28. Insertion of O_2 into a Pd^{IV}–H bond.[91]

Perspective

In the following chapters new modes of reaction between molecular oxygen and Pd and Pt complexes are presented. One reaction involves a five-coordinate Pt^{IV} center and its ligand cooperatively activating molecular oxygen and the second is a transformation of a Pd^{0} complex that results in both C–H and O–O bond cleavages.

Notes to Chapter 1

(1) Hartwig, J.F. *Organotransition Metal Chemistry: From Bonding to Catalysis*, University Science Books, Sausalito, CA, 2010.

(2) Lersch, M.; Tilset, M. *Chem. Rev.* **2005**, *105*, 2471.

(3) Labinger, J. A.; Bercaw, J. E. *Nature* **2002**, *417*, 507.

(4) Periana, R. A.; Bhalla, G.; Tenn, W. J.; Young, K. J. H.; Liu, X. Y.; Mironov, O. A; Jones, C. J.; Ziatdinov, V. R. *J. Mol. Cat. A: Chem*. **2004**, *220*, 7.

(5) Shilov, A. E.; Shul'pin, G. B. *Chem. Rev.* **1997**, *97*, 2879.

(6) Punniyamurthy, T.; Velusamy, S.; Iqbal, J. *Chem. Rev.* **2005**, *105*, 2329.

(7) Cavani, F.; Teles, J. H. *ChemSusChem* **2009**, *2*, 508.

(8) Ishii, Y.; Sakaguchi, S.; Iwahama, T. *Adv. Synth. Catal*. **2001**, *343*, 393.

(9) Shi, Z.; Zhang, C.; Tang, C.; Jiao, N. *Chem. Soc. Rev.* **2012**, 3381.

(10) Stahl, S. S. *Science* **2005**, *309*, 1824.

(11) Stahl, S. S. *Angew. Chem., Int. Ed.* **2004**, *43*, 3400.

(12) Smidt, J.; Hafner, W.; Jira, R.; Sieber, R.; Sedlmeier, J.; Sabel, A. *Angew. Chem., Int. Ed.* **1962**, *1*, 80.

(13) Gligorich, K. M.; Sigman, M. S. *Chem. Commun.* **2009**, 3854.

(14) Takacs, J. M.; Jiang, X. -T. *Curr. Org. Chem*. **2003**, *7*, 369.

(15) Wu, W.; Jiang, H. *Acc. Chem. Res.* **2012**, *45*, 1736.

(16) Sigman, M. S.; Jensen, D. R. *Acc. Chem. Res.* **2006**, *39*, 221.

(17) Schultz, M. J.; Sigman, M. S. *Tetrahedron* **2006**, *62*, 8227.

(18) Izawa, Y.; Pun, D.; Stahl, S. S. *Science* **2011**, *333*, 209.

(19) Campbell, A. N.; Stahl, S. S. *Acc. Chem. Res.* **2012**, *45*, 815.

(20) Wang, A.; Jiang, H. *J. Org. Chem.* **2010**, *75*, 2321.

Zhu, M.-K.; Zhao, J.-F.; Loh, T.-P. *J. Am. Chem. Soc.* **2010**, *132*, 6284.

(21) (a) Jintoku, T.; Nishimura, K.; Takaki, K.; Fujiwara, Y. *Chem. Lett.* **1991**, 193. (b) Jintoku, T.; Takaki, K.; Fujiwara, Y.; Fuchita, Y.; Hiraki, K. *Bull. Chem. Soc. Jpn.* **1990**, *63*, 438. (c) Jintoku, T.; Nishimura, K.; Takaki, K.; Fujiwara, Y. *Chem. Lett.* **1990**, *19*, 1687. (d) Jintoku, T.; Taniguchi, H.; Fujiwara, Y. *Chem. Lett.* **1987**, 1865.

(22) Yamada, S.; Sakaguchi, S.; Ishii, Y. *J. Mol. Cat. A: Chem.* **2007**, *262*, 48.

(23) Chuang, G. J.; Wang, W.; Lee, E.; Ritter, T. *J. Am. Chem. Soc.* **2011**, *133*, 1760.

(24) Zhang, Y.-H.; Yu, J.-Q. *J. Am. Chem. Soc.* **2009**, *131*, 14654.

(25) Yan, Y.; Feng, P.; Zheng, Q.-Z.; Liang, Y.-F.; Lu, J.-F.; Cui, Y.; Jiao, N. *Angew. Chem. Int. Ed.* **2013**, *52*, 5827.

(26) Popp, B. V; Morales, C. M.; Landis, C. R.; Stahl, S. S. *Inorg. Chem.* **2010**, *49*, 8200.

(27) Popp, B. V.; Thorman, J. L.; Stahl, S. S. *J. Mol. Cat. A: Chem.* **2006**, *251*, 2.

(28) Norman, J. G. *Inorg. Chem.* **1977**, *16*, 1328.

(29) Wilke, G.; Schott, H.; Heimbach, P. *Angew. Chem., Int. Ed.* **1967**, *6*, 92.

(30) Aboelella, N. W.; York, J. T.; Reynolds, A. M.; Fujita, K.; Kinsinger, C. R.; Cramer, C. J.; Riordan, C. G.; Tolman, W. B. *Chem. Commun.* **2004**, *1*, 1716.

(31) Yoshida, T.; Tatsumi, K.; Matsumoto, M.; Nakatsu, K.; Nakamura, A.; Fueno, T.; Otsuka, S. *Nouveau Journal de Chimie*. **1979**, *3*, 761.

(32) Yoshida, T.; Otsuka, S. *J. Am. Chem. Soc.* **1977**, *99*, 2134.

(33) Matsumoto, M.; Yoshioka, H.; Nakatsu, K.; Yoshida, T.; Otsuka, S. *J. Am. Chem. Soc.* **1974**, *96*, 3322.

(34) Otsuka, S.; Yoshida, T.; Matsumoto, M.; Nakatsu, K. *J. Am. Chem. Soc.* **1976**, *98*, 5850.

(35) York, J. T.; Llobet, A.; Cramer, C. J.; Tolman, W. B. *J. Am. Chem. Soc.* **2007**, *129*, 7990.

(36) Sergeev, A. G.; Neumann, H.; Spannenberg, A.; Beller, M. *Organometallics* **2010**, *29*, 3368.

(37) Adjabeng, G.; Brenstrum, T.; Frampton, C. S.; Robertson, A. J.; Hillhouse, J.; McNulty, J.; Capretta, A. *J. Org. Chem.* **2004**, *69*, 5082.

(38) Clegg, W.; Eastham, G. R.; Elsegood, M. R. J.; Heaton, B. T.; Iggo, J. A.; Tooze, R. P.; Whyman, R.; Zacchini, S. *J. Chem. Soc., Dalton Trans.* **2002**, 3300.

(39) Gramage-Doria, R.; Armspach, D.; Matt, D.; Toupet, L. *Chem. Eur. J.* **2012**, *18*, 10813.

(40) Fantasia, S.; Nolan, S. P. *Chem. Eur. J.* **2008**, *14*, 6987.

(41) Jurčík, V.; Schmid, T. E.; Dumont, Q.; Slawin, A. M. Z.; Cazin, C. S. J. *Dalton Trans.* **2012**, *41*, 12619.

(42) Konnick, M. M.; Guzei, I. A.; Stahl, S. S. *J. Am. Chem. Soc.* **2004**, *126*, 10212.

(43) Yamashita, M.; Goto, K.; Kawashima, T. *J. Am. Chem. Soc.* **2005**, *127*, 7294.

(44) Otsuka, S.; Nakamura, A.; Tatsuno, Y. *J. Am. Chem. Soc.* **1969**, *91*, 6994.

(45) Labios, L. A; Millard, M. D.; Rheingold, A. L.; Figueroa, J. S. *J. Am. Chem. Soc.* **2009**, *131*, 11318.

(46) Stahl, S. S.; Thorman, J. L.; Nelson, R. C.; Kozee, M. A. *J. Am. Chem. Soc.* **2001**, *123*, 7188.

(47) Cramer, C. J.; Tolman, W. B.; Theopold, K. H.; Rheingold, A. L. *Proc. Natl. Acad. Sci. U.S.A.* **2003**, *100*, 3635.

(48) Erhardt, S.; Grushin, V. V.; Kilpatrick, A. H.; Macgregor, S. A; Marshall, W. J.; Roe, D. C. *J. Am. Chem. Soc.* **2008**, *130*, 4828.

(49) Landis, C. R.; Morales, C. M.; Stahl, S. S. *J. Am. Chem. Soc.* **2004**, *126*, 16302.

(50) Popp, B. V.; Wendlandt, J. E.; Landis, C. R.; Stahl, S. S. *Angew. Chem., Int. Ed.* **2007**, *119*, 607.

(51) Popp, B. V.; Stahl, S. S. *J. Am. Chem. Soc.* **2007**, *129*, 4410.

(52) Lanci, M. P.; Brinkley, D. W.; Stone, K. L.; Smirnov, V. V; Roth, J. P. *Angew. Chem., Int. Ed.* **2005**, *44*, 7273.

(53) Cai, X.; Majumdar, S.; Fortman, G. C.; Cazin, C. S. J.; Slawin, A. M. Z.; Lhermitte, C.; Prabhakar, R.; Germain, M. E.; Palluccio, T.; Nolan, S. P.; Rybak-Akimova, E. V.; Temprado, M.; Captain, B.; Hoff, C. D. *J. Am. Chem. Soc.* **2011**, *133*, 1290.

(54) Huacuja, R.; Graham, D. J.; Fafard, C. M.; Chen, C.-H.; Foxman, B. M.; Herbert, D. E.; Alliger, G.; Thomas, C. M.; Ozerov, O. V *J. Am. Chem. Soc.* **2011**, *133*, 3820.

(55) Denney, M. C.; Smythe, N. A.; Cetto, K. L.; Kemp, R. A.; Goldberg, K. I. *J. Am. Chem. Soc.* **2006**, *128*, 2508.

(56) Keith, J. M.; Muller, R. P.; Kemp, R. A; Goldberg, K. I.; Goddard, W. A; Oxgaard, J. *Inorg. Chem.* **2006**, *45*, 9631.

(57) Chowdhury, S.; Rivalta, I.; Russo, N.; Sicilia, E. *Chem. Phys. Lett.* **2007**, *443*, 183.

(58) Konnick, M. M.; Gandhi, B. A.; Guzei, I. A.; Stahl, S. S. *Angew. Chem., Int. Ed.* **2006**, *45*, 2904.

(59) Konnick, M. M.; Stahl, S. S. *J. Am. Chem. Soc.* **2008**, *130*, 5753.

(60) Keith, J. M.; Goddard, W. A.; Oxgaard, J. *J. Am. Chem. Soc.* **2007**, *129*, 10361.

(61) Popp, B. V.; Stahl, S. S. *J. Am. Chem. Soc.* **2006**, *128*, 2804.

(62) Decharin, N.; Popp, B. V.; Stahl, S. S. *J. Am. Chem. Soc.* **2011**, *133*, 13268.

(63) Popp, B. V.; Stahl, S. S. *Chem. Eur. J.* **2009**, *15*, 2915.

(64) Muzart, J. *Chem. Asian J.* **2006**, *1*, 508.

(65) Chowdhury, S.; Rivalta, I.; Russo, N.; Sicilia, E. *J. Chem. Theory Comput.* **2008**, *4*, 1283.

(66) Konnick, M. M.; Decharin, N.; Popp, B. V.; Stahl, S. S. *Chem. Sci.* **2011**, *2*, 326.

(67) Boisvert, L.; Denney, M. C.; Hanson, S. K.; Goldberg, K. I. *J. Am. Chem. Soc.* **2009**, *131*, 15802.

(68) (a)Vicente, J.; Abad, J.-A.; Franlkand, A. D.; Ramirez de Arellano, M. C. *Chem. Commun.* **1997**, 959. (b) Vicente, J.; Abad, J.-A.; Frankland, A. D.; Ramírez de Arellano, M. C. *Chem. Eur. J.* **1999**, *5*, 3066.

(69) Khusnutdinova, J. R.; Rath, N. P.; Mirica, L. M. *J. Am. Chem. Soc.* **2012**, *134*, 2414.

(70) Tang, F.; Zhang, Y.; Rath, N. P.; Mirica, L. M. *Organometallics* **2012**, *31*, 6690.

(71) Kashiwagi, T.; Yasuoka, N.; Kasai, N.; Kakudo, M.; Takahashi, S.; Hagihara, N. *Chem. Commun.* **1969**, 743.

(72) Boron-Rettore, P.; Grove, D. M.; Venanzi, L. M. *Helvetica Chim. Acta*. **1984**, *67*, 65.

(73) Hwang, W. *Polyhedron* **1984**, *3*, 513.

(74) Lee, H. C.; Oldfield, E. *J. Magn. Reson*. **1986**, *370*, 367.

(75) Litz, K. E.; Banaszak Holl, M. M.; Kampf, J. W.; Carpenter, G. B. *Inorg. Chem.* **1998**, *37*, 6461.

(76) Cygan, Z. T.; Bender, J. E.; Litz, K. E.; Kampf, J. W.; Banaszak Holl, M. M. *Organometallics* **2002**, 7484.

(77) Sarneski, J. E.; McPahil, A. T.; Onan, K. D.; Erickson, L. E.; Reilley, C. N. *J. Am. Chem. Soc.* **1977**, *99*, 7376.

(78) Wieghardt, K.; Koppen, M.; Swiridoff, W.; Weiss, J. *J. Chem. Soc. Dalton Trans.* **1983**, 1981.

(79) Prokopchuk, E. M.; Jenkins, H. A.; Puddephatt, R. J. *Organometallics* **1999**, *18*, 2861.

(80) Vedernikov, A. N.; Binfield, S. A.; Zavalij, P. Y.; Khusnutdinova, J. R. *J. Am. Chem. Soc.* **2006**, *128*, 82.

(81) Khusnutdinova, J. R.; Zavalij, P. Y.; Vedernikov, A. N. *Organometallics* **2007**, *26*, 2402.

(82) Vedernikov, A. N. *Chem. Commun.* **2009**, 4781.

(83) (a) Rostovtsev, V. V.; Henling, L. M.; Labinger, J. A.; Bercaw, J. E. *Inorg. Chem.* **2002**, *41*, 3608. (b) Rostovtsev, V. V.; Labinger, J. A.; Bercaw, J. E.; Lasseter, T. L.; Goldberg, K. I. *Organometallics* **1998**, *17*, 4530.

(84) Davies, M. S.; Hambley, T. W. *Inorg. Chem.* **2006**, *37*, 5408.

(85) (a) Bould, J.; Kilner, C. A.; Kennedy, J. D. *Dalton Trans*. **2005**, 1574. (b) Bould, J.; McInnes, Y. M.; Carr, M. J.; Kennedy, J. D. *Chem. Commun.* **2004**, *4*, 2380.

(86) Dieck, H. . T.; Fendesak, G.; Munz, C. *Polyhedron* **1991**, *10*, 255.

(87) Oppolzer, W. *Angew. Chem., Int. Ed.* **1989**, *28*, 38.

(88) Grice, K. A.; Goldberg, K. I. *Organometallics* **2009**, *28*, 953.

(89) Taylor, R. A.; Law, D. J.; Sunley, G. J.; White, A. J. P.; Britovsek, G. J. P. *Angew. Chem., Int. Ed.* **2009**, *48*, 6014.

(90) Wenzel, T. T. *Stud. Surf. Sci. Catal*. **1991**, *66*, 545.

(91) (a) Look, J. L.; Wick, D. D.; Mayer, J. M.; Goldberg, K. I. *Inorg. Chem.* **2009**, *48*, 1356. (b) Wick, D. D.; Goldberg, K. I. *J. Am. Chem. Soc.* **1999**, *121*, 11900.

Chapter 2: Reactions of five-coordinate Pt^{IV} complexes with molecular oxygen*

Introduction

In this chapter, the reactivity of neutral 16 e^- five-coordinate Pt^{IV} complexes with molecular oxygen is presented. Five-coordinate Pt^{IV} species have been identified as ubiquitous intermediates on the reaction paths of C−H, C−C and C−X bond cleavage and bond formation reactions via oxidative addition to Pt^{II} and reductive elimination from Pt^{IV}, respectively.[1] As oxidative addition and reductive elimination are key reactions in homogeneous catalysis, understanding how these unsaturated intermediate species react with molecular oxygen will be essential to the rational development of novel oxidation catalysts for use with O_2. While five-coordinate Pt species are usually highly reactive, often eluding even spectroscopic observation, a limited number of isolable species have recently been reported and characterized.[1-5] Here the reactivity of several isolable five-coordinate Pt^{IV} trimethyl complexes bearing chelating anionic nitrogen ligands with molecular oxygen is described.[6] We have found that activation of dioxygen by these complexes requires the involvement of both the electrophilic metal center and a Lewis basic site on the ligand.

---

* The material in this chapter was previously published.

Building on previous work in the Goldberg group,[7–9] the five-coordinate complexes ($^{t\text{BuMe2}}$nacnac)PtMe$_3$, (**1**, $^{t\text{BuMe2}}$nacnac$^-$ = [((4-*t*Bu-2,6-Me$_2$C$_6$H$_2$)NC(CH$_3$))$_2$CH]$^-$),[3,10] ($^{\text{Me3}}$Me-nacnac)PtMe$_3$ (**2**, $^{\text{Me3}}$Me-nacnac$^-$ = [((2,4,6-Me$_3$C$_6$H$_2$)NC(CH$_3$))$_2$CCH$_3$]$^-$), ($^{t\text{Bu2}}$PyPyr)PtMe$_3$ (**3**, $^{t\text{Bu2}}$PyPyr$^-$ = 3,5-di-*tert*-butyl-2-(2-pyridyl)pyrrolide),[4] ($^{\text{iPr2}}$AnIm)PtMe$_3$ (**4a**, $^{\text{iPr2}}$AnIm$^-$ = [*o*-C$_6$H$_4$-{N(C$_6$H$_3$^{i}Pr$_2$)}(CH=NC$_6$H$_3$^{i}Pr$_2$)]$^-$),[5] and ($^{\text{Me3}}$AnIm)PtMe$_3$ (**4b**, $^{\text{Me3}}$AnIm$^-$ = [*o*-C$_6$H$_4$-{N(C$_6$H$_2$Me$_3$)}(CH=NC$_6$H$_2$Me$_3$)]$^-$), shown in Figure 2.1, were exposed to oxygen in benzene-d_6 or toluene-d_8 solutions. Complexes **1**-**3** react rapidly forming peroxo intermediates in which one oxygen atom is bound to the platinum center and the other to a carbon atom of the ligand backbone. No reaction was observed with complexes **4a** or **4b**. This difference in reactivity is attributed to the inability of the AnIm ligand to interact with oxygen,thus preventing concurrent binding of oxygen to the metal and the ligand.

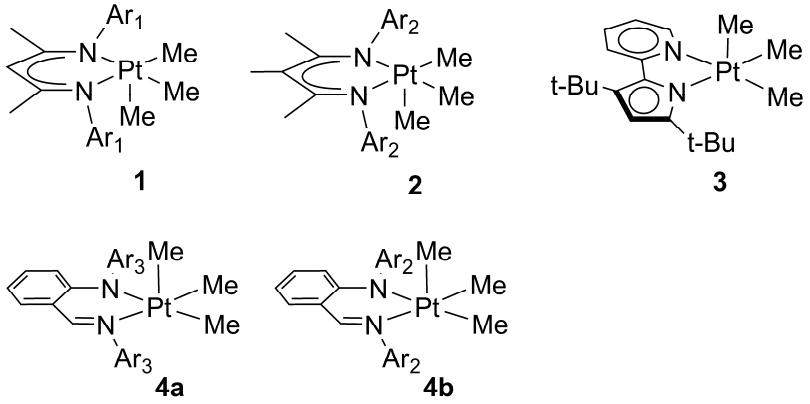

Ar$_1$ = 4-*t*Bu-2,6-dimethylphenyl
Ar$_2$ = 2,4,6-trimethylphenyl
Ar$_3$ = 2,6-diisopropylphenyl

Figure 2.1. Five-coordinate Pt^{IV} complexes studied in our laboratory

Results and discussion

Reactions of five-coordinate Pt complexes with molecular oxygen

Upon mixing a bright orange solution of ($^{t\text{BuMe2}}$nacnac)$PtMe_3$, **1**, in benzene-d_6 or toluene-d_8 with dioxygen, the solution rapidly became pale yellow and a new species, **5** (Figure 2.2), formed.[10] At room temperature, the three Pt−Me groups of **5** are represented by a single broad resonance in the ^{1}H NMR spectrum centered at 0.83 ppm in toluene-d_8. When a sample of **5** in toluene-d_8 was cooled to –40 °C, the ^{1}H NMR spectrum revealed two distinct signals for the Pt−Me groups. A singlet integrating to one methyl group was evident at 0.55 ppm with a $^2J_{\text{Pt–H}}$ = 68 Hz and a singlet integrating to two methyl groups appeared at 1.10 ppm with $^2J_{\text{Pt–H}}$ = 71 Hz. These values are consistent with those expected for an axial and two equivalent equatorial Pt−Me groups, respectively, in an octahedral geometry. The coupling constant between the protons of the axial methyl group and the Pt center ($^2J_{\text{Pt–H}}$), 68 Hz, is of note because it strongly indicates that a ligand is coordinated trans to the axial methyl group. If there was no ligand in this position or only a weakly coordinating one, a significantly larger coupling (> 80 Hz) would be expected.[2e,11] The broad resonance for the three Pt−Me groups that is observed at room temperature is readily explained by a fluxional process in which the Pt−Me groups exchange positions on the NMR timescale. Most likely this exchange proceeds through reversible opening of one of the three ligand arms to generate a transient five-coordinate species in which the Me groups can exchange positions. Five-coordinate d^6 complexes are typically fluxional and the methyl groups of the starting five-coordinate Pt^{IV} trimethyl complexes have been observed to exchange position rapidly on the NMR timescale even at temperatures of −80 °C.[1]

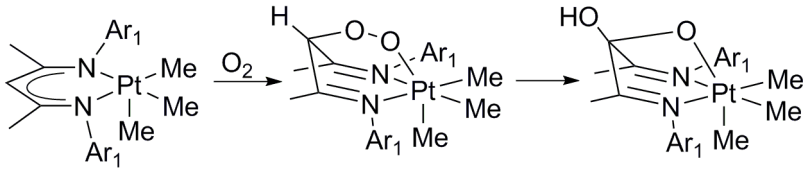

1 **5** **10**

Ar_1 = 4-*t*butyl-2,6-dimethylphenyl

Figure 2.2. Reaction of **1** to form **5** and **10**.

Spectroscopic data for **5** also support the binding of oxygen to the ligand backbone. The one bond carbon−hydrogen coupling constant ($^1J_{C-H}$) of the central carbon of the ligand backbone decreased from 157 Hz in **1** to 144 Hz in **5**. This decrease in the coupling constant is consistent with a hybridization change from sp^2 to sp^3.[12]

Derivatives in which a sixth ligand interacts exclusively with the metal center were prepared by reactions of **1**with CO or *tert*-butyl isonitrile to generate the CO or *tert*-butyl isonitrile adducts **6** and **7** respectively (Figure 2.3). The $^1J_{C-H}$ values for **6** and **7** (158 Hz and 155 Hz respectively) indicate that the $^1J_{C-H}$ value at the central carbon of the ligand backbone is relatively insensitive to a ligand binding exclusively to the metal center.

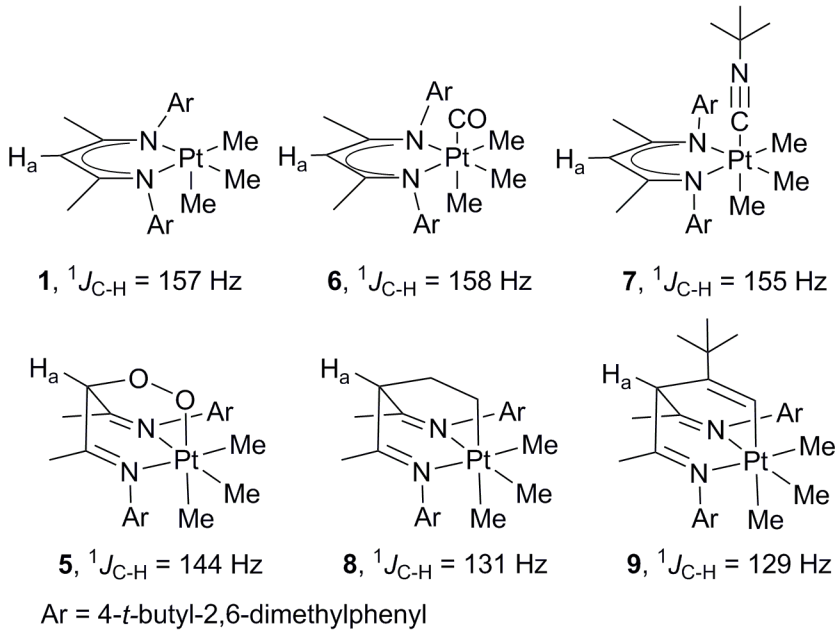

Figure 2.3. $^1J_{C-H}$ values for a series of Pt complexes with sp^2 or sp^3 hybridized carbon atoms in the ligand backbone.

Notably the reaction of **1** with ethylene or 3,3-dimethylbutyne resulted in the formation of six-coordinate Pt species **8** and **9,** respectively (Figure 2.4). While **8** was only stable under a pressure of ethylene, **9** was isolated and crystallographically characterized (Figure 2.5). As seen in Figure 2.5, the central carbon of the ligand backbone in **9** is clearly sp^3 hybridized. Consistent with this assessment, the $^1J_{C-H}$ values of the C–H bond at the center of the ligand backbone in **9** is 129 Hz. The $^1J_{C-H}$ for this carbon in **8** exhibits a similar value of 131 Hz. Observations in organic systems have established that the presence of an electronegative atom will increase coupling constant values, and thus **5** would be expected to have a larger coupling constant than either **8** or **9**.[12] The measured value of 144 Hz observed for this carbon in **5** is then consistent with sp^3 hybridization and an attached oxygen functionality.

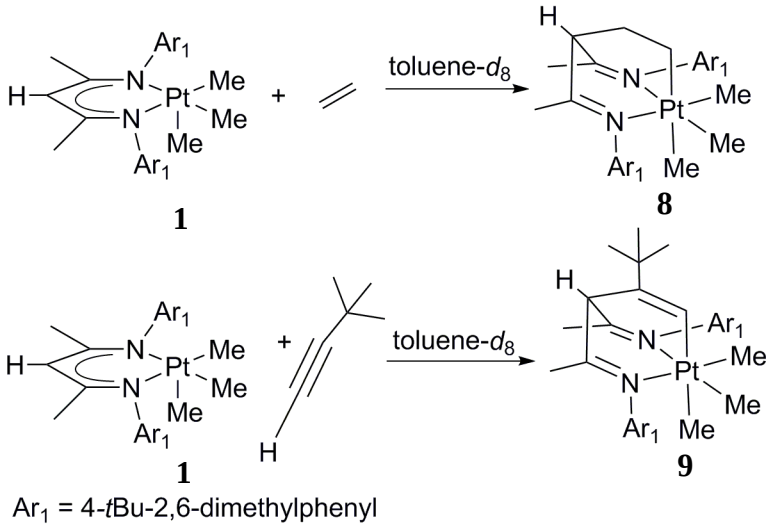

Figure 2.4. Formation of complexes **8** and **9** by reaction of **1** with ethylene and 3,3-dimethylbutyne respectively.

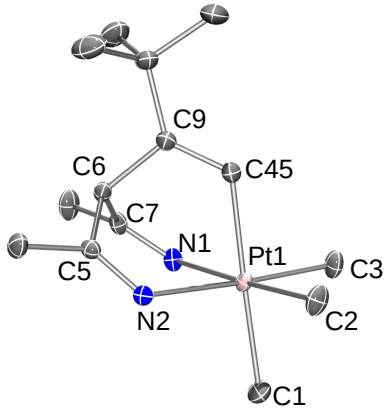

Figure 2.5. POV-Ray rendition of the ORTEP of **9** at the 50% probability level with hydrogen atoms, the aryl rings, and cocrystallized toluene omitted for clarity.[13,14] Selected bond lengths (A˚) and angles (deg) for **9**: Pt1−C1 = 2.126(2), Pt1−C2 = 2.053(2), Pt1−C3 = 2.0461(19), Pt1−C45 = 2.073(2), Pt1−N2 = 2.1894(15), Pt1−N1 = 2.1806(17), C3−Pt1−C45 = 92.35(8), C2−Pt1−C45 = 93.83(8), C3−Pt1−C1 = 86.02(9), C2−Pt1−C1 = 85.98(9), C45−Pt1−N1 = 84.07(7), C45− Pt1−N2 = 84.48(7), N1−Pt1−N2 = 85.73(6).

The structure of **5** as depicted in Figure 2.2 is well supported by NMR spectroscopic evidence and by the characterization of **8** and **9**, carbon analogs of the peroxo group coordination in **5**. Efforts to obtain crystals of **5** suitable for X-ray crystallography were unsuccessful as **5** underwent further reaction under ambient conditions to form the Pt-alkoxide complex (**10**, Figure 2.6).[7] All attempts to grow crystals of **5** yielded complex **10** instead.[10] The alkoxide

complex, **10**, was characterized by NMR spectroscopy, confirming the presence of an OH moiety, and X-ray crystallography confirming the coordination of oxygen to the metal. Complex **10** is structurally similar to Pt hemiketal ring systems prepared by Puddephatt and co-workers.[15] In the room temperature ^{1}H NMR spectrum of **10** in toluene-d_8 resonances for the axial Pt−Me group (0.72 ppm, $^{2}J_{\text{Pt-H}}$ = 72 Hz) and the equatorial Pt−Me groups (1.21 ppm, $^{2}J_{\text{Pt-H}}$ = 70 Hz) could be identified but were somewhat broadened while the resonances of the ligand are sharp. The Pt−Me resonances sharpen at lower temperatures and broaden into the baseline at 50 °C suggesting similar fluxionality to that observed for **5**.

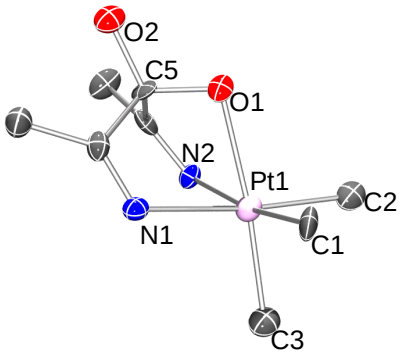

Figure 2.6. POV-Ray rendition of the ORTEP of **10** at the 50 % probability level with hydrogen atoms, aryl rings, and co-crystallized solvent molecules omitted for clarity.[13,14] Selected bond lengths (Å) and angles (deg) for **10**: Pt1–C2 = 2.034(6), Pt1–C3 = 2.021(6), Pt1–C1 = 2.023(6), Pt1–O1 = 2.146(4), Pt1–N1 = 2.206(5), Pt1–N2 = 2.180(5), O1–C6 = 1.397(7), O2–C6 = 1.384(7), C3–Pt1–C1 = 85.8(3), C3–Pt1–C2 = 87.6(2), O1–Pt1–N2 = 75.72(17), O1-Pt1–N1 = 74.17(16), N2–Pt1–N1 = 88.19(18), C6–O1–Pt1 = 100.2(3).

The conversion of the peroxo complex **5** to the alkoxo species **10** involves cleavage of the oxygen−oxygen bond and the formal insertion of an oxygen atom into a carbon−hydrogen bond. We reasoned that replacement of the carbon−hydrogen bond on the central carbon of the nacnac ligand with a more oxidation resistant carbon−carbon bond could inhibit this transformation of the peroxo intermediate. The analogous five-coordinate Pt complex, (^{Me3}Me-nacnac)$PtMe_3$, **2**, was prepared incorporating a recently reported nacnac-based ligand bearing a

methyl group rather than a hydrogen atom at the central carbon of the ligand backbone.[16] In analogy to the method used for preparing **1** and **3**,[4,10 Me3]Me-nacnac-H was deprotonated with KH in THF, and a toluene solution of the deprotonated ligand was then added to a toluene solution of $[PtMe_3OTf]_4$ resulting in immediate formation of bright red **2**.

Upon exposure of a benzene solution of **2** (Figure 2.7) to 1 atm of air or O_2, the bright red color of **2** rapidly disappeared and a pale yellow solution with a pale yellow precipitate of a new species, **11**, was obtained. In addition to being only sparingly soluble in benzene, **11** is also insoluble in THF and acetonitrile. Dissolution of compound **11** in dichloromethane-d_2 allowed for characterization by ^{1}H and ^{13}C NMR spectroscopies. At 25 °C the resonances attributable to the chelating ligand of **11** are sharp, however, the Pt–Me groups appear as a single broad resonance centered at 0.27 ppm. At –40 °C, two distinct resonances for the axial and equatorial Pt–Me groups of **11** can be observed (axial: –0.11ppm, $^2J_{Pt-H}$ = 69 Hz; equatorial 0.30 ppm, $^2J_{Pt-H}$ = 71 Hz). These coupling constants are nearly identical to those of **5**, (vide supra) 68 Hz and 71 Hz for the axial and equatorial Pt−Me groups respectively. As in compound **5**, these data are most consistent with a six-coordinate octahedral Pt^{IV} complex.

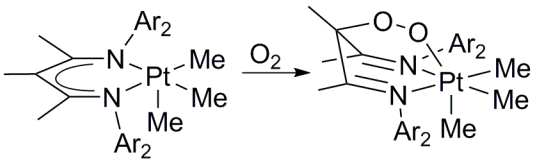

2 **11**

Ar_2 = 2,4,6-trimethylphenyl

Figure 2.7. Reaction of **2** with O_2 to form **11**.

Complex **11** with the methyl group on the central carbon of the ligand backbone is more stable than complex **5** with a hydrogen atom at that position. The peroxo complex, **11**, persists in dichloromethane solution for several days before decaying to a mixture containing multiple species. X-ray quality crystals of **11** were grown from a dichloromethane and pentane solution at

−10 °C. The crystal structure confirms that **11** is indeed a peroxo complex with one oxygen atom bound to the Pt center and the other bound to the central carbon of the ligand backbone (Figure 2.8). Compound **11** has a slightly distorted octahedral geometry about the Pt center with angles between cis ligands ranging from 84.3 to 98.8°. The O–O bond length is 1.465(3) Å. A related iridacyclohexa-2,5-diene-peroxo complex was reported to have an O–O bond length of 1.466(7) Å (Figure 2.9).[17]

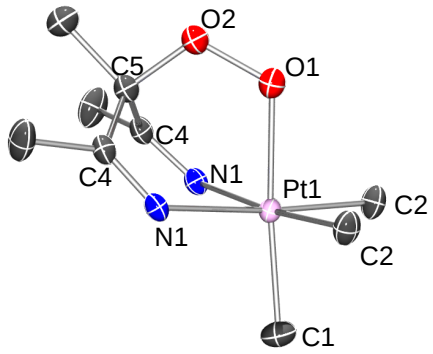

Figure 2.8. POV-Ray rendition of the ORTEP of **11** at the 50 % probability level with hydrogen atoms, aryl rings, and co-crystallized benzene-d_6 omitted for clarity.[13,14] Selected bond lengths (Å) and angles (deg). Pt1–C1 = 2.062(3), Pt1–C2 = 2.041(2), Pt1–N1 = 2.1787(17), Pt1–O1 = 2.103(2), O1–O2 = 1.465(3), O2–C5 = 1.438(4), O2–O1–Pt1 = 117.05(16), C5–O2–O1 = 117.0(2), C2–Pt1–C1 = 84.27(13), C2–Pt1–C1 = 86.46(11), C2–Pt1–O1 = 89.99(8), C2–Pt1–N1 = 94.99(8), C1–Pt1–N1 = 98.78(9), O1–Pt1–N1 = 84.71(7).

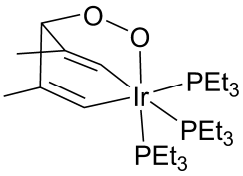

Figure 2.9. Previously reported Ir–peroxo complex with an O–O bond length of 1.466(7) Å.[17]

While complexes with β-diketiminate-based ligands have been shown to cyclize a wide range of substrates with multiple bonds similar to the reactions of 1 with ethylene and 3,3-dimethylbutyne (above), evidence for the formal 4 + 2 cyclization of dioxygen has been more limited.2b,18 Oxidation of the central carbon of a β-diketiminate ligand by dioxygen has been observed in Cu and Zn complexes but in these reactions no peroxo intermediates were detected.[19]

A β-diketiminate-based Co macrocycle was reported to cyclize with dioxygen to form a peroxo complex but no X-ray structural evidence was presented.[20] We recently reported in situ spectroscopic characterization of complex 5,10 however, the crystallographic characterization of **11** provides further confirmation that oxygen can indeed react by cycloaddition involving the β-diketiminate ligand backbone. This new evidence is important in light of the widespread use of β-diketiminate ligands in inorganic chemistry and catalysis.[21] In addition, it should be noted that such peroxo structures wherein the oxygen molecule is bound to both the metal center and the ligand backbone are reminiscent of those proposed in the mechanisms of heme oxygenase[22] and extradiol ring-cleaving dioxygenases.[23]

To better understand the reactivity of a range of five-coordinate Pt^{IV} species with molecular oxygen, we investigated the reaction of (^{tBu2}PyPyr)$PtMe_3$ (**3**, Figure 2.10) with oxygen.[4] A benzene-d_6 solution of **3** was exposed to oxygen and within minutes nearly quantitative formation of a new species, **12**, was observed by ^{1}H and ^{13}C NMR spectroscopies at room temperature. In addition to a single set of well-resolved resonances corresponding the chelating ligand, the ^{1}H NMR spectrum of **12** contains three, well-resolved Pt–Me resonances indicative of a static, six-coordinate Pt complex. This static structure is in contrast to **5** and **11** which both exhibit exchange of the axial and equatorial Pt–Me groups on the NMR time scale at room temperature. Upon warming in toluene-d_8, the Pt–Me resonances of **12** broaden relative to other ligand resonances but were not fully coalesced at 80 °C.

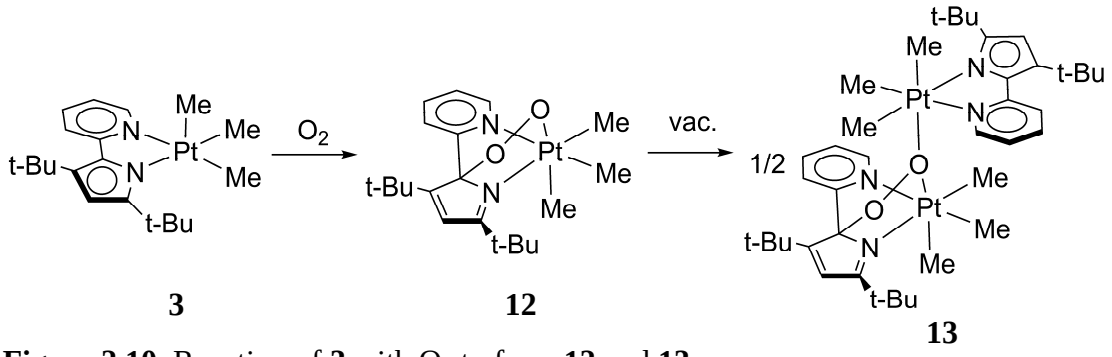

3 **12** **13**

Figure 2.10. Reaction of **3** with O_2 to form **12** and **13**.

In air, a benzene/pentane solution of **12** was allowed to evaporate slowly resulting in small crystals suitable for X-ray diffraction. Analysis of these crystals revealed an asymmetric unit containing two independent molecules of **12** (Figure 2.11). The structure of **12** has a peroxo group that bridges between the Pt center and a carbon atom on the ligand backbone reminiscent of the peroxo complexes **5** and **11**. The Pt−O bond lengths in **11** (2.103(2) Å) and in **12** (2.11 ± 0.02 Å, average of two molecules)[24] are similar, perhaps not surprisingly as the oxygen atoms of both **11** and **12** are trans to strongly donating methyl groups. The O−O bond length in **12** (1.49 ± 0.02 Å average) is slightly longer than that in **11** (1.465(3) Å) and the O–O–Pt bond angles for the two complexes differ substantially with **11** having an angle of 117.05(16)° and **12** an angle of 109 ± 1° (average). The smaller angle in **12** is consistent with the presence of smaller five-membered platinacycles, in contrast to **11** which has only six-membered platinacycles. Efforts to isolate **12** on a large scale were not successful.

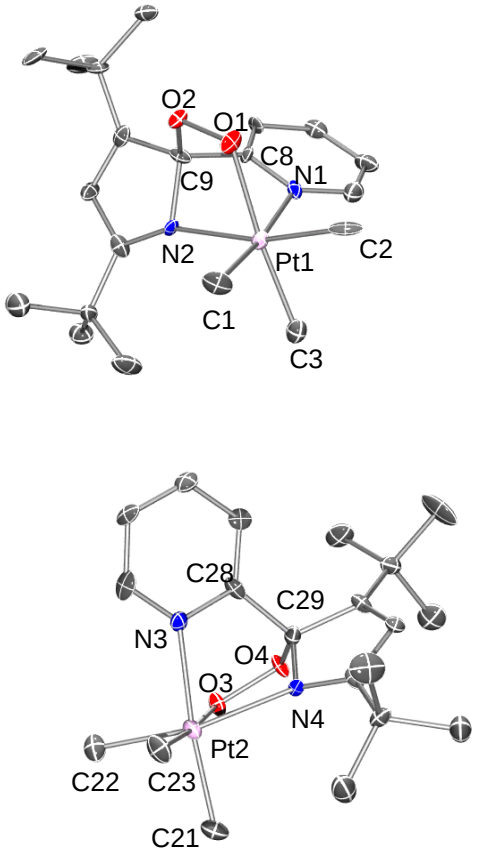

Figure 2.11. POV-Ray rendition of the ORTEP of **12** at the 50 % probability level of the two independent molecules of **12** with hydrogen atoms omitted for clarity.[13,14] The * designation represents that the measurements presented are averages of the two structures. Selected bond lengths (Å) and angles (deg) averaged over the two independent molecules (estimated errors ± 0.02 Å and ± 1 deg):[24] $(C1-Pt1)^*$ = 2.04, $(C2-Pt1)^*$ = 2.01, $(C3-Pt1)^*$ = 2.05, $(N1-Pt1)^*$ = 2.14, $(N2-Pt1)^*$ = 2.21, $(O1-O2)^*$ = 1.49, $(O1-Pt1)^*$ = 2.11, $(O2-C9-N2)^*$ = 110, $(O2-C9-C8)^*$ = 115, $(N2-C9-C8)^*$ = 103, $(C2-Pt1-C1)^*$ = 88, $(C1-Pt1-C3)^*$ = 91, $(C2-Pt1-O1)^*$ = 89, $(C2-Pt1-N1)^*$ = 95, $(O1-Pt1-N1)^*$ = 82, $(C3-Pt1-N2)^*$ = 103, $(N1-Pt1-N2)^*$ = 75, $(O2-O1-Pt1)^*$ = 109, $(C9-O2-O1)^*$ = 111.

Unlike the peroxo complexes **5** and **11**, complex **12** is not stable to vacuum. A benzene solution of **12** was allowed to evaporate slowly under vacuum over one week. Again X-ray-quality crystals were obtained, but analysis of these revealed a new bimetallic peroxo species, **13** (Figure 2.12).[9] Such a structure could form by the loss of O_2 from **12** to form **3** which then coordinates to a second equivalent of **12**. The structure of **13** with a second Pt atom bound to the peroxo oxygen atom proximal to the Pt center suggests that the proximal oxygen atom is a

relatively electron rich and nucleophilic site. Efforts to crystallize **13** on a larger scale were not successful.

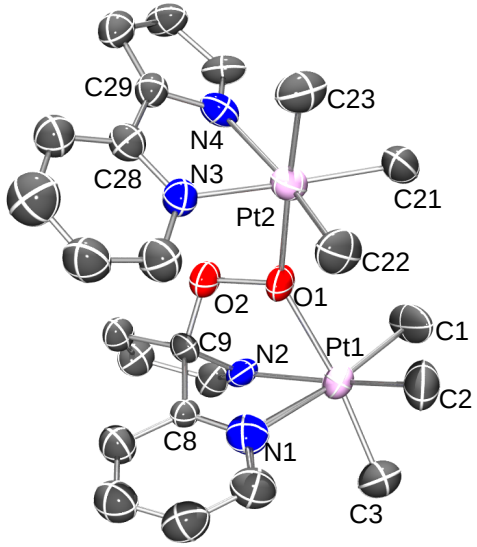

Figure 2.12. POV-Ray rendition of the ORTEP of **13** at the 50 % probability level with hydrogen atoms, *t*Bu groups, and disorder in the pyridine rings omitted for clarity.[13,14] Selected bond lengths (Å) and angles (deg): Pt1–C3 = 2.013(12), Pt–C2 = 2.037(12), Pt1–C1 = 2.082(12), Pt1–N1 = 2.12(3), Pt1–O1 = 2.188(7), Pt1–N2 = 2.198(9), Pt2–C23 = 2.021(12), Pt2–C22 = 2.031(11), Pt2–C21 = 2.076(12), Pt2–N3 = 2.02(3), Pt2–O1 = 2.202(7), Pt2–N4 = 2.209(9), O1–O2 = 1.490(9), O2–C9 = 1.388(12), C3–Pt1–C2 = 85.1(5), C3–Pt1–C1 = 92.7(6), C2–Pt1–C1 = 87.3(6), C3–Pt1–N1 = 91.6(12), C2–Pt1–N1 = 98.6(14), N1–Pt1–O1 = 80.0(12), C3–Pt1–N2 = 100.8(4), C1–Pt1–N2 = 98.2(5), N1–Pt1–N2 = 75.6(13), O1–Pt1–N2 = 77.9(3), C23–Pt2–C22 = 86.2(5), C22–Pt2–C21 = 86.1(5), C22–Pt2–O1 = 89.9(4), N3–Pt2–O1 = 94.3(17), O2–O1–Pt1 = 108.6(5), O2–O1–Pt2 = 106.9(5), Pt1–O1–Pt2 = 144.5(3), C9–O2–O1 = 110.7(7).

Surprisingly, no reaction was observed upon mixing a benzene-d_6 solution of the five-coordinate complex, (^{iPr3}AnIm)PtMe$_3$ (**4a**, Figure 2.1) with dioxygen at room temperature.[8] This contrasts with the five-coordinate Pt species **1**, **2**, and **3** which react with oxygen immediately upon mixing. When a benzene-d_6 solution of **4a** was pressurized with 1 atm O_2, the solution retained its dark red color and no signals other than those attributable to **4a** itself were detected by ^{1}H NMR spectroscopy. Heating **4a** in the presence of dioxygen resulted in loss of ethane followed by a previously reported activation of an aryl isopropyl group.[5] The thermal reactivity of **4a** with oxygen was identical to that observed on heating **4a** in the absence of dioxygen.[5]

To test whether the sterically bulky isopropyl substituents on the aryl rings could be preventing oxygen from accessing the metal center of **4a**, (^{Me3}AnIm)PtMe$_3$ (**4b**, Figure 2.1) was prepared. The steric properties of this complex should be similar to those of complexes **1** and **2** which also have methyl groups at the 2- and 6- positions of the aryl rings. A solution of **4b** was pressurized with 3 atm O_2. After one day, no new species were observed in solution by ^{1}H NMR spectroscopy and the deep red color of the solution persisted. Longer reaction times and heating were avoided as **4b** was found to decompose in the absence of oxygen under these conditions and the details of the decomposition in the absence of air are not well understood.

Each of the five-coordinate Pt complexes studied has an open site at the metal center yet only **1**-**3** react with oxygen. In each reaction, the oxygen molecule forms a bond to the open site at the Pt center and also forms a bond to a carbon atom on the ligand backbone. Of note, each of the carbon atoms in the ligand that participates in the reaction with oxygen is a relatively electron-rich site where a partial anionic charge localization is suggested by a resonance structure. On the basis of the observation that **1**, **2**, and **3** react with oxygen but **4a** and **4b** do not, it seems that subtle structural variations in the ligand are important in controlling the reactivity of five-coordinate Pt species with oxygen. In all five of these Pt^{IV} complexes, the Pt bears a formally anionic bidentate ligand with a delocalized negative charge and all of the atoms in the platinacycle containing the chelating ligand are sp^2 hybridized. Upon cooperative binding of oxygen, one of those sp^2 hybridized atoms must take on sp^3 hybridization and move out of the plane. In complexes **1** and **2** the strain of this conformational change is easily accommodated as the nacnac ligand localizes its electrons to form two imine bonds. The peroxo complexes **5** and **11** are formed rapidly and irreversibly. The monometallic and bimetallic peroxo complexes derived from **3**, complexes **12** and **13**, indicate that the pyridylpyrrolide ligand structure can also

demonstrate this change of hybridization. The lack of reactions involving **4a** and **4b** may be rationalized by considering that a reaction with dioxygen analogous to that seen in **1**, **2**, and **3** would involve breaking the aromaticity of the six-membered arene ring in the ligand backbone, a more thermodynamically uphill transformation.[25]

Reactivity of the Pt^{IV}-peroxo complexes

The reactivity of the new peroxo complexes was also explored. As was noted, the peroxo complex **5** undergoes further reaction in arene solvents in the absence of any added substrate to form the Pt alkoxide complex **10** (Figure 2.2).[10] This reaction to form **10** is interesting as the O−O bond is cleaved and the C−H functionality at the central carbon of the ligand backbone is oxidized to a C−OH, suggesting that Pt^{IV} peroxo complexes might be effective oxidants for incorporating oxygen atoms into organic substrates.

The related Pt^{IV} peroxo complex, **11**, lacks a C−H bond on the central C of the β-diketiminate backbone. The substitution of a methyl group in this position appears to stabilize the peroxo intermediate and has allowed us to probe the reactivity of the peroxo functionality with added substrates. Complex **11** in dichloromethane-d_2 solution was observed to react with PPh_3, SMe_2, and CO. In each reaction, there was no change in the visual appearance of the samples but ^{1}H NMR spectra recorded after four hours revealed complete consumption of **11**. Regardless of which substrate was added, the same new Pt-containing species, **14** (Figure 2.13), formed in > 90% yield (as determined by integration of the ^{1}H NMR resonances relative to an internal standard). In the cases of PPh_3 and SMe_2, $OPPh_3$ and DMSO were also detected respectively. The three Pt−Me groups in the Pt product, **14**, appear as a single broad resonance at 0.53 ppm in the ^{1}H NMR spectrum. Upon cooling to – 5 °C, the broad resonance resolved into two singlets with Pt satellites at 0.58 ppm ($^2J_{Pt-H}$ = 75 Hz) and 0.12 ppm ($^2J_{Pt-H}$ = 71 Hz) for the

equatorial and axial Pt–Me groups respectively. Crystals of **14** were obtained by slow evaporation of a solution containing a mixture of dichloromethane-d_2 and pentane. X-ray crystallography confirmed that complex **14** is an octahedral Pt^{IV} species in which an O−O bond has been broken and one oxygen atom has been lost such that the bridging peroxo moiety from **11** is now an alkoxo (Figure 2.14).

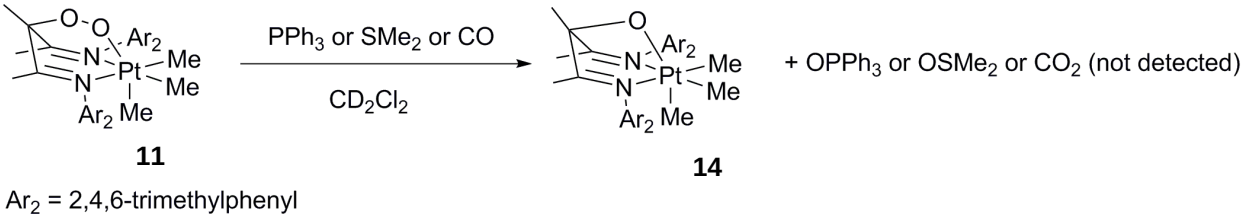

Figure 2.13. Reaction of **11** with oxygen atom acceptors to form **14**.

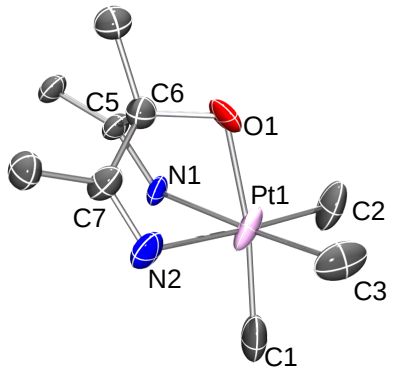

Figure 2.14. POV-Ray rendition of the ORTEP of **14** at the 50 % probability level with hydrogen atoms, aryl groups, and cocrystallized pentane are omitted for clarity.[13,14] Selected bond lengths (Å) and angles (deg): C1–Pt1= 2.028(8), C2–Pt1= 2.028(7), C3–Pt1 = 2.029(7), N1–Pt1 = 2.145(7), N2–Pt1 = 2.248(11), O1–Pt1 = 2.054(9), C2–Pt1–C1 = 83.6(6), C2–Pt1–C3 = 87.2(6), C2–Pt1–O1 = 102.2(5), C3–Pt1–O1 = 97.4(5), C1–Pt1–O1 = 172.1(4), C1–Pt1–N1 = 95.1(5), O1–Pt1–N1 = 79.5(3), O1–Pt1–N2 = 75.6(3).

Summary

The reactivity of oxygen with a series of five-coordinate Pt^{IV} trimethyl species with monoanionic N,N or N,N' chelating ligands was explored. Three of these complexes, **1**, **2**, and **3** react with oxygen immediately to form new Pt^{IV} peroxo species that were characterized

spectroscopically and in two cases, crystallographically. The peroxo products exhibit bonding of one of the oxygen atoms to the metal center and the other to a carbon atom on the chelating ligand. This reaction with oxygen requires the participation of both the metal center and a site on the ligand backbone. In complexes **4a** and **4b**, there is no adequate Lewis basic site on the ligand to participate in the binding of oxygen and consequently no reaction with oxygen is observed. The activation of oxygen by five-coordinate Pt^{IV} species can be regarded as another class of reaction involving metal-ligand cooperation,[26] opening new possibilities for the discovery of other transition metal oxygen activation reactions. Both intra- and intermolecular oxygen transfer from the new Pt ligand peroxo complexes were observed.

Experimental

General Considerations

Unless otherwise specified, all manipulations were carried out in a nitrogen-filled glovebox, using a Schlenk line, or using a high-vacuum manifold. Glassware was oven-dried prior to use. Benzene, dichloromethane, THF, toluene, and pentane were dried by passage through activated alumina and molecular sieve columns under argon. Benzene-d_6 and toluene-d_8 were vacuum-transferred from sodium/benzophenone ketyl. Dichloromethane-$d_2$was vacuum transferred from CaH_2. Complexes **1**,[10] **3**,[4] **4a** and **4b**,[5] $[PtMe_3OTf]_4$,[27] and the neutral proligand for complex **2**, ^{Me3}Me-nacnac-H,[16] were prepared using previously reported procedures. KH was obtained as a suspension in mineral oil and washed with pentane prior to use. All other reagents and gases were obtained from commercial vendors and used as received. Gas pressures in excess of 1 atm were attained using a previously described pressurization apparatus.[28] IR spectra were recorded on a Perkin Elmer Spectrum RX1 FT-IR spectrometer in nujol mull. NMR spectra were recorded

on Bruker DRX500, AV500, AV700, or AV800 spectrometers and were referenced to the residual protiated solvent signal. Data from HMQC and HMBC experiments were used in the assignment of ^{13}C resonances. Abbreviations: s = singlet, d = doublet, dd = doublet of doublets, m = multiplet, br = broad.

Synthesis of (^{Me3}Me-nacnac)PtMe$_3$ (2)

^{Me3}Me-nacnac-H (69 mg, 0.20 mmol) was dissolved in 5 mL THF in a glass reaction vessel with a Teflon stopper. Potassium hydride (40 mg, 1.0 mmol) was added and the solution was stirred 20 hours. The bright yellow suspension was filtered through a 0.2 μm PTFE filter, and the volatiles removed in vacuo giving a yellow residue which was dissolved in 15 mL toluene. This solution was slowly added to a solution of $[PtMe_3OTf]_4$ (78 mg, 0.050 mmol) dissolved in 5 mL toluene. After 30 minutes, the bright red suspension was filtered through a 0.2 μM PTFE filter, and the volatiles removed in vacuo to give a red solid which was recrystallized from pentane at –35 °C to give red crystals of **2** (36 mg, 31 % yield). ^1H NMR of **2** (benzene-d_6, 700 MHz, 298 K) δ 6.90 (s, 4H, Ar–**H**), 2.24 (s, 6H, Ar$_{para}$–C**H$_3$**), 2.07 (s, 12H, Ar$_{ortho}$–C**H$_3$**), 1.97 (s, 3 H, (N=C)$_2$–C**H$_3$**), 1.77 (s, 6 H, N=C–C**H$_3$**), 1.12 (s, 9H, $^2J_{Pt–H}$ = 74 Hz, Pt–**CH$_3$**). ^{13}C NMR of **2** (benzene-d_6, 176 MHz, 298 K) δ 157.1 (N–**C**$_{backbone}$), 148.4 (N–**C**$_{aryl}$), 133.6 (**C**$_{Ar\text{-}para}$), 131.9 (**C**$_{Ar\text{-}ortho}$), 129 (C$_{Ar\text{-}meta}$), 100 (**C**$_{backbone\ center}$), 21.4 (N–C–**C**H$_3$), 20.9 (Ar$_{para}$–**C**H$_3$), 20.4 (C$_{backbone\ center}$–**C**H$_3$), 19.5 (Ar$_{ortho}$–**C**H$_3$), 2.0 (Pt–**C**H$_3$). Anal. Calcd. for $C_{27}H_{40}N_2Pt$: C, 55.18; H, 6.86; N, 4.77. Found: C, 55.26; H, 6.97; N, 4.72.

Reaction between (^{tBuMe2}nacnac)PtMe$_3$ (1) and dioxygen to form 5

Complex **1** (1.0 mg, 0.0015 mmol) and a 1,3,5-trimethoxybenzene internal standard (0.5 mg, 0.003 mmol) were dissolved in toluene-d_8 (0.4 mL) in an aluminum foil-covered NMR tube

fitted with a J. Young style Teflon valve. The tube was then pressurized with dioxygen (1-4 atm) at room temperature or -78 °C resulting in an immediate color change from bright yellow-orange to pale yellow. The yield of **5** was greater than 90% (integration relative to the internal standard). ^{1}H NMR of **5** (toluene-d_8, 233 K) δ 0.55 (s, 3H, $^{2}J_{Pt\text{-}H}$ = 68 Hz, Pt–C**H**$_3$), 1.12 (s, 6H, $^{2}J_{Pt\text{-}H}$ = 71 Hz, Pt–C**H**$_3$), 1.25 (s, 18 H, C(C**H**$_3$)$_3$), 1.40 (s, 6H, N=C–C**H**$_3$),[29] 2.14 (s, 6H, Ar–C**H**$_3$), 2.37 (s, 6H, Ar–C**H**$_3$), 4.62 (s, 1H, N=C–C**H**),[29] 7.17 (s, 2H, Ar–**H**), 7.19 (s, 2H, Ar–**H**). ^{1}H NMR (benzene-d_6, 323 K) δ 0.78 (s, 9H, $^{2}J_{Pt\text{-}H}$ = 70 Hz, Pt–C**H**$_3$), 1.23 (s, 18H, C(C**H**$_3$)$_3$), 1.50 (s, 6H, N=C–C**H**$_3$),[29] 2.12 (s, 6H, Ar–C**H**$_3$), 2.34 (s, 6H, Ar–C**H**$_3$), 4.64 (s, 1H, N=C–C**H**),[29] 7.13 (s, 2H, Ar–**H**), 7.14 (s, 2H, Ar-**H**). ^{13}C NMR (toluene-d_8, 298 K) δ 18.6 (Ar–**C**H$_3$), 19.3 (Ar–**C**H$_3$), 24.1 (N=C–**C**H$_3$), 31.5 (C(**C**H$_3$)$_3$), 34.3 (**C**(CH$_3$)$_3$), 87.9 (O–**C**–H), 125.4 (**C**$_{Ar}$–H), 125.8 (**C**$_{Ar}$–H), 127.5 (**C**$_{Ar}$–CH$_3$), 130.6 (**C**$_{Ar}$–CH$_3$), 141.0 (N–**C**$_{Ar}$) 148.9 (**C**$_{Ar}$–C(CH$_3$)$_3$), 173.8 (N=**C**).

Synthesis of 6 from 1 and CO

Complex **1** (1.0 mg, 0.0015 mmol) and a 1,3,5-trimethoxybenzene internal standard (0.5 mg, 0.003 mmol) were dissolved in toluene-d_8 (0.4 mL) in an aluminum foil-covered NMR tube fitted with a J. Young style Teflon valve. CO gas (1 atm) was added by opening the degassed sample to a CO-filled manifold. The solution turned from yellow-orange to colorless on mixing. The yield of **6** was 92% (integration relative to the internal standard). ^{1}H NMR (toluene-d_8, 233 K) δ 0.70 (s, 6H, $^{2}J_{Pt\text{-}H}$ = 63 Hz, Pt–C**H**$_3$), 1.29 (s, 18H, C(C**H**$_3$)$_3$), 1.53 (s, 6H, N=C–C**H**$_3$), 1.67 (s, 3H, $^{2}J_{Pt\text{-}H}$ = 64 Hz, Pt–C**H**$_3$), 2.33 (s, 6H, Ar–C**H**$_3$), 2.37 (s, 6H, Ar–C**H**$_3$), 4.62 (s, 1H, N=C–C**H**), 7.21 (s, 2H, Ar–**H**), 7.22 (s, 2H, Ar–**H**). ^{1}H NMR (toluene-d_8, 298 K) δ 0.88 (s br, 9H, Pt–C**H**$_3$), 1.27 (s, 18 H, C(C**H**$_3$)$_3$), 1.53 (s, 6H, N=C–C**H**$_3$), 2.30 (s, 12 H, Ar–C**H**$_3$), 4.61 (s, 1H, N=C–C**H**), 7.16 (s, 4H, Ar–**H**).

Synthesis of 7 from 1 and *tert*-butylisonitrile

Complex **1** (5.0 mg, 0.0076 mmol) and a 1,3,5-trimethoxybenzene internal standard (1.0 mg, 0.0076 mmol) were dissolved in toluene-d_8 (0.4 mL) in an aluminum foil-covered NMR tube fitted with a J. Young style Teflon valve. *tert*-Butylisonitrile was added (0.9 μL, 0.008 mmol). The sample turned from yellow-orange to colorless upon mixing. Integration of the ^{1}H NMR spectrum revealed a yield of 95% relative to the internal standard. ^{1}H NMR (toluene-d_8, 298 K) δ 0.62 (s, 6H, $^2J_{Pt\text{-}H}$ = 65 Hz, Pt–C**H**$_3$), 0.89 (s, 9H, N–C(C**H**$_3$)$_3$), 1.29 (s, 18 H, Ar–C(C**H**$_3$)$_3$), 1.43 (s, 3H, $^2J_{Pt\text{-}H}$ = 65 Hz, Pt–C**H**$_3$), 1.59 (s, 6H, N=C–C**H**$_3$), 2.39 (s, 6H, Ar–C**H**$_3$), 2.44 (s, 6H, Ar-C**H**$_3$), 4.62 (s, 1H, N=C–C**H**), 7.15 (s, 2H, Ar–**H**), 7.17 (s, 2H, Ar–**H**). ^{13}C NMR (toluene-d_8, 298 K) δ -7.6 (Pt–**C**H$_3$), 5.3 (Pt–**C**H$_3$), 19.8 (Ar–**C**H$_3$), 20.4 (Ar–**C**H$_3$), 24.7 (N=C–**C**H$_3$), 29.4 (N–C(**C**H$_3$)$_3$), 31.7 (Ar–C(**C**H$_3$)$_3$), 34.1 (Ar–C(**C**H$_3$)$_3$), 56.2 (N–**C**(CH$_3$)$_3$), 96.0 (N=C–**C**–C=N), 124.8 (**C**$_{Ar}$–H), 124.9 (**C**$_{Ar}$–H), 132.2 (**C**$_{Ar}$–CH$_3$), 134.1 (**C**$_{Ar}$–CH$_3$), 137.2 (Pt–**C**≡N), 146.2 (**C**$_{Ar}$–C(CH$_3$)$_3$), 147.1 (**C**$_{Ar}$–N), 159.0 (**C**=N). IR (cm^{-1}): 2192 (ν_{CN}).

Synthesis of 8 from 1 and ethylene

Complex **1** (1.0 mg, 0.0015 mmol) and a 1,3,5-trimethoxybenzene internal standard (0.5 mg, 0.003 mmol) were dissolved in toluene-d_8 (0.4 mL) in an aluminum foil-covered NMR tube fitted with a J. Young style Teflon valve. Ethylene (4 atm) was condensed into the tube from a known-volume bulb. The sample turned from yellow-orange to pale yellow upon warming and mixing. Integration of the ^{1}H NMR spectrum revealed a yield of 85% relative to the internal standard. ^{1}H NMR (toluene-d_8, 298 K) δ 0.01 (s, 3H, $^2J_{Pt\text{-}H}$ = 46 Hz, Pt–C**H**$_3$), 0.92 (s, 6H, $^2J_{Pt\text{-}H}$ = 73 Hz, Pt–C**H**$_3$), 0.93 (br m, 2H, Pt–C**H**$_2$), 1.24 (s, 18 H, C(C**H**$_3$)$_3$), 1.39 (s, 6H, N=C–C**H**$_3$), 1.74 (br m, 2H, Pt–CH$_2$C**H**$_2$), 2.03 (s, 6H, Ar–C**H**$_3$), 2.20 (s, 6H, Ar-C**H**$_3$), 3.50 (s, 1H, N=C-C**H**), 7.12 (s, 2H, Ar–**H**), 7.17 (s, 2H, Ar–**H**). ^{13}C NMR (toluene-d_8, 298 K) δ –5.5 (Pt–**C**H$_3$), 2.3

(Pt–**C**H_3), 16.8 (Pt–**C**H_2), 18.7 (Ar–**C**H_3), 19.9 (Ar–**C**H_3), 23.4 (N=C–**C**H_3), 24.0 (Pt–CH_2–**C**H_2), 31.5 (C(**C**$H_3)_3$), 34.2 (**C**$(CH_3)_3$), 65.9 (N=C–**C**–C=N), 125.4 ($\mathbf{C}_{Ar}$–H), 125.5 ($\mathbf{C}_{Ar}$–H), 128.2 ($\mathbf{C}_{Ar}$–CH_3), 129.5 ($\mathbf{C}_{Ar}$–CH_3), 142.5 ($\mathbf{C}_{Ar}$–N), 148.2 ($\mathbf{C}_{Ar}$–$C(CH_3)_3$), 173.9 (**C**=N).

Synthesis of 9 from 1 and 3,3-dimethylbutyne

Complex **1** (1.0 mg, 0.0015 mmol) and a 1,3,5-trimethoxybenzene internal standard (0.5 mg, 0.003 mmol) were dissolved in toluene-d_8 (0.4 mL) in an aluminum foil-covered NMR tube fitted with a J. Young style Teflon valve. 3,3-Dimethylbutyne was added (2 μL, 0.2 mmol). The sample turned from yellow-orange to colorless upon mixing. Integration of the ^{1}H NMR spectrum revealed a yield of 95% relative to the internal standard. Material for elemental analysis was precipitated from pentane solution and rinsed with several portions of pentane. ^{1}H NMR (toluene-d_8, 298 K) δ 0.12 (s, 3H, $^2J_{Pt\text{-}H}$ = 45 Hz, Pt–C**H**$_3$), 0.93 (s, 6H, $^2J_{Pt\text{-}H}$ = 75 Hz, Pt–C**H**$_3$), 1.13 (s, 9H, C(C**H**$_3)_3$), 1.23 (s, 18 H, Ar–C(C**H**$_3)_3$), 1.63 (s, 6H, N=C–C**H**$_3$), 1.81 (s, 6H, Ar–C**H**$_3$), 2.25 (s, 6H, Ar–C**H**$_3$), 4.72 (d, 1H, $^4J_{H\text{-}H}$ = 2 Hz, N=C–C**H**), 7.07 (s, 2H, Ar–**H**), 7.17 (s, 2H, Ar–**H**), 7.56 (d, 1H, $^4J_{H\text{-}H}$ = 2 Hz, $^2J_{Pt\text{-}H}$ = 35 Hz). ^{13}C NMR (toluene-d_8, 298 K) δ –7.7 (Pt-**C**H_3), 0.4 (Pt–**C**H_3), 18.6 (Ar–**C**H_3), 19.9 (Ar–**C**H_3), 24.8 (N=C–**C**H_3), 30.4 (C(**C**$H_3)_3$), 31.5 (Ar–C(**C**$H_3)_3$), 34.2 (Ar–**C**$(CH_3)_3$), 37.8 (**C**$(CH_3)_3$), 69.5 (N=C–**C**–C=N), 125.4 ($\mathbf{C}_{Ar}$–H), 125.5 ($\mathbf{C}_{Ar}$–H), 128.2 ($\mathbf{C}_{Ar}$–CH_3), 130.5 ($\mathbf{C}_{Ar}$–CH_3), 137.8 (Pt–C=**C**), 141.7 ($\mathbf{C}_{Ar}$–N), 148.4 ($\mathbf{C}_{Ar}$–$C(CH_3)_3$), 161.0 (Pt–**C**=C), 172.7 (**C**=N). Anal. Calcd for $C_{38}H_{60}N_2Pt$ (739.97): C, 61.68; H, 8.17; N, 3.79. Found: C, 61.81; H, 8.27; N, 3.77.

Formation of 10 from 5

Over time, the formation of **10** was observed in greater than 60% yield relative to a 1,3,5-trimethoxybenzene internal standard. Material for elemental analysis was precipitated from

benzene solution and rinsed with several portions of pentane. ^{1}H NMR of **10** (toluene-d_8, 298 K) δ 0.72 (s, 3H, $^{2}J_{Pt\text{-}H}$ = 72 Hz, Pt–C**H**$_3$), 1.21 (s, 6H, $^{2}J_{Pt\text{-}H}$ = 70 Hz, Pt–C**H**$_3$), 1.29 (s, 18 H, C(C**H**$_3$)$_3$), 1.99 (s, 6H, N=C–C**H**$_3$), 2.19 (s, 6H, Ar–C**H**$_3$), 2.45 (s, 6H, Ar–C**H**$_3$), 7.16 (s, 2H, Ar–**H**), 7.27 (s, 2H, Ar–**H**), 11.25 (s, 1H, C–O**H**). ^{13}C NMR (toluene-d_8, 298 K) δ –14.4 (Pt–**C**H$_3$), –9.9 (Pt–**C**H$_3$), 19.3 (Ar–**C**H$_3$), 20.0 (Ar–**C**H$_3$), 20.0 (N=C–**C**H$_3$), 31.5 (C(**C**H$_3$)$_3$), 34.2 (**C**(CH$_3$)$_3$), 109.8 (O–**C**–OH), 125.4 (**C**$_{Ar}$–H), 126.0 (**C**$_{Ar}$–H), 128.7 (**C**$_{Ar}$–CH$_3$), 130.6 (**C**$_{Ar}$–CH$_3$), 140.8 (N–**C**$_{Ar}$) 148.6 (**C**$_{Ar}$–C(CH$_3$)$_3$), 191.1 (N=**C**). Anal. Calcd for $C_{32}H_{50}N_2O_2Pt$ (689.53): C, 55.72; H, 7.31; N, 4.06. Found: C, 55.32; H, 7.38; N, 4.12.

Reaction of 2 with air to form 11

Complex **2** (27.6 mg, 0.0470 mmol) was partially dissolved in 2 mL benzene. The suspension was exposed to air upon which the solution color changed from orange to pale yellow accompanied by the formation of a pale yellow precipitate. The suspension was allowed to settle and after 1 hour the benzene supernatant was pipetted away. In air the remaining solid was rinsed with 3 x 1mL THF and then dried under vacuum yielding **11** (21.7 mg, 0.036 mmol, 76%). Crystals suitable for X-ray diffraction were obtained by cooling a solution of **9** in dichloromethane/pentane to approx. −10 °C. ^{1}H NMR of **11** (dichloromethane-d_2, 500 MHz, 298 K) δ 6.98 (s, 2H, Ar–**H**), 6.95 (s, 2H, Ar–**H**), 2.31 (s, 6H, Ar$_{para}$–C**H$_3$**), 2.17 (s, 6H, Ar$_{ortho}$–C**H$_3$**), 2.07 (s, 6H, Ar$_{ortho}$–C**H$_3$**), 2.02 (s, 6 H, N=C–C**H$_3$**), 1.92 (s, 3H, O–O–C–C**H$_3$**), 0.27 (br, 9H, Pt–C**H$_3$**). ^{1}H NMR of **11** (dichloromethane-d_2, 500 MHz, 233 K) δ 6.95 (s, 2H, Ar–**H**), 6.93 (s, 2H, Ar–**H**), 2.28 (s, 6H, Ar$_{para}$–C**H$_3$**), 2.11 (s, 6H, Ar$_{ortho}$–C**H$_3$**), 2.02 (s, 6H, Ar$_{ortho}$–C**H$_3$**), 2.01 (s, 6 H, N=C–C**H$_3$**), 1.91 (s, 3H, O–O–C–C**H$_3$**), 0.30 (s, 6H, $^{2}J_{Pt–H}$ = 71 Hz, Pt–C**H$_3$**), –0.11 (s, 3H, $^{2}J_{Pt–H}$ = 69 Hz, Pt–C**H$_3$**). ^{13}C NMR of **11** (dichloromethane-d_2, 201 MHz, 298 K) δ 177.5 (N=**C**), 141.7 (N–**C**$_{aryl}$), 136.1 (**C**$_{Ar\text{-}para}$), 130.7 (**C**$_{Ar\text{-}ortho}$), 129.6 (**C**$_{Ar\text{-}meta}$), 129.4 (**C**$_{Ar\text{-}meta}$), 128.0 (**C**$_{Ar\text{-}}$

$_{ortho}$), 88.1 (O–O–**C**, $^{3}J_{Pt–H}$ = 48 Hz), 23.6 (O–O–C–**C**H$_3$), 21.6 (N=C–**C**H$_3$), 21.0 (Ar$_{para}$–**C**H$_3$), 19.4 (Ar$_{ortho}$–**C**H$_3$), 18.3 (Ar$_{ortho}$–**C**H$_3$).[30] Anal. Calcd. for $C_{27}H_{40}N_2O_2Pt$: C, 52.33; H, 6.51; N, 4.52. Found: C, 51.96; H, 6.61; N, 4.39.

Generation of 12 from 3 and O_2

An orange benzene-d_6 (0.4 mL) solution of ($^{t\text{Bu2}}$PyPyr)PtMe$_3$, **3** (2.3 mg, 0.0046 mmol) containing toluene as an internal standard was prepared in an NMR tube fitted with a Teflon stopcock. O_2 gas (1 atm) was added to the tube. The solution became bright yellow and complex **12** formed in > 90 % yield as measured by integration of the ^{1}H NMR spectrum. Crystals of **12** suitable for X-ray diffraction were obtained by slow evaporation of a benzene/pentane solution of **12** in air. ^{1}H NMR of **12** (benzene-d_6, 500 MHz, 298 K) δ 8.00 (d, $^{2}J_{H–H}$ = 5 Hz, $^{3}J_{Pt–H}$ = 19 Hz, 1H, C$_{pyridyl}$–**H**), 7.21 (d, $^{2}J_{H–H}$ = 8.0 Hz, 1H, C$_{pyridyl}$–**H**), 6.73 (t, $^{2}J_{H–H}$ = 7.5 Hz, 1H, C$_{pyridyl}$–**H**), 6.33 (t, $^{2}J_{H–H}$ = 7.0 Hz, 1H, C$_{pyridyl}$–**H**), 6.22 (s, 1H, N=C–C–**H**), 1.79 (s, 3H, $^{2}J_{Pt–H}$ = 73 Hz, Pt–C**H$_3$**), 1.60 (s, 3H, $^{2}J_{Pt–H}$ = 77 Hz, Pt–C**H$_3$**), 1.29 (s, 9 H, (C**H$_3$**)$_3$), 1.12 (s, 3H, $^{2}J_{Pt–H}$ = 68 Hz, Pt–C**H$_3$**), 0.99 (s, 9H, (C**H$_3$**)$_3$). ^{13}C NMR of **12** (benzene-d_6, 126 MHz, 298 K) δ 184.2 ($^{2}J_{Pt–C}$ = 15 Hz, **C**−C−(CH$_3$)$_3$), 175.0 (**C**−C−(CH$_3$)$_3$), 158.9($^{2}J_{Pt–C}$ = 8 Hz, **C**$_{pyridyl}$), 145.5 ($^{2}J_{Pt–C}$ = 16 Hz, **C**$_{pyridyl}$–H), 137.7 (**C**$_{pyridyl}$–H), 127 (N=C–**C**), 125.3 ($J_{Pt–C}$ = 15 Hz, **C**$_{pyridyl}$–H), 122.8 (**C**$_{pyridyl}$–H), 119.1 ($^{2}J_{Pt–C}$ = 23 Hz, N−**C**$_{sp3}$), 36.6(**C**−(CH$_3$)$_3$), 35.5 (**C**−(CH$_3$)$_3$), 32.6(**C**H$_3$)$_3$), 28.1 (**C**H$_3$)$_3$), −6.5 ($^{1}J_{Pt–C}$ = 735 Hz, Pt–**C**H$_3$), −9.8 ($^{1}J_{Pt–C}$ = 707 Hz, Pt–**C**H$_3$), −15.2 ($^{1}J_{Pt–C}$ = 683 Hz, Pt–**C**H$_3$).

Crystallization of 13

In a glass reaction vessel fitted with a teflon stopcock ($^{t\text{Bu2}}$PyPyr)PtMe$_3$, **3** (20 mg, 0.040 mmol) was dissolved in benzene (4 mL).[9] The solution was degassed by three freeze-pump-thaw cycles and then oxygen gas (1 atm) was introduced causing a color change from red to greenish-yellow.

The solvent volume was reduced under vacuum over one week resulting in crystals of the bimetallic species, **13**, which were suitable for X-ray diffraction.

Typical procedure for testing 4a and 4b for reaction with O_2

A benzene-d_6 solution of **4b** (10 mM) and the internal standard 1,3,5-trimethoxybenzene in an NMR tube fitted with a Teflon valve was pressurized with 3 atm O_2 and monitored by ^{1}H NMR.

Generation of 14 by oxygen-atom transfer from 11

An NMR tube fitted with a Teflon valve was charged with **2** (2.2 mg, 3.7 mmol) and benzene (0.4 mL) with a small amount of 1,3,5-trimethoxybenzene added as an internal standard. The sample was pressurized with 3 atm O_2. After 20 min. all of the volatiles were removed in vacuo, dichloromethane-d_2 was added by vacuum transfer, and an initial spectrum of **11** was recorded and integrated relative to the internal standard. PPh_3 (1.7 mg, 6.5 mmol) was added. Within four hours, **14** was observed in >90% yield (integration of ^{1}H NMR spectrum relative to 1,3,5-trimethoxybenzene). A similar procedure was used when testing the reactivity of **11** with other potential oxygen atom acceptors. ^{1}H NMR of **14** (dichloromethane-d_2, 500 MHz, 298 K) δ 6.95 (s, 2H, Ar–**H**), 6.91 (s, 2H, Ar–**H**), 2.29 (s, 6H, Ar_{para}−C**H**$_3$), 2.07 (s, 6H, Ar_{ortho}−C**H**$_3$), 2.07 (s, 6H, Ar_{ortho}−C**H**$_3$), 1.95 (s, 6 H, N=C–C**H$_3$**), 1.84 (s, 3H, O–C–C**H$_3$**), 0.53 (br, 9H, Pt–C**H$_3$**). ^{1}H NMR of **14** (dichloromethane-d_2, 500 MHz, 268 K) δ 6.95 (s, 2H, Ar–**H**), 6.91 (s, 2H, Ar–**H**), 2.28 (s, 6H), 2.05 (s, 6H), 2.04 (s, 6H), 1.94 (s, 6 H, N=C–C**H$_3$**), 1.85 (s, 3H, O–C–C**H$_3$**), 0.58 (s, 6H, $^2J_{Pt–H}$ = 75 Hz, Pt–C**H$_3$**), 0.12 (s, 3H, $^2J_{Pt–H}$ = 71 Hz, Pt–C**H$_3$**). ^{13}C NMR of **14** (dichloromethane-d_2, 201 MHz, 298 K) δ 190.8 (N=**C**), 140.8 (N–**C**$_{aryl}$), 135.6 (**C**$_{Ar\text{-}para}$), 130.4 (**C**$_{Ar\text{-}ortho}$), 129.5 (**C**$_{Ar\text{-}meta}$), 129.2 (**C**$_{Ar\text{-}meta}$), 129.1 (**C**$_{Ar\text{-}ortho}$), 94.6 (O–**C**), 27.2 (O–C–**C**H$_3$), 20.8 (Ar_{para}–**C**H$_3$), 20.7 (N=C–**C**H$_3$), 19.9 (Ar_{ortho}–**C**H$_3$), 18.2 (Ar_{ortho}–**C**H$_3$).[30]

Generation of 14 using CO

A solution of **11** in dichloromethane-d_2 was prepared as above and then pressurized with 3 atm of CO. Within four hours, **14** was observed in >90% yield (integration of ^{1}H NMR spectrum relative to 1,3,5-trimethoxy benzene).

Crystallographic characterization of 9

A colorless prism, measuring 0.22 x 0.05 x 0.03 mm^3 was mounted on a glass capillary with oil. Data was collected at −163 °C on a Bruker APEX II single crystal X-ray diffractometer, Mo-radiation. The crystal-to-detector distance was 40 mm and the exposure time was 20 seconds per degree for all sets. The scan width was 0.5°. Data collection was 100% complete to 25° in ϑ. A total of 122416 (merged) reflections were collected covering the indices, h = –15 to 15, k = –18 to 18, l = –32 to 31. 19150 reflections were symmetry independent and the R_{int} = 0.0587 indicated that the data was of average quality. Indexing and unit cell refinement indicated a triclinic P lattice. The space group was found to be P $\bar{1}$ (No.2). The data was integrated and scaled using SAINT, SADABS within the APEX2 software package by Bruker.[31] Solution by direct methods (SHELXS, SIR97[32]) produced a complete heavy atom phasing model consistent with the proposed structure. The structure was completed by difference Fourier synthesis with SHELXL97.[33,34] Scattering factors are from Waasmair and Kirfel.[35] Hydrogen atoms were placed in geometrically idealized positions and constrained to ride on their parent atoms with C–H distances in the range 0.95 - 1.00 Å. Isotropic thermal parameters U_{eq} were fixed such that they were 1.2U_{eq} of their parent atom U_{eq} for CH's and 1.5U_{eq} of their parent atom U_{eq} in case of methyl groups. All non-hydrogen atoms were refined anisotropically by full-matrix least-squares.

One disordered toluene molecule, was found. Further disorder required some restraints to be applied for ensuring convergence of the refinement of thermal parameters of the disordered moieties. Structural parameters are reported in Table 2.1.

Table 2.1. Crystallographic data for **9**.

Parameter	**9**
Empirical formula	$C_{83}H_{128}N_4Pt_2$
Formula weight	1572.07
Temperature	110(2) K
Wavelength	0.71073 Å
Crystal system	Triclinic
Space group	P -1
Unit cell dimensions	a = 9.264(5) Å α= 89.109(5)° b = 11.244(5) Å β= 78.762(5)° c = 19.100(5) Å γ = 76.840(5)°
Volume	1899.3(14) $Å^3$
Z	1
Density (calculated)	1.374 Mg/m^3
Absorption coefficient	3.723 mm^{-1}
F(000)	810
Crystal size	0.22 x 0.05 x 0.03 mm^3
Theta range for data collection	1.86 to 37.37°
Index ranges	$-15 \leq h \leq 15$, $-18 \leq k \leq 18$, $-32 \leq l \leq 31$
Reflections collected	122416
Independent reflections	19150 [R(int) = 0.0587]
Completeness to theta = 25.00°	100.0 %
Absorption correction	Semi-empirical from equivalents
Max. and min. transmission	0.8965 and 0.4947
Refinement method	Full-matrix least-squares on F^2
Data / restraints / parameters	19150 / 162 / 559
Goodness-of-fit on F^2	1.025
Final R indices [I>2sigma(I)]	R1 = 0.0283, wR2 = 0.0542
R indices (all data)	R1 = 0.0400, wR2 = 0.0579
Largest diff. peak and hole	1.222 and -1.860 e.$Å^{-3}$

Crystallographic details for compound 10

A colorless prism, measuring 0.24 x 0.20 x 0.18 mm^3 was mounted on a glass capillary with oil. Data was collected at –143 °C on a Nonius Kappa CCD FR590 single crystal X-ray diffractometer, Mo-radiation. Crystal-to-detector distance was 30 mm and exposure time was 35 seconds per degree for all sets. The scan width was 2^o. Data collection was 92.9% complete to 28.25^o and 99.3% complete to 25° in ϑ. A total of 62342 partial and complete reflections were collected covering the indices, h = –13 to 15, k = –15 to 18, l = –20 to 19. 10886 reflections were symmetry independent and the R_{int} = 0.0951 indicated that the data was of a little less than average quality (0.07). Indexing and unit cell refinement indicated a triclinic P lattice. The space group was found to be P $\bar{1}$ (No.2). The data was integrated and scaled using hkl-SCALEPACK.[36] This program applies a multiplicative correction factor (S) to the observed intensities (I) and has the following form:

$$S = (e^{-2B(\sin^2\theta)/\lambda^2})/\text{scale}$$

S is calculated from the scale and the B factor determined for each frame and is then applied to I to give the corrected intensity (I_{corr}). Solution by direct methods (SHELXS, SIR97[32], DIRDIF[37]) produced a complete heavy atom phasing model consistent with the proposed structure. The structure was completed by difference Fourier synthesis with SHELXL97.[33,34] Scattering factors are from Waasmair and Kirfel.[35]All hydrogen atoms were located using a riding model. All non-hydrogen atoms were refined anisotropically by full-matrix least-squares. 3.5 deuterated benzene rings accompany the complex. C18-C20 of one of the terminal *t*-butyl groups is rotating and refined with a disorder model. Structural parameters are shown in Table 2.2.

Table 2.2. Crystallographic data for **10.**

parameter	**10**
Empirical Formula	$C_{32}H_{50}N_2O_2Pt$, 3.5(C_6 D_6)'
Formula Weight	984.33
Temperature K	130(2)
Wavelength Å	0.71073
Color and habit	colorless prism
Crystal System, space group	Triclinic, $P\bar{1}$ (No. 2)
Unit Cell Dimensions	a = 12.0695(9)Å, α = 80.727(3)° b = 13.6977(11)Å, β = 84.903(3)° c = 15.1780(16)Å, γ = 72.956(7)°
Volume	2365.4(4) $Å^3$
Density	1.382 Mg/m^3
Absorption coefficient	3.006 mm^{-1}
F(000)	994
theta range for data collection	2.18° to 25.75°
Index ranges	$-13 \leq h \leq 15$, $-15 \leq k \leq 18$, $-20 \leq l \leq 19$
Reflections Collected/Unique	20342 / 12420
Rint / Rσ	0.0951 / 0.2105
ϑm / completeness	25° / 99.3%
R1, wR2, [I>2σ(I)]	0.0565, 0.0920
R1, wR2, (all data)	0.1242, 0.1085
Absorption correction	Semi-empirical from equivalents
Max. and min. transmission	0.6137 and 0.5323
Refinement method	Full-matrix least-squares on F^2
Data / restraints / parameters	10886 / 0 / 535
Goodness-of-fit on F^2	0.905

Crystallographic details for compound 11

A yellow prism, measuring 0.19 x 0.15 x 0.10 mm^3 was mounted on a loop with oil. Data was collected at –163 °C on a Bruker APEX II single crystal X-ray diffractometer, Mo-radiation. Crystal-to-detector distance was 40 mm and exposure time was 10 seconds per frame for all sets.

The scan width was 0.5°. Data collection was 100% complete to 25° in ϑ. A total of 99922 reflections were collected covering the indices, h = –27 to 27, k = –15 to 15, l = –28 to 27. 3365 reflections were symmetry independent and the R_{int} = 0.0375 indicated that the data was brilliant average (quality 0.07). Indexing and unit cell refinement indicated a C-centered orthorhombic lattice. The space group was found to be *Cmca* (No.64). The data was integrated and scaled using SAINT, SADABS within the APEX2 software package by Bruker.[31] Solution by direct methods (SHELXS, SIR97[32]) produced a complete heavy atom phasing model consistent with the proposed structure. The structure was completed by difference Fourier synthesis with SHELXL97.[33,34] Scattering factors are from Waasmair and Kirfel.[35] Hydrogen atoms were placed in geometrically idealized positions and constrained to ride on their parent atoms with C–H distances in the range 0.95 - 1.00 Å. Isotropic thermal parameters U_{eq} were fixed such that they were 1.2U_{eq} of their parent atom U_{eq} for CH's and 1.5U_{eq} of their parent atom U_{eq} in case of methyl groups. All non-hydrogen atoms were refined anisotropically by full-matrix least-squares. Structural parameters are reported in Table 2.3.

Table 2.3. Crystallographic data for **11**.

Parameter	**11**
Empirical formula	$C_{27}H_{40}N_2O_2Pt$
Formula weight	619.70
Temperature	110(2) K
Wavelength	0.71073 Å
Crystal system	Orthorhombic
Space group	C m c a
Unit cell dimensions	a = 20.498(3) Å α= 90° b = 11.969(3) Å β= 90° c = 21.056(4) Å γ = 90°
Volume	5166.2(16) $Å^3$
Z	8
Density (calculated)	1.593 Mg/m^3
Absorption coefficient	5.457 mm^{-1}
F(000)	2480
Crystal size	0.19 x 0.15 x 0.10 mm^3
Theta range for data collection	1.93 to 28.63°
Index ranges	$-27 \leq h \leq 27, -15 \leq k \leq 15, -28 \leq l \leq 27$
Reflections collected	99922
Independent reflections	3365 [R(int) = 0.0375]
Completeness to theta = 25.00°	100.0 %
Max. and min. transmission	0.6114 and 0.4237
Refinement method	Full-matrix least-squares on F^2
Data / restraints / parameters	3365 / 0 / 159
Goodness-of-fit on F^2	1.101
Final R indices [I>2sigma(I)]	R1 = 0.0171, wR2 = 0.0384
R indices (all data)	R1 = 0.0192, wR2 = 0.0390
Largest diff. peak and hole	1.440 and -1.098 e.$Å^{-3}$

Crystallographic details for compound 12

From a batch of colorless material was taken one leg of a cross like twin, measuring 0.15 x 0.07 x 0.04 mm^3 which was mounted on a loop with oil. Data was collected at –173°C on a Bruker

APEX II single crystal X-ray diffractometer, Mo-radiation. Crystal-to-detector distance was 40 mm and exposure time was 20 seconds per degree for all sets. The scan width was 0.5°. Data collection was 100% complete to 25° in ϑ. The sample (Figure 2.15) clearly showed concave interceptions on its edges which are typical signs of twinning. Additionally, twinning was investigated by birefringence and optical eigenray directions across the sample, indicating that the rotation axis may be almost parallel to the twin rotation axis (negligible extinction angle difference between twin components).

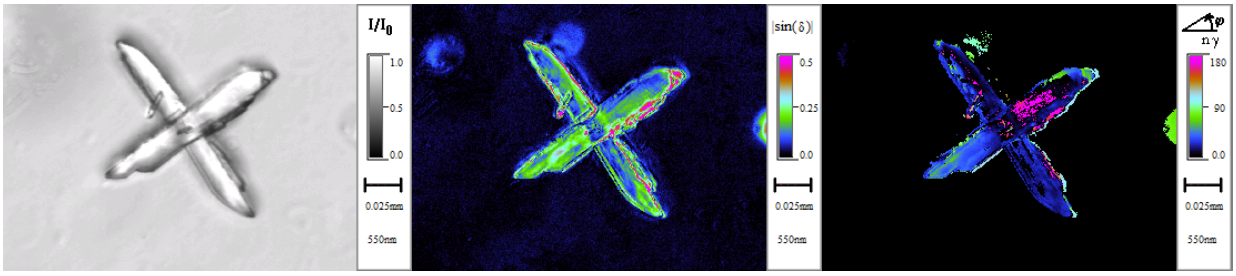

Figure 2.15. Crystal with signs of twinning, seen in (from left to right) transmission, birefringence, and extinction.[38]

The raw data still appeared twinned to some extent. With CELL_NOW[39] a 180° twin operation about (0 0 1) was found which, if unresolved, would have caused overlapping diffraction peak intensities from different domains of the sample. Multi-domain integration with SAINT within the APEX2 software package by Bruker[31] and absorption correction with twinabs[40] removed the remaining overlap. A total of 77780 reflections were collected with 8536 symmetry independent reflections covering the indices, h = –12 to 12, k = –14 to 11, l = 0 to 23 with R_{int} = 0.1049 (all data) indicated that the twin-refined data was acceptable (average quality 0.07). Indexing and unit cell refinement indicated then a triclinic P lattice. The space group was found to be $P\bar{1}$ (No.2).

Solution by direct methods (SHELXS, SIR97[32]) produced a complete heavy atom phasing model consistent with the proposed structure. The structure was completed by difference Fourier synthesis with SHELXL97.[33,34] Scattering factors are from Waasmair and Kirfel.[35] Hydrogen atoms were placed in geometrically idealized positions and constrained to ride on their parent atoms with C–H distances in the range 0.95–1.00 Å. Isotropic thermal parameters U_{eq} were fixed such that they were $1.2U_{eq}$ of their parent atom U_{eq} for CH's and $1.5U_{eq}$ of their parent atom U_{eq} in case of methyl groups. All non-hydrogen atoms were refined anisotropically by full-matrix least-squares. The structure shows two independent molecules in the asymmetric unit. Structural parameters are reported in Table 2.4.

Table 2.4. Crystallographic data for **12**.

Parameter	**12**
Empirical formula	$C_{20}H_{32}N_2O_2Pt$
Formula weight	527.57
Temperature	100(2) K
Wavelength	0.71073 Å
Crystal system	Triclinic
Space group	$P\bar{1}$
Unit cell dimensions	a = 9.7826(19) Å α= 91.239(9)° b = 11.383(2) Å β= 91.586(8)° c = 18.509(4) Å γ = 90.924(10)°
Volume	2059.4(7) $Å^3$
Z	4
Density (calculated)	1.702 Mg/m^3
Absorption coefficient	6.828 mm^{-1}
F(000)	1040
Crystal size	0.07 x 0.05 x 0.01 mm^3
Theta range for data collection	1.79 to 26.37°
Index ranges	$-12 \leq h \leq 12, -14 \leq k \leq 14, 0 \leq l \leq 23$
Reflections collected	77780
Independent reflections	8536 [R(int) = 0.1049]
Completeness to theta = 25.00°	100.0 %
Max. and min. transmission	0.9349 and 0.6465
Refinement method	Full-matrix least-squares on F^2
Data / restraints / parameters	8536 / 0 / 471
Goodness-of-fit on F^2	1.026
Final R indices [I>2sigma(I)]	R1 = 0.0456, wR2 = 0.0705
R indices (all data)	R1 = 0.0699, wR2 = 0.0776
Largest diff. peak and hole	1.741 and −1.202 $e.Å^{-3}$

Crystallographic details for compound 13

A yellow piece, measuring 0.19 x 0.10 x 0.05 mm^3 was mounted on a glass capillary with oil. Data was collected at –143^{o}C on a Nonius Kappa CCD FR590 single crystal X-ray diffractometer, Mo-radiation. Crystal-to-detector distance was 30 mm and exposure time was 20

seconds per degree for all sets. The scan width was 2°. Data collection was 92.8% complete to 24.71° in ϑ. A total of 71296 partial and complete reflections were collected covering the indices, h = –12 to 12, k = –11 to 13, l = –20 to 21. 10053 reflections were symmetry independent and the R_{int} = 0.0815 indicated that the data was of average quality. Indexing and unit cell refinement indicated a triclinic lattice. The space group was found to be P $\bar{1}$ (No.2). The data was integrated and scaled using hkl-SCALEPACK.[36] This program applies a multiplicative correction factor (S) to the observed intensities (I) and has the following form:

$$S = (e^{-2B(\sin^2\theta)/\lambda^2}) / \text{scale}$$

S is calculated from the scale and the B factor determined for each frame and is then applied to I to give the corrected intensity (I_{corr}). Solution by direct methods (SHELXS, SIR97[32]) produced a complete heavy atom phasing model consistent with the proposed structure. The structure was completed by difference Fourier synthesis with SHELXL97.[33,34] Scattering factors are from Waasmair and Kirfel.[35] Hydrogen atoms were placed in geometrically idealized positions and constrained to ride on their parent atoms with C–H distances in the range 0.95 - 1.00 Å. Isotropic thermal parameters U_{eq} were fixed such that they were $1.2U_{eq}$ of their parent atom U_{eq} for CH's and $1.5U_{eq}$ of their parent atom U_{eq} in case of methyl groups. All non-hydrogen atoms were refined anisotropically by full-matrix least-squares. Structural parameters are reported in Table 2.5.

Table 2.5. Crystallographic data for **13**.

Parameter	**13**
Empirical formula	$C_{40}H_{64}N_4O_2Pt_2$
Formula weight	1023.13
Temperature	130(2) K
Wavelength	0.71073 Å
Crystal system	Triclinic
Space group	$P\ \bar{1}$
Unit cell dimensions	a = 11.0170(5) Å α= 73.939(2)° b = 11.1590(6) Å β= 82.311(2)° c = 17.9080(11) Å γ = 87.392(4)°
Volume	2096.5(2) $Å^3$
Z	2
Density (calculated)	1.621 Mg/m^3
Absorption coefficient	6.701 mm^{-1}
F(000)	1008
Crystal size	0.19 x 0.10 x 0.05 mm^3
Theta range for data collection	3.02 to 24.71°
Index ranges	$-12 \leq h \leq 12, -11 \leq k \leq 13, -20 \leq l \leq 21$
Reflections collected	10053
Independent reflections	6616 [R(int) = 0.0815]
Completeness to theta = 24.71°	92.8 %
Max. and min. transmission	0.7305 and 0.3625
Refinement method	Full-matrix least-squares on F^2
Data / restraints / parameters	6616 / 0 / 452
Goodness-of-fit on F^2	0.923
Final R indices [I>2sigma(I)]	R1 = 0.0552, wR2 = 0.1032
R indices (all data)	R1 = 0.1265, wR2 = 0.1269
Extinction coefficient	0.00041(19)
Largest diff. peak and hole	0.941 and -1.112 $e.Å^{-3}$

Crystallographic details for compound 14

A colorless piece, measuring 0.09 x 0.05 x 0.02 mm^3 was mounted on a loop with oil. Data was collected at –133^oC on a Bruker APEX II single crystal X-ray diffractometer, Mo-radiation. Crystal-to-detector distance was 40 mm and exposure time was 10 seconds per frame for all sets. The scan width was 0.5°. Data collection was 96.2% complete to 25° in ϑ. A total of 42182 reflections were collected covering the indices, h = –26 to 26, k = –10 to 10, l = –17 to 17. 5036 reflections were symmetry independent and the R_{int} = 0.08977 indicated that the data was of slightly less than average quality (0.07). Indexing and unit cell refinement indicated a primitive monoclinic lattice. The space group was found to be P $2_1/c$ (No.14). The data was integrated and scaled using SAINT, SADABS within the APEX2 software package by Bruker.[31] Solution by direct methods (SHELXS, SIR97[32]) produced a complete heavy atom phasing model consistent with the proposed structure. The structure was completed by difference Fourier synthesis with SHELXL97.[33,34] Scattering factors are from Waasmair and Kirfel.[35] Hydrogen atoms were placed in geometrically idealized positions and constrained to ride on their parent atoms with C–H distances in the range 0.95 - 1.00 Å. Isotropic thermal parameters U_{eq} were fixed such that they were 1.2U_{eq} of their parent atom U_{eq} for CH's and 1.5U_{eq} of their parent atom U_{eq} in case of methyl groups. All non-hydrogen atoms were refined anisotropically by full-matrix least-squares. The structure exhibited a pseudo symmetry obscuring the true space group. This could be coincident or twinning, however, no twin-law was found by the software packages PLATON or CellNow. The pentane appears to be disordered. Structural parameters are reported in Table 2.6.

Table 2.6. Crystallographic data for **14**.

Parameter	**14**
Empirical formula	$C_{59}H_{92}N_4O_2Pt_2$
Formula weight	1279.55
Temperature	140(2) K
Wavelength	0.71073 Å
Crystal system	Monoclinic
Space group	P 2_1/c
Unit cell dimensions	a = 22.313(4) Å α= 90° b = 8.9467(16) Å β= 91.256(9)° c = 14.309(2) Å γ = 90°
Volume	2855.9(8) $Å^3$
Z	2
Density (calculated)	1.488 Mg/m^3
Absorption coefficient	4.936 mm^{-1}
F(000)	1292
Crystal size	0.09 x 0.05 x 0.02 mm^3
Theta range for data collection	2.69 to 25.35°
Index ranges	$-26 \leq h \leq 26$, $-10 \leq k \leq 10$, $-17 \leq l \leq 17$
Reflections collected	42182
Independent reflections	5036 [R(int) = 0.0977]
Completeness to theta = 25.00°	96.2 %
Max. and min. transmission	0.9077 and 0.6650
Refinement method	Full-matrix least-squares on F^3
Data / restraints / parameters	5036 / 44 / 310
Goodness-of-fit on F^2	1.178
Final R indices [I>2sigma(I)]	R1 = 0.0926, wR2 = 0.1517
R indices (all data)	R1 = 0.1400, wR2 = 0.1705
Largest diff. peak and hole	2.030 and -1.587 $e.Å^{-3}$

Coauthor contributions

Avery T. Luedtke performed initial experiments involving complexes **3** and **12**, and grew the crystals of **13**. Investigations of complex **4a** were conducted by Susan K. Hanson. Preliminary

observations of complexes **5** and **10** were made by Ulrich Fekl. Collection of crystallographic data and solutions of the structures were completed by Werner Kaminsky assisted by Thomas R. Porter and Jason B. Benedict.

Notes to chapter 2

(1) Grice, K. A.; Scheuermann, M. L.; Goldberg, K. I. *Top. Organomet. Chem.* **2011**, *35*, 1.

(2) (a) Zhao, S.-B.; Cui, Q.; Wang, S. *Organometallics* **2010**, *29*, 998. (b) West, N. M.; White, P. S.; Templeton, J. L.; Nixon, J. F. *Organometallics* **2009**, *28*, 1425. (c) McBee, J. L.; Tilley, T. D. *Organometallics* **2009**, *28*, 3947. (d) Sangtrirutnugul, P.; Tilley, T. D. *Organometallics* **2008**, *27*, 2223. (e) Zhao, S.-B.; Wu, G.; Wang, S. *Organometallics* **2008**, *27*, 1030. (f) Luedtke, A. T.; Goldberg, K. I. *Angew. Chem., Int. Ed.* **2008**, *47*, 7694. (g) Karshtedt, D.; McBee, J. L.; Bell, A. T.; Tilley, T. D. *Organometallics* **2006**, *25*, 1801. (h) Fekl, U.; Kaminsky, W.; Goldberg, K. I. *J. Am. Chem. Soc*. **2001**, *123*, 6423. (i) Reinartz, S.; White, P. S.; Brookhart, M.; Templeton, J. L. *J. Am. Chem. Soc.* **2001**, *123*, 6425.

(3) Fekl, U.; Kaminsky, W.; Goldberg, K. I. *J. Am. Chem. Soc.* **2003**, *125*, 15286.

(4) Luedtke, A. T.; Goldberg, K. I. *Inorg. Chem*. **2007**, *46*, 8496.

(5) Kloek, S. M.; Goldberg, K. I. *J. Am. Chem. Soc*. **2007**, *129*, 3460.

(6) Scheuermann, M. L.; Luedtke, A. T.; Hanson, S. K.; Fekl, U.; Kaminsky, W.; Goldberg, K. I. *Organometallics* **2013**, in press.

(7) Fekl, U. unpublished results.

(8) Hanson, S. K. PhD. Dissertation, University of Washington, 2007.

(9) Luedtke, A. T. PhD. Dissertation, University of Washington, 2007.

(10) Scheuermann, M. L.; Fekl, U.; Kaminsky, W.; Goldberg, K. I. *Organometallics* **2010**, *29*, 4749.

(11) Hill, G. S.; Puddephatt, R. J. *J. Am. Chem. Soc*. **1996**, *118*, 8745.

(12) Silverstein, R. M.; Bassler, G. C.; Morrill, T. C. *Spectrometric Identification of Organic Compounds,* 5th ed.; John Wiley & Sons, Inc.: New York, 1991.

(13) Persistence of Vision Ray-Tracer (POV-Ray), available at http://www.povray.org/.

(14) ORTEP plots were created using Ortep-3 for Windows. See: Farrugia, L. J. *J. Appl. Crystallogr.* **1997**, *30*, 565.

(15) Zhang, F.; Broczkowski, M. E.; Jennings, M. C.; Puddephatt, R. J. *Can. J. Chem.* **2005**, *83*, 595.

(16) Rodriguez, M. M.; Bill, E.; Brennessel, W. W.; Holland, P. L. *Science* **2011**, *334*, 780.

(17) Bleeke, J. R.; Xie, Y.-F.; Bass, L.; Chiang, M. Y. *J. Am. Chem. Soc.* **1991**, *113*, 4703.

(18) For example see: (a) Yao, S.; van Wüllen, C.; Driess, M. *Chem. Commun.* **2008**, 5393. (b) Phillips, A. D.; Laurenczy, G.; Scopelliti, R.; Dyson, P. J. *Organometallics* **2007**, *26*, 1120. (c) Gregory, E. A.; Lachicotte, R. J.; Holland, P. L. *Organometallics* **2005**, *24*, 1803. (d) Basuli, F.; Huffman, J. C.; Mindiola, D. J. *Inorg. Chem.* **2003**, *42*, 8003. (e) Carey, D. T.; Cope-Eatough, E. K.;Vilaplana-Mafé, E.; Mair, F. S.; Pritchard, R. G.; Warren, J. E.; Woods, R. J. *Dalton Trans.* **2003**, 1083. (f) Radzewich, C. E.; Coles, M. P.; Jordan, R. F. *J. Am. Chem. Soc.* **1998**, *120*, 9384.

(19) Yokota, S.; Tachi, Y.; Itoh, S. *Inorg. Chem.* **2002**, *41*, 1342.

(20) Weiss, M. C.; Goedken, V. L. *J. Am. Chem. Soc.* **1976**, *98*, 3389.

(21) For reviews on β-diketiminate chemistry see: (a) Zhu, D.; Budzelaar, P. H, M. *Dalton Trans.* **2013**, *42*, 11343. (b) Mindiola, D. J. *Angew. Chem., Int. Ed.* **2009**, *48*, 6198. (c) Holland, P. L. *Acc. Chem. Res.* **2008**, *41*, 905. (d) Roesky, H. W.; Singh, S.; Jancik, V.; Chandrasekhar, V. *Acc. Chem. Res.* **2004**, *37*, 969. (e) Piers, W.; Emslie, D. J. H. *Coord. Chem. Rev.* **2002**, *233-234*, 131. (f) Bourget-Merle, L.; Lappert, M. F.; Severn, J. R. *Chem. Rev.* **2002**, *102*, 3031.

(22) Kamachi, T.; Shestakov, A. F.; Yoshizawa, K. *J. Am. Chem. Soc.* **2004**, *126*, 3672.

(23) Kovaleva, E. G.; Lipscomb, J. D. *Science* **2007**, *316*, 453.

(24) Error margins were estimated by calculating the standard deviation for the average difference between corresponding measurements in the two structures.

(25) Anslyn, E. V.; Dougherty, D. A. *Modern Physical Organic Chemistry*; University Science Books: Sausalito, CA, 2006; pp 116-117.

(26) For recent reviews on other classes of reactions involving metal-ligand cooperation see: (a) Schneider, S.; Meiners, J.; Askevold, B. *Eur. J. Inorg. Chem.* **2012**, 412. (b) Gelman, D.; Musa, S. *ACS Catal.* **2012**, *2*, 2456. (c) Crabtree, R. H. *New J. Chem.* **2011**, *35*, 18. (d) van der Vlugt, J. I.; Reek, J. N. H. *Angew. Chem., Int. Ed.* **2009**, *48*, 8832. (e) Grützmacher, H. *Angew. Chem., Int. Ed.* **2008**, *47*, 1814. (f) Ikariya, T.; Blacker, A. J. *Acc. Chem. Res.* **2007**, *40*, 1300. (g) Grotjahn, D. B. *Chem. Eur. J.* **2005**, *11*, 7146.

(27) Baldwin, J. C.; Kaska, W. C. *Inorg. Chem.* **1979**, 18, 686.

(28) Fulmer, G. R.; Herndon, A. N.; Kaminsky, W.; Kemp, R. A.; Goldberg, K. I. *J. Am. Chem. Soc.* **2011**, 133, 17713. See supporting information for details on the pressurization apparatus used.

(29) The chemical shift of this resonance varies as a function of the sample concentration. The resonance shifts downfield at higher concentrations and the magnitude of this variation is temperature-dependant. Resonances were observed as much as 0.5 ppm downfield of the reported value for N=C–CH and 0.3 ppm downfield for N=C–CH_3. Other resonances do not shift significantly as a function of concentration.

(30) The resonance corresponding to the Pt–Me group was not observed in ^{13}C spectrum recorded at 298 K. It is likely broadened because of the fluxionality of the complex on the NMR timescale.

(31) Bruker (**2007**) APEX2 (Version 2.1-4), SAINT (version 7.34A), SADABS (version 2007/4), BrukerAXS Inc, Madison, Wisconsin, USA.

(32) (a) Altomare, A.; Burla, C.; Camalli M.; Cascarano L.; Giacovazzo C.; Guagliardi A.; Moliterni A.G.G.; Polidori G.; Spagna R. *J. Appl. Cryst.* **1999**, *32*, 115-119; (b) Altomare, A., Cascarano, G., Giacovazzo, C., Guagliardi, A., *J. Appl. Cryst.* **1993**, *26*, 343.

(33) Sheldrick, G. M. SHELXL-97: Program for the Refinement of Crystal Structures 1997 University of Gottingen, Germany.

(34) Mackay, S.; Edwards, C.; Henderson, A.; Gilmore, C.; Stewart, N.; Shankland, K.; Donald, A.; *MaXus: a computer program for the solution and refinement of crystal structures from diffraction data*. University of Glasgow, Scotland, 1997.

(35) Waasmaier, D.; Kirfel, A. *Acta Crystallogr. A.* **1995**, *51*, 416.

(36) Otwinowsky, Z.; Minor, W. In: *Methods in Enzymology*; Carter, C. W., Jr., Sweet, R. M., Eds.; Academic Press: New York, 1997, **276**, 307-326.

(37) Beurskens, P.T.; Admiraal, G.; Beurskens, G.; Bosman, W. P.; Garcia-Granada, S.; Gould, R. O.; Smits, J. M. M; Smykalla, C. (1996) *The DIRDIF96 Program System.* Technical Report of the Crystallography Laboratory, University of Nijmegen, The Netherlands.

(38) (a) Kaminsky, W.; Gunn, E.; Sours, R.; Kahr, B. *J. Microscopy* **2008**, *228*, 153-164. (b) Kaminsky, W.: Real-time linear-birefringence-detecting polarization microscope. April 21st 2009, US Patent 7522278.

(39) Sheldrick, G. M. (2005). CELL_NOW. University of Goettingen, Germany.

(40) Sheldrick, G. M. (2007). TWINABS. University of Goettingen, Germany.

Chapter 3: Oxygen-promoted C–H bond cleavage at Pd

Introduction

There is great interest in using oxygen as an oxidant for organic transformations and the use of transition metal catalysts has emerged as a promising strategy for controlling the selectivity of such reactions.[1–3] Pd-based, oxidase-type catalysts, which employ oxygen as an oxidant and proton acceptor, are widely used to oxidize existing functional groups such as alcohols[4] and olefins.[5] However, to incorporate an oxygen atom into an unfunctionalized C–H bond, oxygenase catalysts, which employ oxygen as both the oxidant and oxygen atom source have shown promise.

Presently the majority of the Pd-oxygenase catalysts capable of C–H functionalization employ oxidants other than molecular oxygen,[6] however some examples in which molecular oxygen serves as the oxidant are known. Benzene and biphenyl have been hydroxylated using O_2, a Pd catalyst, and CO but the yields and selectivities are modest.[7,8] Though not strictly a C−H oxidation, the groups of Loh and Jiang recently developed Pd-catalyzed methods for the oxygenation of alkenes using O_2 as the oxidant and oxygen atom source.[9] Using a catalyst proposed to involve $Pd^{II/III}$, Ritter and coworkers can affect the α-hydroxylation of ketones.[10] Yu and coworkers reported the hydroxylation of substituted benzoic acids using $Pd(OAc)_2$ with air or O_2 as the oxidant and oxygen atom source.[11] Most recently a method to hydroxylate phenyl-pyridine derivatives using a Pd catalyst and NHPI (NHPI = *N*-hydroxy- phthalimide) with the toluene solvent serving as a co-reductant was reported.[12]

In this chapter the stoichiometric reaction of a Pd^0 complex with air or O_2 to generate a Pd^{II} hydroxide dimer is presented. Intermediates are observed that suggest a mechanism involving initial oxidation of the Pd^0 by dioxygen followed by C–H activation and O–H bond formation steps. These observations suggest a previously unexplored mechanism for oxygen-promoted C–H activation at Pd.

Results and discussion

Preparation and characterization of Pd(P(Ar)(*t*Bu)$_2$)$_2$ (Ar = naphthyl)

The bright orange Pd^0 complex Pd(P(Ar)(*t*Bu)$_2$)$_2$ (**15**, Ar = naphthyl) was prepared by reaction of (tmeda)$PdMe_2$[13] (tmeda = N,N,N,N-tetramethylethylenediamine) with two equivalents of di-*tert*-butyl-napthtyl-phosphine[14] in benzene at 60 °C for 18 hours. The ^{31}P NMR spectrum of **15** in benzene-d_6 is unremarkable exhibiting one singlet at 43.5 ppm. The ^{1}H NMR spectrum contains a virtual triplet for the ^{t}Bu groups integrating to 36 protons. Simulation of this resonance suggests a phosphorus-phosphorus coupling constant ($^2J_{P-P}$) of 450 Hz. Caulton reports that J_{PP} values > 250 Hz are typical for trans phosphines.[15] There are seven resonances for the protons of the naphthyl ring each integrating to two protons. Of interest is that one of these naphthyl protons has a chemical shift of 12.2 ppm, significantly different from the other naphthyl protons (7.25 - 8.05 ppm). In contrast, the carbon atom attached to this unusual proton has a chemical shift of 130.8 ppm, a typical value for a carbon atom in an aromatic system and near the middle of the 123.7 - 138.3 ppm range observed for the naphtyl carbons in **15**.

In an effort to better understand this surprising chemical shift, we obtained an X-ray crystal structure of **15** (Figure 3.1). The structure confirms a nearly linear molecule with a P–Pd–P bond angle of 172.615(11)° and P–Pd bond lengths of 2.2973(3) and 2.29173(3) Å. With hydrogen atoms placed at geometrically idealized positions relative to the aromatic carbons, this

structure revealed unusually short distances between the Pd center and the protons on the naphthyl carbons labeled C9 and C19 of approximately 2.30 and 2.33 Å respectively.

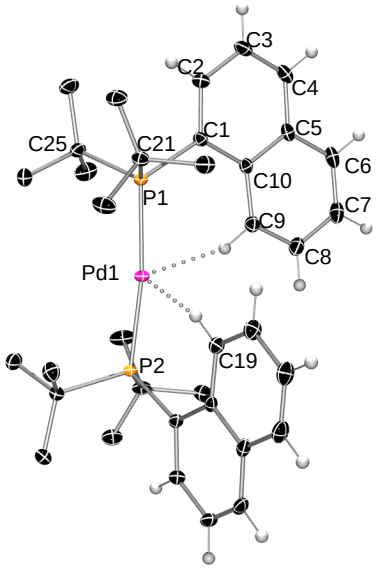

Figure 3.1. POV-Ray rendition of the ORTEP of **15** at the 50% probability level with hydrogen atoms on the *t*Bu groups omitted for clarity.[16,17] Selected bond lengths (A˚) and angles (deg) for **15**: P1−Pd1 = 2.2973(3), C1−P1 = 1.8559(11), P2−Pd1 = 2.2917(3), C21−P1 = 1.8992(12), C25−P1 = 1.8906(12), C7−C8 = 1.4099(18), C8−C9 = 1.3744(16), C9−C10 = 1.4214(16), C6−C7 = 1.3651(19), C5−C6 = 1.4226(17), C4−C5 = 1.4162(17), C3−C4 1.3636(18), C2−C3 = 1.4126(16), C1−C2 = 1.3825(16), P2−Pd1−P1 = 172.615(11), C1−P1−C25 = 103.21(5), C1−P1−C21 = 104.08(5), C25−P1−C21 = 112.02(5), C1−P1−Pd1 = 118.16(4), C25−P1−Pd1 = 109.37(4), C21−P1−Pd1 = 109.83(4).

To further investigate the unusual spectroscopic and crystallographic data, the gas phase structure of **15** was optimized at the DFT level with BP86,[18] and B3LYP[19] functionals. Optimization using the BP86 functional gave Pd---H distances of 2.289 and 2.290 Å and optimization using the B3LYP functional gave Pd---H distances of 2.364 and 2.362 Å. Although these calculated values are not identical to those from the crystal structure, they are in agreement with the Pd atom and a proton from the naphthyl rings being in close proximity. The optimized structures reveal Pd---H−C bond angles of 159.6 and 159.8° for the BP86 and B3LYP optimizations respectively.

Taken together, the unusual chemical shifts, short Pd---H distances, and Pd---H−C bond angles are indicative of what Brookhart, Green, and Parkin refer to as anagostic interactions.[20] These primarily electrostatic interactions are characterized by M---H distances of approximately 2.3 to 2.9 Å, M---H−C bond angles between 110 and 170°, and ^{1}H chemical shifts downfield relative to those of protons not involved in an anagostic interaction.

Reaction of 15 with O_2

Prolonged heating of **15**, in benzene-d_6, with or without added water, results in formation of a Pd "mirror" on the glass reaction vessel and the generation of free phosphine ligand which was observed by ^{1}H and ^{31}P NMR spectroscopies. In contrast, exposure of an arene solution of **15** (approx. 10 - 15 mM) to 1 - 3 atm of air or O_2 at room temperature results in a color change from yellow to orange/brown accompanied by the disappearance of the NMR resonances associated with **15**. In the initial NMR spectra after oxygen addition, ^{1}H and ^{31}P resonances corresponding to one equivalent of free phosphine per starting Pd were observed. Over several days, the free phosphine partially oxidized to the corresponding phosphine oxide (^{31}P NMR 57.7 ppm). Two additional resonances were observed by ^{31}P NMR spectroscopy at 99.6 and 100.5 ppm.

When the reaction was repeated using a saturated suspension of **15**, crystals formed in the reaction mixture. These were crystallographically characterized as trans-[($^{t\mathrm{Bu}2}$PC)PdOH]$_2$ **16a** (Figure 3.2). The Pd atoms, connected by two bridging hydroxides, are in identical, approximately square planar environments. The O1–Pd–(O1) bond angle is 78.30(3)° while the O1–Pd1–P1 angle is 102.19(2)°. Once formed, these crystals have poor solubility in a range of solvents. An isolated yield of 75% was measured and purity for the formula $C_{36}H_{50}O_2P_2Pd_2 \cdot C_6H_6$ was verified by elemental analysis.

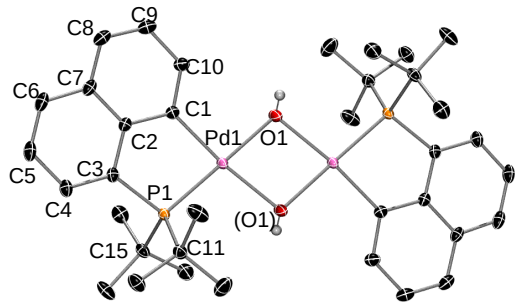

Figure 3.2. POV-Ray rendition of the ORTEP for the growth fragment of **16a** at the 50% probability level with hydrogen atoms (except on OH groups) and co-crystallized benzene-d_6 omitted for clarity.[16,17] Selected bond lengths (Å) and angles (deg) for **16a**: C1−Pd1= 1.9864(9), C3−P1 = 1.8180(9), O1−H1 0.761(18), O1−Pd1= 2.0920(7), O1−Pd1 = 2.1148(7), P1−Pd1 = 2.2191(2), C1−Pd1−O1 95.96(3), O1−Pd1−O1 = 78.30(3), C1−Pd1−P1 = 83.61(3), O1−Pd1−P1 = 102.19(2), C3−P1−Pd1 = 104.48(3), C11−P1−Pd1 = 112.74(3), C15−P1−Pd1 = 111.83(3).

The crystal structure shows a C_2-symmetric complex and on this basis only one ^{31}P NMR resonance is expected. However two signals of unequal intensity but with chemical shifts separated by less than 2 ppm are observed in the ^{31}P NMR spectrum in benzene-d_6 or dichloromethane-d_2. The ^{31}P NMR data suggests that in solution, two similar species are present. The ^{1}H NMR spectrum also suggests the presence of two species in solution. Two *t*Bu resonances are present suggesting cyclometallated phosphine ligands in two different environments. The upfield portion of the spectrum, where M–OH resonances would be expected, contains three resonances that disappear on addition of D_2O.[21] One of these resonances appears at −0.86 ppm (doublet, $^{3}J_{P-H}$ = 2.5 Hz) in benzene-d_6 and integrates as one proton relative to an aryl proton of the major species. ^{1}H{^{31}P} NMR experiments confirm that the observed coupling is to phosphorus. The NMR data suggest that the major species in solution is the C_2-symmetric complex, **16a** which was observed in the solid state. The other two upfield resonances that incorporated deuterium (−2.70 ppm, singlet, and 0.49 ppm, triplet, $^{3}J_{P-H}$ = 2.0 Hz in benzene-d_6) are present in a 1:1 ratio and each integrates to half the intensity of an aromatic proton in the minor species. This data is consistent with the minor species being a dimer having C_{2v} symmetry,

cis-[(^{tBu2}PC)PdOH]$_2$ **16b** (Figure 3.3), an isomer of **16a**. Gas phase DFT calculations carried out on the optimized structures of **16a** and **16b** suggest that the difference in energy between **16a** and **16b** is less than 1 kcal/mol in the absence of solvent interactions. In benzene-d_6 **16a** and **16b** are present in a ratio of approximately 6:1 while in the more polar solvent dichloromethane-d_2, **16a** and **16b** are present in a ratio of approximately 3:1. That different ratios are observed upon dissolution of the same crystalline sample in different solvents suggest that **16a** and **16b** are in equilibrium.

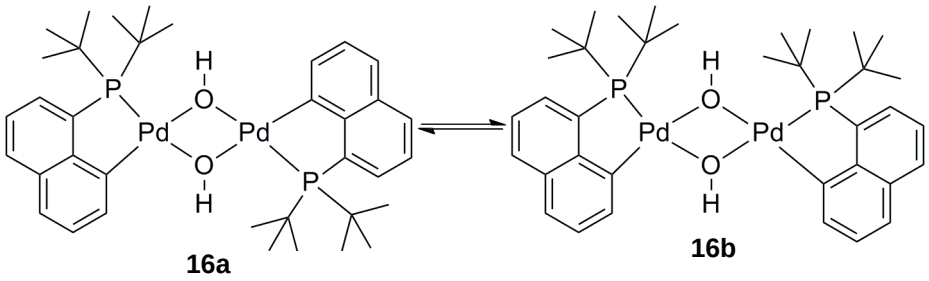

Figure 3.3. Structures of **16a** and its isomer **16b**.

An effort to independently synthesize **16a** also yielded both **16a** and **16b**. Based on literature precedent for related complexes,[22] K_2PdCl_4 was stirred with the free phosphine in methanol resulting in the formation of cis/trans-[(^{tBu2}PC)PdCl]$_2$ which was characterized by ^{1}H NMR.[23] The mixture of cis/trans-[(^{tBu2}PC)PdCl]$_2$ was then treated with tetrabutylammonium hydroxide in acetone yielding **16a** and **16b** in the same ratio as was seen in the reaction of **15** with oxygen.[24] This result again points to an equilibrium between the two structures. If isomers **16a** and **16b** are in equilibrium as the data suggests then their ratio must not be a mechanistic consequence of the reaction involving oxygen.

The reaction of **15** with O_2 to form **16a** and **16b** is surprising since there have been numerous studies of reactions of Pd^0 bis phosphine species with oxygen and none of these reactions involve the cleavage of a C–H bond. In most cases where a product could be identified, the result is the formation of P_2Pd^{II}-η^2peroxo complexes, several of which have been

characterized crystallographically.[25-30] Similar reactivity has also been seen with Pd^0 species bearing carbene, nitrogen-based ligands, or mixed ligands. The mechanism for the binding of dioxygen to Pd^0 centers has been investigated computationally and is thought to involve an η^1-superoxo complex as an intermediate.[31,32] Despite the limited thermal stability of many of these Pd^{II}-η^2-peroxo complexes, to our knowledge there have been no reports describing the formation of further metal-containing species in the absence of added reagents. While Pd^{II}-peroxo complexes are the most commonly reported products of reactions between Pd^0 complexes and O_2, in one instance, a Pd^{II}-bis superoxo complex was characterized upon addition of O_2 to $(IPr)_2Pd$ (IPr =1,3-bis(diisopropyl)phenylimidazol-2-yli-dene), but again no C–H activation was observed.[33]

Characterization of two intermediates at low temperature

In an effort to better understand the formation of **16a** and **16b** from **15**, and to learn how oxygen might be involved in the promotion of C–H activation, we studied the reaction of **15** with O_2 at low temperature. Oxygen was added to a solution of **15** in toluene-d_8 cooled in a dry ice/isopropanol bath and the sample was inserted into an NMR probe that was precooled to −80 °C. At −80 °C. Signals assignable to a minor (**A**) and a major species (**B**) were observed. Upon warming the sample to −60 °C the resonances for **A** disappeared and a single species, **B**, was present in a yield of > 80 % (^{1}H NMR integration versus 1,3,5-trimethoxybenzene internal standard). The ^{31}P NMR spectrum of **B** consists of two sets of doublets at 103.5 ppm and 55.2 ppm. A ^{31}P COSY experiment confirmed that the doublets arise from phosphorus-phosphorus coupling and a coupling constant of 20 Hz was measured. This coupling constant is consistent with two inequivalent phosphorus atoms bound to the same palladium atom but not trans to one another.[15]

The chemical shift of metal bound phosphines is strongly correlated with ring size and the metal–phosphorus–R group angle.[34] It has been noted that a phosphine in a six membered metallacycle will shift approximately 14 ppm upfield relative to an electronically similar phosphine that is not part of a metallacycle. In contrast, a phosphine in a five-membered metallacycle with its smaller metal-phosphine-R group angle will typically shift approximately 33 ppm downfield. In the context of this system, in the starting material, the phosphine is effectively in a six membered ring as a consequence of the anagostic C−H interaction with the metal center. In the cyclometalated product however the phosphines are in five-membered palladacycles. The 48.3 ppm difference in chemical shift between these two resonances would be consistent with a structure in which the phosphorus corresponding to the resonance at 55.2 ppm retains the anagostic interaction observed in the starting material, while for the phosphine resonating at 103.5 ppm the phosphorus has acquired some of the geometric parameters of the cyclometalated phosphine in **16a** and **16b**.

Much of the ^{1}H NMR spectrum is obscured by the toluene solvent residual, however two resonances at 11.21 and 4.9 ppm are of note. A COSY spectrum revealed that these protons, which have unusual chemical shifts for aromatic protons, couple to other aromatic protons. Thus these protons are still a part of the aromatic system. From an HMQC experiment at −40 °C, ^{13}C chemical shifts for the carbons bound to these protons were found to be 129.5 and 122.0 ppm. These chemical shifts in the typical region for aryl carbons argue against an agostic interaction between a C–H bond and the metal center as an explanation for the unusually upfield proton shift.

The reaction of **15** with oxygen was also studied in THF-d_8 at low temperature. Although the reaction of **15** with oxygen to generate **16a** and **16b** is significantly less clean in THF-d_8 than

in arene solvents, it appears that intermediates **A** and **B** still form in THF-d_8. The ^{1}H NMR spectrum of intermediate **B** in THF-d_8 allows for the identification of 14 distinct aromatic protons. The observation of resonances integrating to 14 protons confirms that in intermediate **B** the C−H activation and cyclometalation of the phosphine naphthyl group has not yet occurred. Exposure of a solution of intermediate **B** at −78 °C to vacuum for two minutes did not result in a back reaction suggesting that under these conditions the formation of intermediate **B** is irreversible.

When pentane was added to a THF or toluene solution of intermediate **B** at −78 °C, a yellow precipitate was obtained. A rapid color change from yellow to orange-brown indicates the instability of intermediate **B** in solution at room temperature, however in the solid state no such color change occurred on warming to room temperature. A cold suspension of intermediate **B** was added to a salt plate, the solvent was quickly removed under a stream of nitrogen gas followed by exposure to vacuum, and an IR spectrum was recorded. A $\upsilon_{^{16}O-^{16}O}$ was observed at 924 cm^{-1} (Figure 3.4). If **B** was prepared in the presence of $^{18}O_2$ a peak corresponding to $\upsilon_{^{18}O-^{18}O}$ was observed at 874 cm^{-1}. This shift of 50 cm^{-1} is similar to the 47 cm^{-1} observed in a bis carbene Pd^{II}-η^2 peroxo complex,[31a] and to the 52 cm^{-1} predicted by treating the O−O vibration as a simple diatomic.[31a]

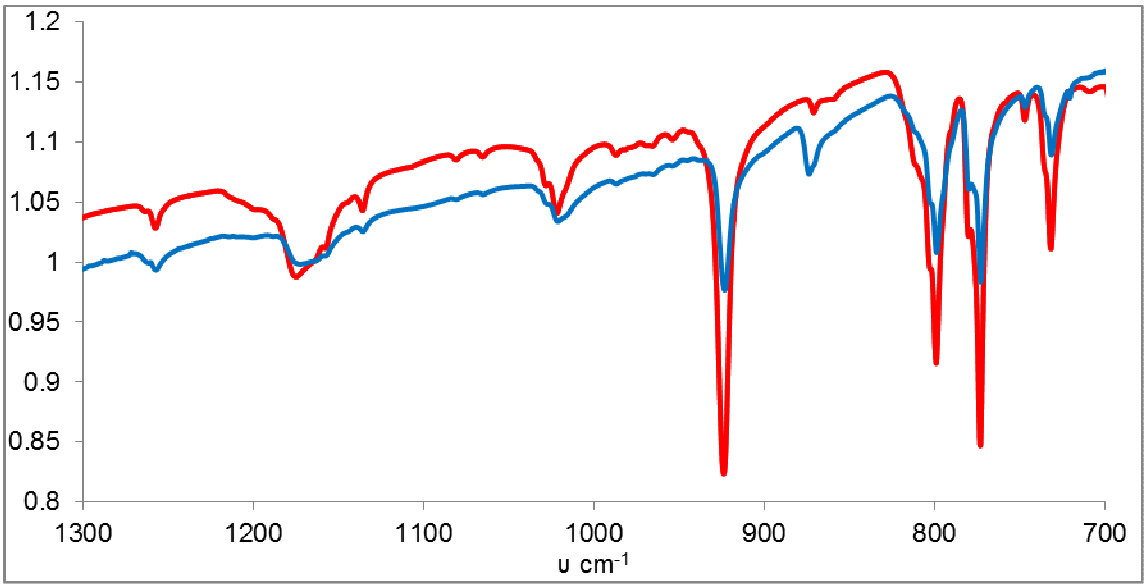

Figure 3.4. IR spectra of intermediate **B**. Red $^{16}O_2$, Blue $^{18}O_2$ then $^{16}O_2$.

Together the data suggest that intermediate **B** is a bis phosphine Pd^{II}-peroxo complex. Unfortunately a crystal of intermediate **B** was not obtained. Semi-empirical PM6 calculations were used to explore potential geometries for this sterically encumbered Pd complex.[35,36] The most promising of these structures was then optimized at the DFT level using the BP86 functional[18] (Figure 3.5). Consistent with the experimental data this structure has two inequivalent phosphine ligands. In one of these phosphines, the naphthyl group is not in close proximity to the bound O_2 fragment. For this phosphine, the Pd−P−C_{naphth} angle is 121.6°, in close agreement with the value of 120.5° for this same measurement in **15**. This phosphine would likely correspond with the ^{31}P NMR resonance observed at 55 ppm. The corresponding Pd---H_{napth} distance is 2.596 Å, longer than the 2.289 Å in **15** but still a relatively close contact perhaps accounting for the downfield resonance in the ^{1}H NMR spectrum at 11.21 ppm in toluene-d_8. As in compound **15** the geometry and NMR chemical shifts are consistent with an anagostic interaction. For the other phosphine, the naphthyl group is located in close proximity to the O_2 fragment. In this second phosphine the Pd−P−C_{naphth} angle is only 113.5° while the same

measurement in **16a** is 103.5°. Although this contraction is not as dramatic as in **16a**, it may be sufficient to account for the ^{31}P NMR resonance observed at 103 ppm. The Pd---H_{napth} distance was calculated to be 2.304 Å while the O---H_{napth} distance is 2.583 Å. It is plausible to suggest that this aromatic proton in relatively close proximity to an oxygen atom is responsible for the ^{1}H NMR resonance at 4.90 ppm. Finally the O−O bond length of 1.387 Å and the Pd−O bond lengths of 2.100 and 2.075 Å are consistent with the description of a Pd^{II}-peroxo complex.[25-30]

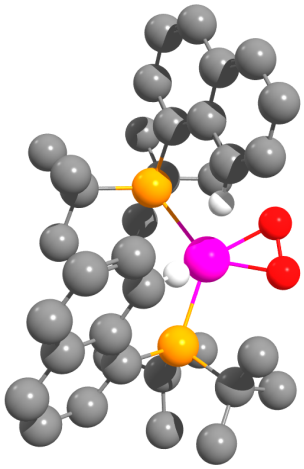

Figure 3.5. Proposed structure for intermediate **B**.

At temperatures above −30 °C, the resonances corresponding to intermediate **B** rapidly disappeared and approximately one equivalent of free phosphine (per starting Pd) was observed by ^{1}H and ^{31}P NMR. No Pd species could be identified in the NMR spectra, however by EPR spectroscopy, several overlapping signals appeared to grow in on approximately the same timescale which intermediate **B** disappears. These EPR signals then lose intensity on approximately the same timescale that **16a** and **16b** appear suggesting that paramagnetic species may be involved as intermediates between intermediate **B** and the products **16a** and **16b**.

Noting that intermediate **A** was only seen at −80 °C, disappeared on warming, and did not reappear upon re-cooling, we wondered whether at lower temperatures intermediate **A** might

be the major species. To study intermediate **A**, oxygen was added to a solution of **15** in THF-d_8 at −95 °C which was then inserted into an NMR probe pre-cooled to −100 °C. Under these conditions, intermediate **A** was the major species in solution, present in >80% yield (NMR integration). The ^{31}P NMR spectrum of intermediate **A** consists of two sets of doublets at 57.8 and 51.8 ppm. These chemical shifts suggest that the phosphorus atoms in intermediate **A** are in more similar chemical environments than those of intermediate **B**. Their chemical environment likely resembles that of the starting material, **15**. As with **15** and intermediate **B**, intermediate **A** also has aromatic protons with unusual chemical shifts, in this case 11.25 and 4.26 ppm. Exposure of a solution of intermediate **A** to vacuum for two minutes at −95 °C did not result in any back reaction suggesting that the binding of oxygen to **A** is also irreversible. Of note, the resonances of intermediate **A** broaden substantially as the sample is warmed above −80 °C making detection and quantification difficult. This broadening could suggest a complex with paramagnetic character such as a Pd^{I}-superoxo complex or a Pd^{II}-bis superoxo complex, with the temperature dependence of the linewidth correlated with the relative populations of antiferromagnetically vs. ferromagnetically coupled states. The previously reported bis-carbene-Pd^{II} bis superoxo complex also generated a ^{1}H NMR spectrum with broad resonances.[33]

Perhaps supporting the assertion that intermediate **A** could be a superoxo complex, an O−O stretch was identified by resonance Raman spectroscopy in a reaction mixture prepared by the addition of O_2 to **15** at −80 °C in THF. Under these conditions a mixture of intermediates **A** and **B** would be expected. Spectra of samples prepared with $^{16}O_2$ contained non-solvent peaks at 1383 and 1363 cm^{-1} (Figure 3.6(a)), while a sample prepared with $^{18}O_2$, a single sharp peak at 1290 cm^{-1} appeared (Figure 3.6 (b)); the features at 1383 and 1363 cm^{-1} are still present, but at reduced intensity. These non-solvent peak intensities decreased upon warming (Figure 3.6 (c)).

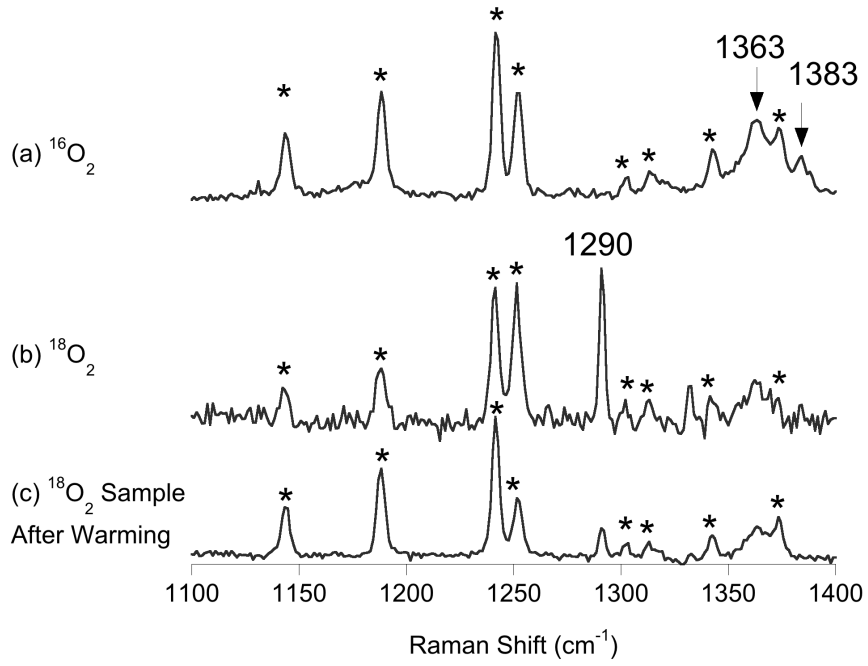

Figure 3.6. Resonance Raman spectra of solution resulting from treatment of **15** with O_2 in THF at -80 °C (λ_{ex}: 406.7 nm, 77 K). * = solvent peak.

The two peaks in the ^{16}O spectrum at 1383 and 1363 cm^{-1} could be consistent with a Fermi doublet centered at 1373 cm^{-1}. Such doublets have been seen in resonance Raman spectra of other metal-oxygen species.[37] The features at 1383 and 1363 cm^{-1} ($^{16}O_2$) and 1290 cm^{-1} ($^{18}O_2$) are assigned as ν_{O-O} for a coordinated superoxide ligand based on the magnitude of the ^{18}O-isotope shift from the average value of 1373 cm^{-1} to1290 cm^{-1} ($\Delta^{18}O_{exp}$ = 83 cm^{-1}). This difference agrees closely with that calculated using an O−O harmonic oscillator approximation which predicts a shift of 78 cm^{-1} to 1295 cm^{-1}. The observed ν_{O-O} is higher than those reported for most other metal-superoxide complexes, which typically exhibit ν_{O-O} between 1000 and 1300 cm^{-1}.[38] Further computational effort would be needed to propose an explanation for this unusual peak location.

Kinetic study of Intermediates A and B

The reaction of **15** with O_2 is rapid, even at −100 °C. In contrast, the conversion of intermediate **A** to intermediate **B** proceeded more slowly and could be conveniently monitored by ^{1}H NMR at −70 °C over approximately 80 minutes in THF-d_8. The resonances corresponding to intermediate **A** were too broad to integrate reliably at this temperature and so the appearance of intermediate **B** was followed through integration of the aromatic protons at 10.85 and 4.71 ppm. Fitting the appearance of intermediate **B** to a first order rate law suggests (Figure 3.7) that the reaction of intermediate **A** → intermediate **B** is first order in [Pd].

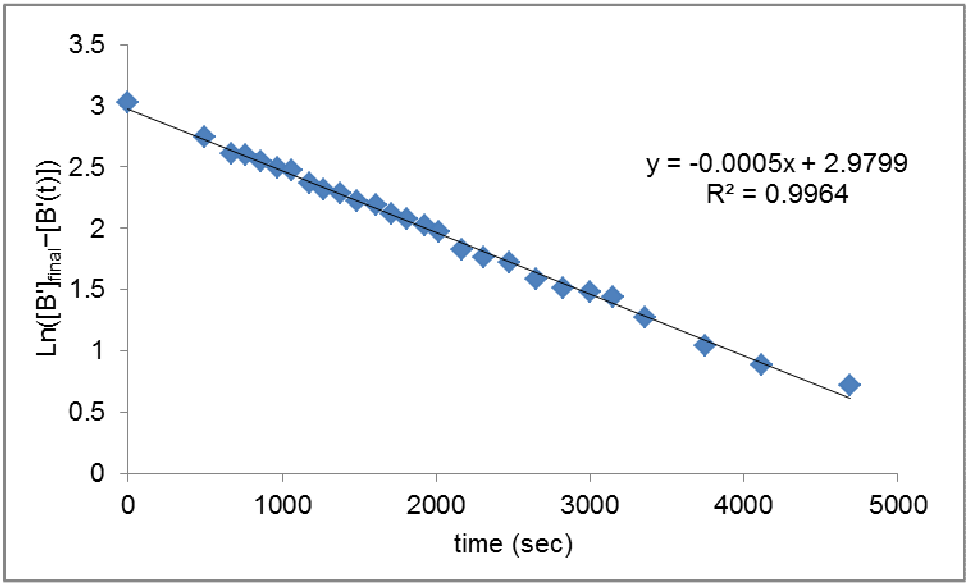

Figure 3.7. First order plot for the appearance of intermediate **B**. The [B'] designation refers to integration relative to an internal standard which is proportional to [B].

The kinetics of intermediate **B** reacting to form one equivalent of free phosphine and an NMR silent Pd species were found to be first order in the disappearance of intermediate **B** (Figure 3.8). That the reaction is first order in [Pd] can also be determined based on data for the appearance of free phosphine. The kinetics of this reaction were measured between −30 °C and −10 °C. An Arrhenuis plot revealed the energy of activation (E_a) to be 16.8 ±1.0 kcal/mol.

Eyring analysis of the data (Figure 3.9) found $\Delta H^{\ddagger}$ to be 16.3 ±1.0 kcal/mol and $\Delta S^{\ddagger}$ to be 6±4 e.u. These values suggest that at −20 °C $\Delta G^{\ddagger}$ would equal 17.8±2.0 kcal/mol.

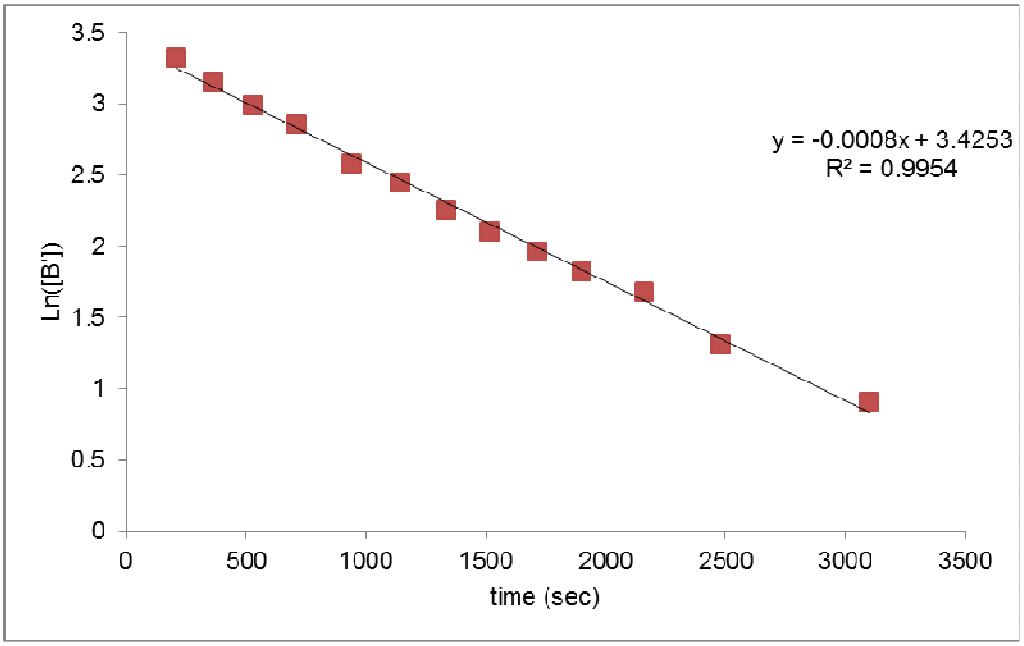

Figure 3.8. First order plot for the disappearance of intermediate **B**. The [B'] designation refers to integration relative to an internal standard which is proportional to [B].

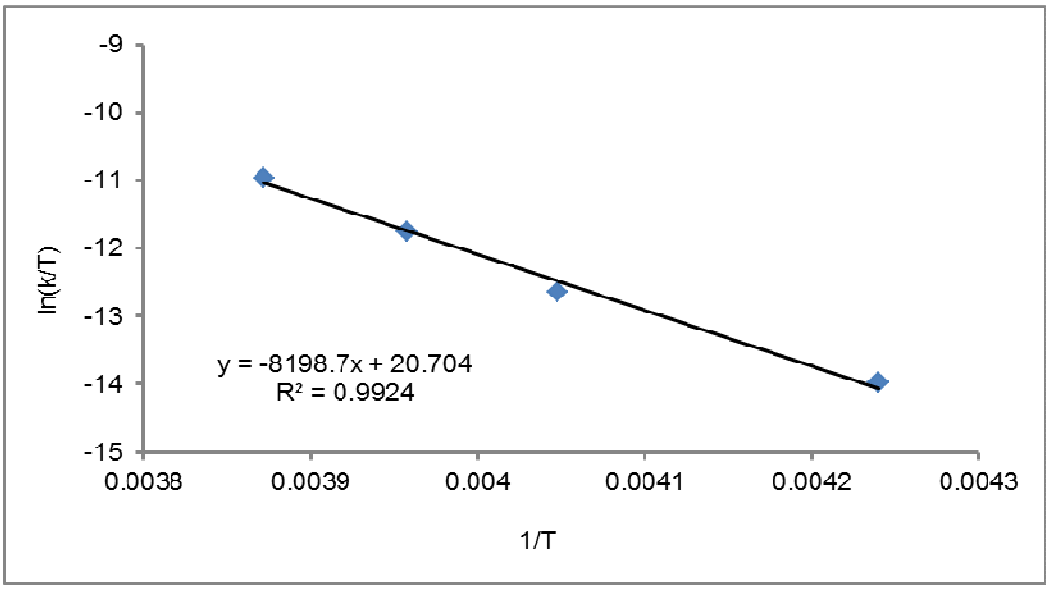

Figure 3.9. Eyring plot for the disappearance of intermediate **B**

The first order behavior for both the formation and disappearance of intermediate **B** would be consistent with intermediates **A** and **B** both having monometallic structures.

Mechanistic consideration

Despite the incomplete picture of the structures for intermediates **A**, **B**, and the paramagnetic species observed at room temperature, some consideration has been given to plausible mechanisms for the overall transformation, and especially the C−H bond cleavage step.

It is clear from the experimental data that the first step of this mechanism involves the interaction of the Pd^0 species with oxygen to eventually form intermediate **B** which is likely a Pd^{II}-η^2 peroxo complex. This seems to be in keeping with the extensive precedent for ligated Pd^0 species being oxidized by molecular oxygen.[39] Also supporting an oxygen-first pathway is a computational study that found C−H oxidative addition to a Pd^0 center to be an endothermic process.[40]

From intermediate **B**, one plausible mechanism could be addition of a C−H bond across a Pd−O bond with concurrent phosphine loss to generate a cyclometalated [(^{t}Bu$_2$PC)Pd−OOH] fragment which rapidly reacts further to dimerize and lose one oxygen atom per Pd. There is ample precedent for metal–OOH complexes "losing" an oxygen atom to form the corresponding metal–OH complexes.[41]

The addition of a C−H bond across a Pd−O bond is favored over an oxidative addition followed by insertion of oxygen into a Pd−H bond because of the lack of precedent for a Pd−peroxo moiety remaining intact in an oxidation state higher than Pd^{II}. In contrast, there is precedent for the addition of a C–H bond across a metal-oxygen bond (Figure 3.10).[42] There is also an example of the O–H bond of phenol adding across a Pt–O bond in a Pt-η^2-peroxo species (Figure 3.11).[43]

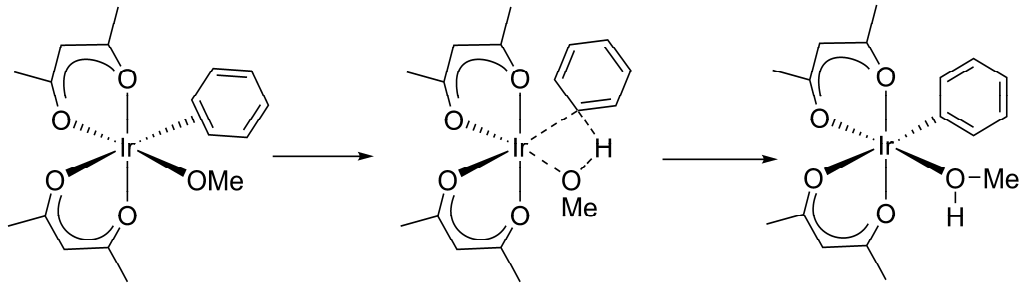

Figure 3.10. Addition of a C–H bond across an Ir–O bond.

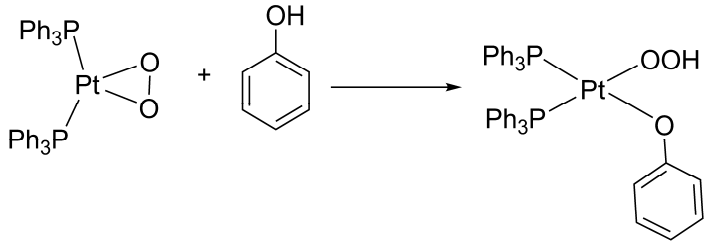

Figure 3.11. Addition of an O–H bond to a Pt-peroxo.

Computational study was undertaken to assess whether the addition of a C–H bond across a Pd–O bond could be a viable mechanism in this system. Initial studies considered the possibility of this C–H bond activation occurring after phosphine loss (Figure 3.12), however this pathway was found to be prohibitively high in energy regardless of the computational method used. The computational efforts were then turned toward a reaction involving addition of a C–H bond across a Pd–O bond occurring concurrently with the loss of one equivalent of phosphine (Figure 3.13). The transition state that was located is shown in Figure 3.14. The reaction was found to be exothermic and the gas phase enthalpy of activation was calculated to be 24 kcal/mol. When solvation (dielectric continuum) and entropy are taken into account, the $\Delta G^{\ddagger}$ of the reaction at 240 K was found to be 21 kcal/mol.[44] The vibrational spectrum was calculated to confirm that a saddle point had been located.

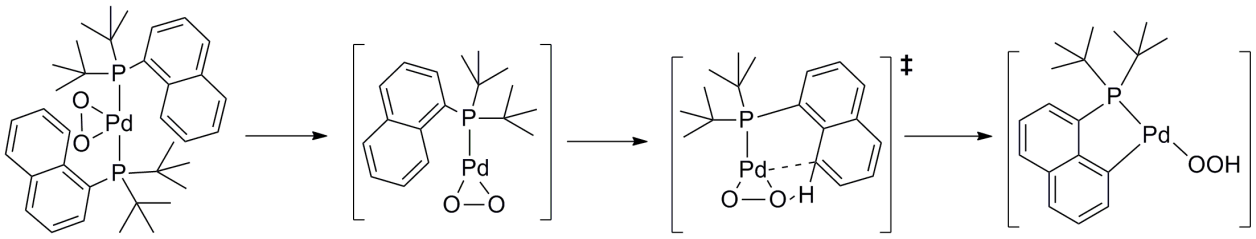

Figure 3.12. Addition of a C–H bond across a Pd–O bond after phosphine loss.

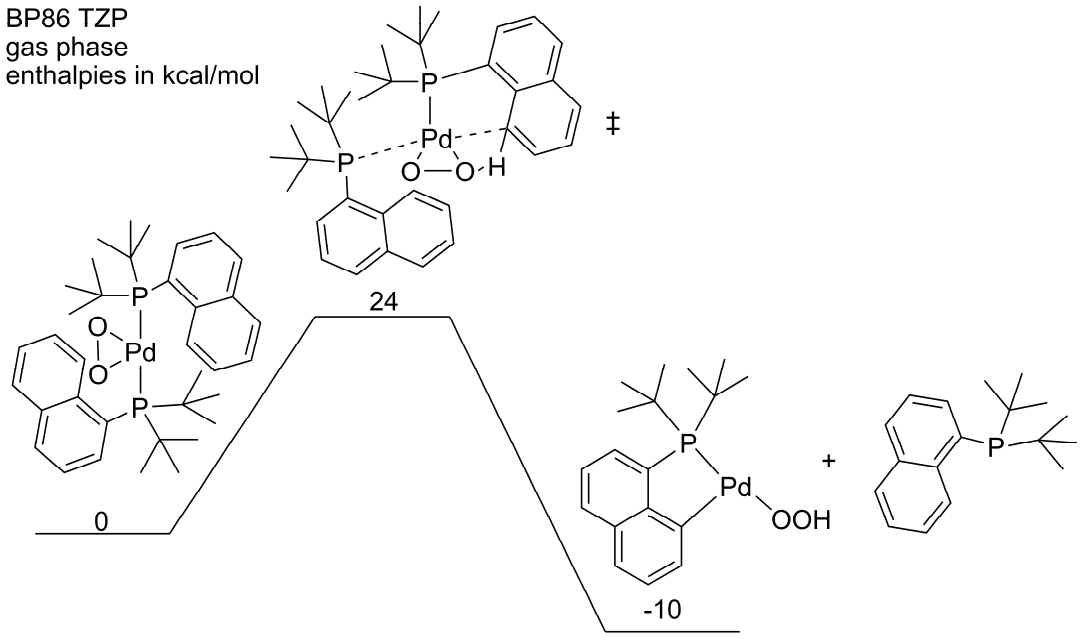

Figure 3.13. Addition of a C–H bond across a Pd–O bond concurrent with phosphine loss.

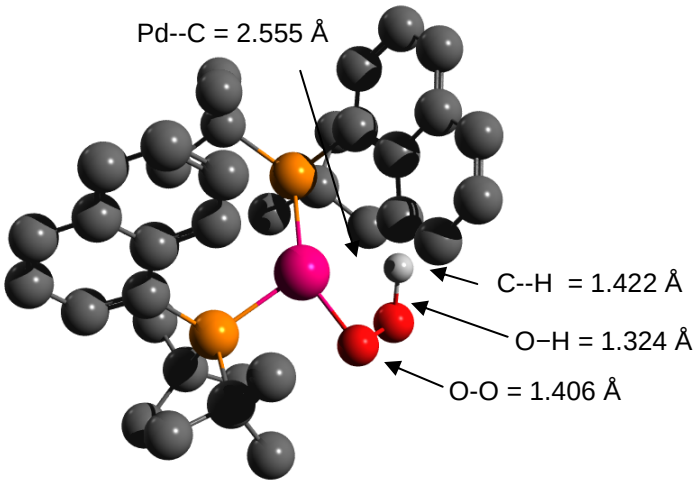

Figure 3.14. BP86 calculated transition state for the addition of a C–H bond across a Pd–O bond.

There are many other plausible mechanisms for this C−H bond cleavage process which have yet to be investigated. Still the accessibility of adding a C−H bond across a metal−peroxo bond could offer a potential pathway for C−H functionalization in this and other systems.

Summary

In summary, the reaction of the Pd^0 bisphosphine complex, **15** with dioxygen results in the formation of dimeric Pd^{II} hydroxide complexes **16a** and **16b**, a transformation that requires activation of both O–O and C–H bonds. The isomeric products were characterized by NMR spectroscopy, X-ray crystallography, elemental analysis, and quantum chemical calculations. Observation of low-temperature intermediates with all of the napthyl C−H bonds intact suggests that this transformation likely represents initial O−O activation followed by C−H bond activation at a Pd center. Such a scheme seems consistent with the propensity of Pd^0 to react with O_2 and the greater favorability of C−H bond activation at Pd^{II}. We have considered the possibility that this system could represent a model system for the arene C−H hydroxylation observed by Yu and coworkers.[11] In our hands, the catalyst in the Yu system was poisoned by Hg^0 suggesting that a

low-ligated Pd^0 species could be important in that mechanism as well.[45] The reaction of **15** with dioxygen represents a previously unexplored pathway for the functionalization of C–H bonds by Pd complexes in which molecular oxygen is employed as the oxidant.

Experimental

General considerations

Benzene, ether, acetonitrile, toluene, and pentane were dried by passage through activated alumina and molecular sieve columns under argon. Benzene-d_6, THF-d_8, and toluene-d_8 were vacuum transferred from sodium/benzophenone ketyl. Dichloromethane-d_2 was vacuum transferred from CaH_2. (tmeda)$PdMe_2$was prepared by a literature method.[46] All other reagents and gases were obtained from commercial vendors and used as received. NMR spectra were recorded on Bruker DRX500, AV500, AV700, or AV800 spectrometers. ^{1}H NMR spectra were referenced to the residual protiated solvent signal. ^{13}C NMR spectra were referenced to the solvent signal. ^{31}P NMR spectra acquired at 298 K were referenced to an 85% H_3PO_4 external standard (0 ppm). Low temperature ^{31}P NMR spectra were referenced to the deuterated solvent via the lock channel. Data from COSY, HMQC, and HMBC experiments were used in the assignments and some signal identifications. Abbreviations: s = singlet, d = doublet, dd = doublet of doublets, m = multiplet, br = broad. Resonance Raman spectra were collected using an ACTON AM-506M3 monochromator and Princeton Instruments ACTON PyLoN LN/CCD-1340 x 400 detector. The spectra were obtained at −196 °C using backscattering geometry. Excitation at 406.7 nm was provided by a Spectra-Physics BeamLok 2060-KR-V Krypton ion laser. Raman shifts were externally referenced to indene and internally referenced to solvent (THF).

Synthesis of 1-napthtyl-di-*tert*-butylphosphine

In a modification of a literature procedure[14] an oven-dried Schlenk flask was charged with 1-bromonaphthalene (5.0 g, 24.2 mmol) and dry ether (100 mL). The solution was deoxygenated by sparging with N_2 then cooled in a dry-ice/acetone bath. *n*-BuLi solution (12 mL, 2.5 M hexanes) was added dropwise and the solution was allowed to warm to room temperature over one hour. The mixture was then placed back in the dry-ice/acetone bath and chloro-di-*tert*-butylphosphine (5 mL, 26.3 mM) was slowly added. The mixture was again warmed to room temperature and the volatiles were removed in vacuo. In a nitrogen-filled glovebox the residue was extracted with pentane and filtered to a give a yellow solution. The volatiles were removed to give a yellow oil which was stirred with acetonitrile (50 mL) yielding white solid 1-napthtyl-di-*tert*-butylphosphine which was collected by vacuum filtration (4.09 g, 62%). Spectroscopic data in chloroform-*d* match those previously reported.[13] ^{1}H NMR (benzene-d_6, 500 MHz, 298 K) δ 9.57 (t, *J* = 8.0 Hz, 1H), 7.94 (d, *J* = 7.1 Hz, 1H), 7.68 (d, *J* = 7.7 Hz, 1H), 7.64 (d, *J* = 7.7, 1H), 7.39 (m, 1H), 7.27 (m, 2H), 1.20 (d, $^3J_{P-H}$ = 11.5 Hz, 18H). ^{31}P NMR (benzene-d_6, 202 MHz, 298 K) δ 10.77.

Synthesis of Pd(P(Ar)(*t*Bu)$_2$)$_2$ (15, Ar = naphthyl)

A reaction vessel with teflon stopper was oven-dried and in a glovebox charged with 1-napthtyl-di-*tert*-butylphosphine (800 mg, 2.9 mmol), (tmeda)$PdMe_2$ (370 mg, 1.5 mmol), and benzene (30 mL). The vessel was heated at 60 °C for 18 hours then cooled to room temperature and the volatiles removed in vacuo. In a nitrogen-filled glovebox the yellow residue was extracted with the minimal amount of toluene needed to dissolve the material. The extracts were filtered through a 0.2 μm PTFE syringe filter, layered with an equal volume of pentane and left at −35 °C for six days yielding orange crystals of **15** (310 mg, 32 %). Further recrystallization of the

supernatant resulted in a second crop of crystalline **15** (290 mg, 30%). X-ray quality crystals were obtained from a benzene-d_6 solution of **15** layered with pentane at room temperature. ^{1}H NMR (benzene-d_6, 500 MHz, 298 K) δ 12.21 (m, 2H), 8.06 (m, 2H), 7.71 (d, J = 7.7, 2H), 7.62 (d, J = 7.6, 2H), 7.35 (m, 2H), 7.27 (m, 2H), 7.25 (m, 2H), 1.58 (m, 36 H). ^{1}H NMR (toluene-d_8, 500 MHz, 193 K) δ 12.34 (br, 2H), 8.00 (br, 2H), 7.65 (br-d, 2H), 7.59 (br-d, 2H), 7.49 (br-t, 2H), 7.31 (br-t, 2H), 7.26 (br-t, 2H), 1.56 (br, 36H). ^{1}H NMR (THF-d_8, 500 MHz, 173 K) δ 11.87 (br, 2H), 8.18 (br, 2H), 8.06 (br-d, 2H), 7.92 (br-d, 2H), 7.62 (br-t, 2H), 7.50 (br-t, 2H), 7.40 (br-t, 2H), 1.51 (br, 36H). ^{13}C NMR (benzene-d_6, 126 MHz, 298 K) δ 138.3 (m), 134.9 (m), 133.3, 133.0 (m), 130.7 (m), 130.7, 128.5, 126.1, 125.4, 123.7 (m), 36.4 (m), 32.0 (m). ^{31}P NMR (benzene-d_6, 202 MHz, 298 K) δ 43.45. Anal. Calcd. for $C_{36}H_{50}P_2Pd$: C, 66.40; H, 7.74. Found: C, 66.36; H, 7.78.

Generation of intermediate A

In a N_2-filled glovebox, an oven-dried NMR tube with a PTFE-lined screw cap was charged with Pd(P(Ar)(*t*Bu)$_2$)$_2$ (2-15 mg), 1,3,5-trimethoxybenzene (internal standard) and freshly vacuum-transferred THF-d_8 (0.5 mL). After an initial spectra was recorded, the sample was cooled in a toluene/LN_2 cold bath and oxygen gas was bubbled through for one to two minutes. The sample was then inserted into an NMR probe pre-cooled to 173 K. ^{1}H NMR (THF-d_8, 500 MHz, 173 K) δ 11.23 (br, 1H), 8.90 (br, 1H), 8.20 (br, 1H), 8.11 (br, 1H), 7.96 (br, 1H), 7.82 (br, 1H), 7.74 (br, 1H), 7.66 (br, 1H), 7.52 (br, 2H), 7.45 (br, 1H), 6.71 (br, 1H), 4.25 (br, 1H), *t*Bu groups appear as multiple resonances between 0.0 and 2.5. ^{31}P NMR (THF-d_8, 202 MHz, 273 K) δ 58 (d, J = 16 Hz), 55 (d, J = 21 Hz).

Generation of intermediate B

In a N_2-filled glovebox, an oven-dried NMR tube with a PTFE-lined screw cap was charged with $Pd(P(Ar)(tBu)_2)_2$ (2-5 mg), 1,3,5-trimethoxybenzene (internal standard) and freshly vacuum transferred toluene-d_8 (0.5 mL). After an initial spectra was recorded, the sample was cooled in a dry ice/acetone cold bath and oxygen gas was bubbled through for one to two minutes.[47] The sample was then inserted into an NMR probe pre-cooled to 193 K. Alternatively, Intermediate **B** could be generated by warming a solution of Intermediate **A** to 213 K in the NMR probe. Either method gives yields of intermediate **B** at 213 K in excess of 80 % by integration relative to the internal standard. Addition of pentane to a solution containing predominantly intermediate **B** results in the formation of a non-crystalline yellow solid. ^{1}H NMR (THF-d_8, 500 MHz, 213 K) δ 10.85 (br-m, 1H), 8.26 (br-m, 2H), 8.13 (br-m, 2H), 8.03 (br-d, 2H), 7.72 (br-m, 2H), 7.61 (br-t, 1H) 7.53 (br-m, 2H), 7.39 (br-m, 2H), 4.71 (t, 1H), *t*Bu groups appear as multiple resonances between 0.5 and 2.5. ^{1}H NMR (toluene-d_8, 500 MHz, 233 K) δ 11.19 (m, 1H), 8.31 (dd, 1H), 8.23 (d, 1H), 7.78 (t, 1H), 7.71 (d, 1H), 7.52 (d, 1H), 7.30 (t, 1H), 7.23 (COSY only), 7.19 (COSY only), 7.17 (COSY only), 7.15 (COSY only) 7.04 (COSY only), 6.94 (COSY only), 4.90 (t, 1H), *t*Bu groups appear as multiple resonances between 0.0 and 2.0. ^{31}P NMR (THF-d_8, 202 MHz, 203 K) δ 103 (d, J = 21 Hz), 55 (d, J = 21 Hz). ^{31}P NMR (toluene-d_8, 202 MHz, 203 K) δ 103 (d, J = 21 Hz), 55 (d, J = 21 Hz).

Synthesis of 16a and 16b from 15

In a N_2-filled glovebox, a tared vial was charged with $Pd(P(Ar)(tBu)_2)_2$ (30.3 mg, 0.0466 mmol). In air, 0.6 mL benzene was added. The suspension was mixed and after about one hour all the solid had dissolved giving a deep red solution. After 12 days the supernatant was pipetted away leaving crystals of **16a**·C_6H_6 which were rinsed with 3 x 1 mL portions of pentane. The crystals were dried under vacuum yielding pure **16a**·C_6H_6 (15.5 mg, 76.7 %). Anal. Calcd. for

$C_{36}H_{50}O_2P_2Pd_2 \cdot C_6H_6$: C, 58.14; H, 6.51. Found: C, 58.39; H, 6.45. Crystals suitable for X-ray diffraction were obtained from a sample in dry C_6D_6 and using 3 atm O_2 rather than air.

Spectroscopic characterization of mixtures containing 16a and 16b

Note that in solution compounds **16a** and **16b** appear as equilibrium mixtures. ^{1}H NMR data are reported separately for**16a** and **16b**. The ^{13}C NMR data represents a compilation of peaks corresponding to both isomers some of which were identified based on HMQC and HMBC data. ^{1}H NMR of **16a** (dichloromethane-d_2, 500 MHz, 298 K) δ 7.82 (m, overlap with a resonance of **16b**), 7.77 (m, overlap with a resonance of **16b**), 7.66 (dd, J = 7.66 Hz, 2H), 7.49 (dd, J = 7.66 Hz, 2H), 7.44 (m, overlap with a resonance of **16b**), 7.22 (t, J = 7.61 Hz, 2H), 1.51 (d, $^3J_{P-H}$= 14 Hz, 36H), −0.91 (d, $^3J_{P-H}$ = 2.5 Hz, 2H). ^{31}P NMR of **2a** (dichloromethane-d_2, 202 MHz, 298 K) δ 100.9. ^{1}H NMR of **16b** (dichloromethane-d_2, 500 MHz, 298 K) δ 7.86 (dd, J = 7.86 Hz, 2H), 7.82 (m, overlap with a resonance of **16a**), 7.77 (m, overlap with a resonance of **16b**), 7.52 (dd, J = 7.51 Hz, 2H), 7.44 (m, overlap with a resonance of **16b**), 7.31 (t, J = 7.31 Hz, 2H), 1.47 (d, $^3J_{P-H}$= 14 Hz, 36H), 0.19 (t, $^3J_{P-H}$ = 3.5 Hz, 1H), −2.51 (s, 1H). ^{31}P NMR of **16b** (dichloromethane-d_2, 202 MHz, 298 K) δ 100.5. ^{13}C NMR data for **16a** and **16b** (dichloromethane-d_2, 176 MHz, 298 K) δ 153, 153, 152, 152, 135, 135, 134, 134, 131, 131, 131, 130, 129.8, 129.7, 126.3, 126.2, 125.1 (d, J = 7 Hz), 125.0 (d, J = 7 Hz),123.1, 123.0, 37.1(d, J = 18 Hz), 36.9 (d, J = 18 Hz), 30.3 (d, overlap), 30.2 (d, overlap).

Independent synthesis of 16a and 16b

In air 1-napthtyl-di-*tert*-butylphosphine (197 mg, 0.72 mmol) and K_2PdCl_4 (242 mg, 0.74 mmol) were suspended in methanol (40 mL). The headspace was purged with N_2 gas and the mixture was stirred at reflux for 20 hours resulting in a white solid with a pale yellow supernatant. The highly insoluble solid was collected on a frit, washed with small portions of water, methanol, and

ether. The product was found to contain two species. ^{1}H NMR (dichloromethane-d_2, 500 MHz, 298 K) δ 8.22(minor), 8.14 (major), 7.86 (both species), 7.82 (both species), 7.57 (minor), 7.55 (major), 7.31 (minor), 7.23 (major), 1.55/1.53 (*t*Bu groups). ^{31}P NMR (dichloromethane-d_2, 202 MHz, 298 K) δ 111.66 (major) and 111.37 (minor). Poor solubility prevented the collection of good quality ^{13}C NMR data. A sample of this solid (100 mg) was then suspended in acetone (1 mL). The suspension was treated with NBu_4OH solution (1M, 250 μL) and stirred at room temperature overnight. The resulting solid was collected on a frit and washed with water. ^{1}H and ^{31}P NMR resonances matched those of **16a** and **16b**.

Crystallographic characterization of 15

An orange cut-block, measuring 0.25 x 0.20 x 0.10 mm^3 was mounted on a glass capillary with oil. Data was collected at –173^{o}C on a Bruker APEX II single crystal X-ray diffractometer, Mo-radiation. Crystal-to-detector distance was 40 mm and exposure time was 10 seconds per degree for all sets. The scan width was 0.5^o. Data collection was 99.2% complete to 25^o in ϑ. A total of 253915 (merged) reflections were collected covering the indices, h = –11 to 11, k = –34 to 34, l = –46 to 46. 9911 reflections were symmetry independent and the R_{int} = 0.0321 indicated that the data was brilliant (average quality 0.07). Indexing and unit cell refinement indicated primitive orthorhombic lattice. The space group was found to be P b c a (No.61). The data was integrated and scaled using SAINT, SADABS within the APEX2 software package by Bruker.[48] Solution by direct methods (SHELXS, SIR97[49]) produced a complete heavy atom phasing model consistent with the proposed structure. The structure was completed by difference Fourier synthesis with SHELXL97.[50,51] Scattering factors are from Waasmair and Kirfel.[52] Hydrogen atoms were placed in geometrically idealized positions and constrained to ride on their parent atoms with C---H distances in the range 0.95-1.00 Angstrom. Isotropic thermal parameters U_{eq}

were fixed such that they were $1.2U_{eq}$ of their parent atom U_{eq} for CH's and $1.5U_{eq}$ of their parent atom U_{eq} in case of methyl groups. All non-hydrogen atoms were refined anisotropically by full-matrix least-squares.

Table 3.1. Crystallographic data for **15**.

Parameter	**15**
Empirical formula	C_{36} H_{50} P_2 Pd
Formula weight	651.10
Temperature	100(2) K
Wavelength	0.71073 Å
Crystal system	Orthorhombic
Space group	P b c a
Unit cell dimensions	a = 8.2897(3) Å, α= 90° b = 23.8619(10) Å, β= 90° c = 32.6736(14) Å, γ = 90°
Volume	6463.1(5) $Å^3$
Z	8
Density (calculated)	1.338 Mg/m^3
Absorption coefficient	0.696 mm^{-1}
F(000)	2736
Crystal size	0.25 x 0.20 x 0.10 mm^3
Theta range for data collection	1.82 to 30.65°
Index ranges	$-11 \leq h \leq 11$, $-34 \leq k \leq 34$, $-46 \leq l \leq 46$
Reflections collected	253915
Independent reflections	9911 [R(int) = 0.0321]
Completeness to theta = 25.00°	99.2 %
Max. and min. transmission	0.9336 and 0.8452
Refinement method	Full-matrix least-squares on F^2
Data / restraints / parameters	9911 / 0 / 364
Goodness-of-fit on F^2	1.025
Final R indices [I>2sigma(I)]	R1 = 0.0215, wR2 = 0.0488
R indices (all data)	R1 = 0.0267, wR2 = 0.0522
Largest diff. peak and hole	0.489 and -0.546 e.$Å^{-3}$

Crystallographic characterization of 16a

An orange prism, measuring 0.20 x 0.18 x 0.15 mm^3 was mounted on a glass capillary with oil. Data was collected at –173^{o}C on a Bruker APEX II single crystal X-ray diffractometer, Mo-radiation. Crystal-to-detector distance was 40 mm and exposure time was 10 seconds per degree for all sets. The scan width was 0.5^o. Data collection was 100% complete to 25^o in ϑ. A total of 99546 (merged) reflections were collected covering the indices, h = –33 to 33, k = –19 to 19, l = –24 to 24. 7479 reflections were symmetry independent and the R_{int} = 0.0189 indicated that the data was brilliant (average quality 0.07). Indexing and unit cell refinement indicated a C-centered monoclinic lattice. The space group was found to be C 2/c (No.15). The data was integrated and scaled using SAINT, SADABS within the APEX2 software package by Bruker.[48] Solution by direct methods (SHELXS, SIR97[49]) produced a complete heavy atom phasing model consistent with the proposed structure. The structure was completed by difference Fourier synthesis with SHELXL97.[50,51] Scattering factors are from Waasmair and Kirfel.[52] Hydrogen atoms were placed in geometrically idealized positions and constrained to ride on their parent atoms with C---H distances in the range 0.95-1.00 Angstrom. Isotropic thermal parameters U_{eq} were fixed such that they were 1.2U_{eq} of their parent atom Ueq for CH's and 1.5U_{eq} of their parent atom U_{eq} in case of methyl groups. All non-hydrogen atoms were refined anisotropically by full-matrix least-squares. The hydrogen of the bridging hydroxyl has no acceptor in this structure, however, the hydrogen was unambiguously visible in the electron density and refined with isotropic thermal parameter. The dimer exhibits centrosymmetry.

Table 3.2. Crystallographic data for **2a**.

Parameter	**2a**
Empirical formula	$C_{42}H_{50}D_6O_2P_2Pd_2$
Formula weight	873.64
Temperature	100(2) K
Wavelength	0.71073 Å
Crystal system	Monoclinic
Space group	C 2/c
Unit cell dimensions	a = 21.4703(7) Å, α = 90° b = 12.6614(7) Å, β =115.970(2)° c = 15.7412(7) Å, γ = 90°
Volume	3847.1(3) $Å^3$
Z	4
Density (calculated)	1.508 Mg/m^3
Absorption coefficient	1.053 mm^{-1}
F(000)	1784
Crystal size	0.20 x 0.18 x 0.15 mm^3
Theta range for data collection	1.92 to 33.45°
Index ranges	$-33 \leq h \leq 33$, $-19 \leq k \leq 19$, $-24 \leq l \leq 24$
Reflections collected	99546
Independent reflections	7479 [R(int) = 0.0189]
Completeness to theta = 25.00°	100.0 %
Max. and min. transmission	0.8581 and 0.8171
Refinement method	Full-matrix least-squares on F^2
Data / restraints / parameters	7479 / 0 / 221
Goodness-of-fit on F^2	1.078
Final R indices [I>2sigma(I)]	R1 = 0.0159, wR2 = 0.0414
R indices (all data)	R1 = 0.0178, wR2 = 0.0430
Largest diff. peak and hole	0.745 and -0.747 $e.Å^{-3}$

Simulated NMR spectra

Selected NMR resonances for compound **15** were simulated using gNMR version 5.1.[53] The experimental and simulated spectra for the *t*Bu resonance are shown in Figure 3.15. The simulated spectrum represents a spin system as described in Table 3.3. The experimental and

simulated spectra of the aromatic proton in close proximity to the Pd center are shown in Figure 3.16. The simulated spectrum represents a spin system as described in Table 3.4.

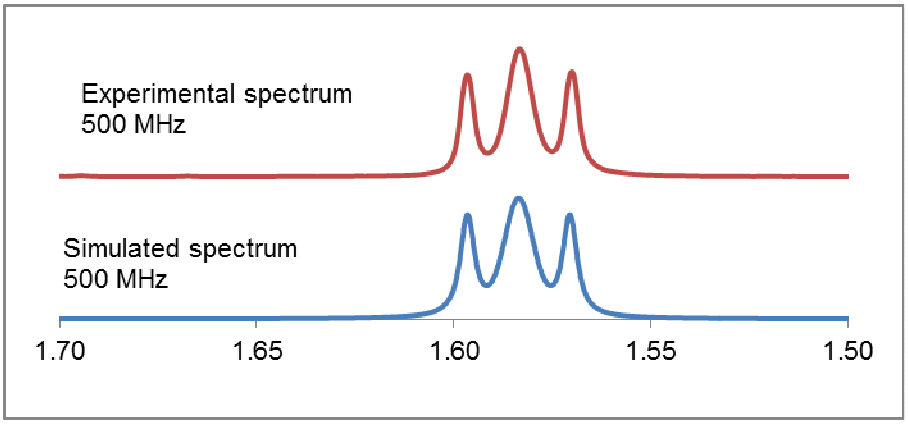

Figure 3.15. Experimental and simulated spectra for the *t*Bu resonance of **15**.

Table 3.3. Spin system for the simulated *t*Bu resonance of **15**.

	Nucleus	**Number**	**Shift**	***J*[1]**	***J*[2]**	***J*[3]**
1	^{1}H	9	1.455	-	-	-
2	^{1}H	9	1.456	0	-	-
3	^{31}P	1	43.45	21	21	-
4	^{31}P	1	43.45	−8	−8	450

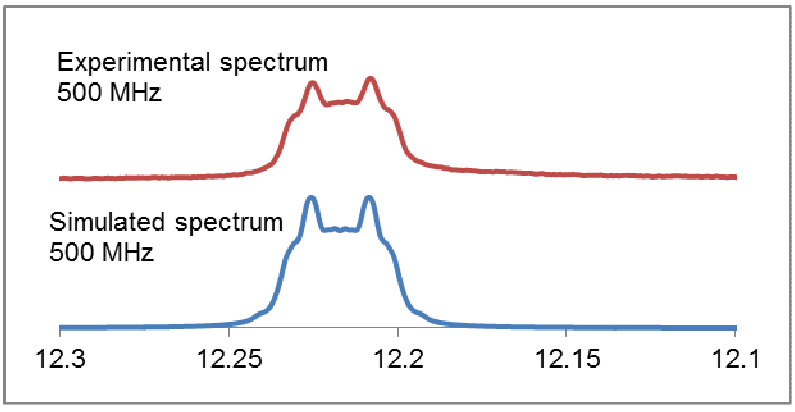

Figure 3.16. Experimental and simulated spectra for the aromatic proton in close proximity to the metal center.

Table 3.4. Spin system the aromatic proton in close proximity to the metal center in **15**.

	Nucleus	Number	Shift	*J*[1]	*J*[2]	*J*[3]	*J*[4]
1	^{1}H	9	12.082	-	-	-	-
2	^{1}H	9	7.350	6.50	-	-	-
3	^{31}P	1	43.45	−42.50	1.00	-	-
4	^{31}P	1	43.45	31.00	0.30	450	-
5	^{1}H	1	12.082	4.00	0.01	31.00	−42.50

General computational methods

DFT calculations were carried out using the ADF program.[54,55,56] The BP86[18] and B3LYP[19] density functionals were employed as described in the text. The ZORA framework for treatment of relativitic effects was employed throughout.[57] Slater-type triple zeta plus polarization (TZP) basis sets, optimized for use with the ZORA method, were used for all atoms.[58]

Coauthor contributions

Kyle Grice made the initial observation of **15** (in situ) and noted that it reacted with oxygen. Raman experiments were performed and analyzed by David Boyce under the supervision of Bill Tolman. Werner Kaminsky collected crystallographic data and solved the structures for **15** and **16a**. Ole Swang offered instruction in computational methods.

Notes to Chapter 3

(1) Stahl, S. S. *Science* **2005**, *309*, 1824.

(2) Cavani, F.; Teles, J. H. *ChemSusChem* **2009**, *2*, 508.

(3) (a) Boisvert, L.; Goldberg, K. I. *Acc. Chem. Res.* **2012**, *45*, 899. (b) Campbell, A. N.; Stahl, S. S. *Acc. Chem. Res.* **2012**, *45*, 851. (c) Shi, Z.; Zhang, C.; Tang, C.; Jiao, N. *Chem. Soc. Rev.* **2012**, *41*, 3381. (d) Sigman, M. S.; Jensen, D. R. *Acc. Chem. Res.* **2006**, *39*, 221. (e) Gligorich, K. M.; Sigman, M. S. *Angew. Chem., Int. Ed.* **2006**, *45*, 6612. (f) Punniyamurthy, T.; Velusamy, S.; Iqbal, J. *Chem. Rev.* **2005**, *105*, 2329.

(4)(a) Sigman, M. S.; Jensen, D. R. *Acc. Chem. Res.* **2006**, *39*, 221. (b) Schultz, M. J.; Sigman, M. S. *Tetrahedron* **2006**, *62*, 8227.

(5)(a) Wu, W.; Jiang, H. *Acc. Chem. Res.* **2012**, *45*, 1736. (b) Gligorich, K. M.; Sigman, M. S. *Chem. Commun.* **2009**, 3854. (c) Takacs, J. M.; Jiang, X. -t. *Curr.Org. Chem.* **2003**, *7*, 369. (d) Smidt, J.; Hafner, W.; Jira, R.; Sieber, R.; Sedlmeier, J.; Sabel, A. *Angew. Chem., Int. Ed.* **1962**, *1*, 80.

(6) (a) Granell, J.; Martínez, M. *Dalton Trans.* **2012**, *41*, 11243. (b) Neufeldt, S. R.; Sanford, M. S. *Acc. Chem. Res.* **2012**, *45*, 936. (c) Engle, K. M.; Mei, T.; Wasa, M.; Yu, J. *Acc. Chem. Res.* **2012**, *45*, 788. (d) Li, H.; Li, B.-J.; Shi, Z.-J. *Catal. Sci. & Tech.* **2011**, *1*, 191. (e) Zhou, M.; Crabtree, R. H. *Chem. Soc. Rev.* **2011**, *40*, 1875. (f) Lyons, T. W.; Sanford, M. S. *Chem. Rev* **2010**, *110*, 1147. (g) Günay, M. E.; Ilyashenko, G.; Richards, C. J. *Tetrahedron: Asymmetry* **2010**, *21*, 2782.

(7) (a) Jintoku, T.; Nishimura, K.; Takaki, K.; Fujiwara, Y. *Chem. Lett.* **1991**, 193. (b) Jintoku, T.; Nishimura, K.; Takaki, K.; Fujiwara, Y. *Chem. Lett.* **1990**, *19*, 1687. (c) Jintoku, T.; Takaki, K.; Fujiwara, Y.; Fuchita, Y.; Hiraki, K. *Bull. Chem. Soc. Jpn.* **1990**, *63*, 438. (d) Jintoku, T.; Taniguchi, H.; Fujiwara, Y. *Chem. Lett.* **1987**, 1865.

(8) Yamada, S.; Sakaguchi, S.; Ishii, Y. *J. Mol. Cat. A: Chem.* **2007**, *262*, 48.

(9) (a) Zhu, M.-K.; Zhao, J.-F.; Loh, T.-P. *J. Am. Chem. Soc.* **2010**, *132*, 6284. (b) Wang, A.; Jiang, H. *J. Org. Chem.* **2010**, *75*, 2321.

(10) Chuang, G. J.; Wang, W.; Lee, E.; Ritter, T. *J. Am. Chem. Soc.* **2011**, *133*, 1760.

(11) Zhang, Y.-H.; Yu, J.-Q. *J. Am. Chem. Soc.* **2009**, *131*, 14654.

(12) Yan, Y.; Feng, P.; Zheng, Q.-Z.; Liang, Y.-F.; Lu, J.-F.; Cui, Y.; Jiao, N. *Angew. Chem. Int.*

Ed. **2013**, *52*, 5827.

(13) de Graaf, W.; Boersma, J.; Smeets, W. J. J.; Spek, A. L.; van Koten, G. *Organometallics* **1989**, *8*, 2907.

(14) Karaçar, A.; Freytag, M.; Thönnessen, H.; Jones, P. G.; Bartsch, R.; Schmutzler, R. *J. Organomet. Chem.* **2002**, *643–644*, 68.

(15) Fan, H.; Fullmer, B. C.; Pink, M.; Caulton, K. G. *Angew. Chem., Int. Ed.* **2008**, *47*, 9112.

(16) ORTEP plots were created using Ortep-3 for Windows. See: Farrugia, L. J. *J. Appl. Crystallogr.* **1997**, *30*, 565.

(17) Persistence of Vision Ray-Tracer (POV-Ray), available at http://www.povray.org/.

(18) Perdew, J. *Phys.Rev. B* **1986**, *33*, 8822.

(19) Becke, A. D. *J. Chem. Phys.* **1993**, *98*, 5648.

(20) Brookhart, M.; Green, M. L. H.; Parkin, G. *Proc. Natl. Acad. Sci. U.S.A.* **2007**, *104*, 6908.

(21) Grushin, V. V.; Alper, H. *Organometallics* **1993**, *12*, 1890.

(22) Cockburn, B. N.; Howe, D. V.; Keating, T.; Johnson, B. F. G.; Lewis, J. *J. Chem. Soc. Dalton Trans.* **1973**, 404.

(23) Limited solubility and phosphorus coupling prevented the collection of good quality ^{13}C data.

(24) Pérez, J.; Serrano, J. L.; Galiana, J. M.; Cumbrera, F. L.; Ortiz, a L.; Sánchez, G.; García, J. *Acta Crystallogr. Sect. B, Struct. Sci.* **2007**, *63*, 75.

(25) Aboelella, N. W.; York, J. T.; Reynolds, A. M.; Fujita, K.; Kinsinger, C. R.; Cramer, C. J.; Riordan, C. G.; Tolman, W. B. *Chem. Commun.* **2004**, *1*, 1716.

(26) Clegg, W.; Eastham, G. R. .; Elsegood, M. R. J.; Heaton, B. T.; Iggo, J. a.; Tooze, R. P.; Whyman, R.; Zacchini, S. *J.Chem. Soc., Dalton Trans*. **2002**, 3300.

(27) Gramage-Doria, R.; Armspach, D.; Matt, D.; Toupet, L. *Chem. Eur. J.* **2012**, *18*, 10813.

(28) (a) Yoshida, T.; Tatsumi, K.; Matsumoto, M.; Nakatsu, K.; Nakamura, A.; Fueno, T.; Otsuka, S. *Nouveau Journal de Chimie* **1979**, *3*, 761. (b) Otsuka, S.; Yoshida, T.; Matsumoto, M.; Nakatsu, K. *J. Am. Chem. Soc.* **1976**, *98*, 5850. (c) Matsumoto, M.; Yoshioka, H.; Nakatsu, K.; Yoshida, T.; Otsuka, S. *J. Am. Chem. Soc.* **1974**, *96*, 3322.

(29) Sergeev, A. G.; Neumann, H.; Spannenberg, A.; Beller, M. *Organometallics* **2010**, *29*, 3368.

(30) Adjabeng, G.; Brenstrum, T.; Frampton, C. S.; Robertson, A. J.; Hillhouse, J.; McNulty, J.; Capretta, A. *J. Org. Chem.* **2004**, *69*, 5082.

(31) for example see: (a) Labios, L. A; Millard, M. D.; Rheingold, A. L.; Figueroa, J. S. *J. Am. Chem. Soc.* **2009**, *131*, 11318. (b) Fantasia, S.; Nolan, S. P. *Chem. Eur. J.* **2008**, *14*, 6987. (c) Erhardt, S.; Grushin, V. V.; Kilpatrick, A. H.; Macgregor, S. a; Marshall, W. J.; Roe, D. C. *J. Am. Chem. Soc.* **2008**, *130*, 4828. (d) Yamashita, M.; Goto, K.; Kawashima, T. *J. Am. Chem. Soc.* **2005**, *127*, 7294. (e) Konnick, M. M.; Guzei, I. A.; Stahl, S. S. *J. Am. Chem. Soc.* **2004**, *126*, 10212. (f) Stahl, S. S.; Thorman, J. L.; Nelson, R. C.; Kozee, M. A. *J. Am. Chem. Soc.* **2001**, *123*, 7188. (g) Otsuka, S.; Nakamura, A.; Tatsuno, Y. *J. Am. Chem. Soc.* **1969**, *91*, 6994.

(32) Landis, C. R.; Morales, C. M.; Stahl, S. S. *J. Am. Chem. Soc.* **2004**, *126*, 16302.

(33) Cai, X.; Majumdar, S.; Fortman, G. C.; Cazin, C. S. J.; Slawin, A. M. Z.; Lhermitte, C.; Prabhakar, R.; Germain, M. E.; Palluccio, T.; Nolan, S. P.; Rybak-Akimova, E. V.; Temprado, M.; Captain, B.; Hoff, C. D. *J. Am. Chem. Soc.* **2011**, *133*, 1290.

(34) Garrou, P. E. *Chem. Rev.* **1981**, *81*, 229.

(35) Stewart, J. J. P. *J. Mol. Modeling*, **2007**, *13*, 1173.

(36) MOPAC2012, James J. P. Stewart, Stewart Computational Chemistry, Colorado Springs, CO, USA, HTTP://OpenMOPAC.net (2012)

(37) (a) York, J. T.; Llobet, A.; Cramer, C. J.; Tolman, W. B., *J. Am. Chem. Soc.* **2007,** *129*, 7990. (b) Spencer, D. J. E.; Reynolds, A. M.; Holland, P. L.; Jazdzewski, B. A.; Duboc-Toia, C.; Pape, L. L.; Yokota, S.; Tachi, Y.; Itoh, S.; Tolman, W. B., *Inorg. Chem.* **2002,** *41*, 6307.

(38) Valentine, J. S. *Chem. Rev.* **1973**, *73*, 235.

(39) See Chapter 1 for a full treatment of this subject

(40) Low, J. J.; Goddard, W. A. *Organometallics* **1986**, *5*, 609.

(41) For example see: (a) Look, J. L.; Wick, D. D.; Mayer, J. M.; Goldberg, K. I. *Inorg. Chem.* **2009**, *48*, 1356. (b) Denney, M. C.; Smythe, N. A.; Cetto, K. L.; Kemp, R. A.; Goldberg, K. I. *J. Am. Chem. Soc.* **2006**, *128*, 2508. (c) Rostovtsev, V. V.; Henling, L. M.; Labinger, J. A.; Bercaw, J. E. *Inorg. Chem.* **2002**, *41*, 3608.

(42) Tenn, W. J.; Young, K. J. H.; Bhalla, G.; Oxgaard, J.; Goddard, W. A; Periana, R. A. *J. Am. Chem. Soc*. **2005**, *127*, 14172.

(43) Cenini, S.; Porta, F.; Pizzotti, M. *J. Organomet. Chem*. **1985**, *296*, 291.

(44) Ho, J.; Klamt, A.; Coote, M. L. *J. Phys. Chem.* **2010**, *114*, 13442.

(45) (a) Crabtree, R. H. *Chem. Rev*. **2012**, *112*, 1536. (b) Widegren, J.; Finke, R. G. *J. Mol. Cat. A: Chem.* **2003**, *198*, 317.

(46) (a) Byers, P. K.; Canty, A. J.; Jin, H.; Kruis, D.; Markies, B. A.; Boersma, J.; van Koten, G. *Inorg. Synth.* **1998**, *32*, 162. (b) de Graaf, W.; Boersma, J.; Smeets, W. J. J.; Spek, A. L.; van Koten, G. *Organometallics* **1989**, *8*, 2907.

(47) When $^{18}O_2$ was used the sample was attached to a lecture bottle and charged with 10 psi $^{18}O_2$.

(48) Bruker (**2007**) APEX2 (Version 2.1-4), SAINT (version 7.34A), SADABS (version 2007/4), BrukerAXS Inc, Madison, Wisconsin, USA.

(49) (a) Altomare, A.; Burla, C.; Camalli M.; Cascarano L.; Giacovazzo C.; Guagliardi A.; Moliterni A.G.G.; Polidori G.; Spagna R. *J. Appl. Cryst.* **1999**, *32*, 115. (b) Altomare, A.; Cascarano, G.; Giacovazzo, C.; Guagliardi, A. *J. Appl. Cryst.* **1993**, *26*, 343.

(50) Sheldrick, G. M. SHELXL-97: Program for the Refinement of Crystal Structures 1997 University of Gottingen, Germany.

(51) Mackay, S.; Edwards, C.; Henderson, A.; Gilmore, C.; Stewart, N.; Shankland, K.; Donald, A.; *MaXus: a computer program for the solution and refinement of crystal structures from diffraction data*. University of Glasgow, Scotland, 1997.

(52) Waasmaier, D.; Kirfel, A. *Acta Crystallogr. A.* **1995**, *51*, 416.

(53) gNMR is available for download at http://home.cc.umanitoba.ca/~budzelaa/gNMR/gNMR.html

(54) ADF2010, SCM, Theoretical Chemistry, Vrije Universiteit, Amsterdam, The Netherlands, http://www.scm.com

(55) Te Velde, G.; Bickelhaupt, F. M.; Baerends, E. J.; Fonseca Guerra, C.; van Gisbergen, S. J. A.; Snijders, J. G.; Ziegler, T. *J. Comp. Chem.* **2001**, *22*, 931.

(56) Guerra, C. F.; Snijders, J. G.; Velde, G.; Baerends, E. J. *Theor. Chem. Acc.* **1998**, *99*, 391.

(57) (a) van Lenthe, E.; Ehlers, A.; Baerends, E.-J. *J. Chem. Phys.* **1999**, *110*, 8943. (b) van Lenthe, E.; Baerends, E. J.; Snijders, J. G. *Chem. Phys.* **1994**, *101*, 9783. (c) van Lenthe, E.; Baerends, E. J.; Snijders, J. G. *Chem. Phys.* **1993**, *99*, 4597.

(58) van Lenthe, E.; Baerends, E. J. *J. Comp. Chem.* **2003**, *24*, 1142.

Chapter 4: Generation and Structural Characterization of a Gold^{III} Alkene Complex*

Introduction

Gold complexes are effective catalysts for a range of organic transformations including the coupling of alkenes and alkynes to other organic fragments.[1-10] A key step in these catalytic reactions is assumed to be the coordination of a C–C multiple bond to the gold center.[1,2,6] Although various catalytic cycles involving Au^{III} π complexes have been proposed,[2,6,11,12] until very recently, no Au^{III} alkene,[13] alkyne, allene, or arene complexes had been conclusively detected and characterized.[1,6,14,15] In 1964, Chalk proposed the generation of $[C_8H_{12}\cdot AuCl_3]$, based solely on an IR spectrum and elemental analysis of mixtures containing two species.[16] Gas phase calculations of $AuCl_3$ and ethylene suggest that alkene binding is exothermic.[17,18] Several groups have attempted to prepare olefin complexes of Au^{III} chlorides and bromides, but clear identification of an Au^{III} alkene complex remained elusive.[14,15,19-23] The first conclusive spectroscopic evidence for Au^{III} alkene complexes was presented by Bochmann and coworkers in 2013.[13b] They reported cationic Au^{III} complexes of cyclopentene, norbornene, and ethylene supported by a 2,6-bis(4-*t*BuC_6H_3)$_2$pyridine ligand. In contrast to Au^{III}, Au^{I} alkene complexes have been known for some time with several examples reported. [1-3,16,24-35]

---

* The material in this chapter was previously published: Langseth, E.; Scheuermann, M. L.; Balcells, D.; Kaminsky, W.; Goldberg, K. I.; Eisenstein, O.; Heyn, R. H.; Tilset, M. *Angew. Chem., Int. Ed.* **2013**, *52*, 1660–1663.

Recent interest in the characterization of potential Au^{III} intermediates has resulted in the isolation of both an Au^{III} hydride[36] and an Au^{III} vinyl[37]complex. Herein, we describe the preparation of the first crystallographically characterized Au^{III} alkene complex in which the Au center is directly bonded solely to carbon atoms.[13a]

Results and Discussion

Spectroscopic and structural characterization of Au^{III} species

The cyclometalated tolylpyridine (tpyH) complex (tpy)$AuMe_2$ (**17**, Figure 4.1) was prepared as recently described.[38] Addition of triflic acid (HOTf, ca. 2.2 equiv) to a dichloromethane-d_2 solution of **17** at –78 °C followed by warming to –40 °C yielded the Au^{III} dimethyl species (tpyH)$AuMe_2OTf$, **18**. Selective protonolysis of the Au–C(sp^2) bond, as has been observed in other Au^{III} complexes,[39] is confirmed in the ^1H NMR spectrum by the two inequivalent Au–Me groups, the absence of methane, and the symmetry of the tolyl group. NOE interactions between the protons of one Au–Me group and aromatic protons of tpyH suggest that tpyH is coordinated to Au as a monodentate ligand in **18** through the N atom. Triflate presumably occupies the fourth site of the square plane around the Au^{III} center.

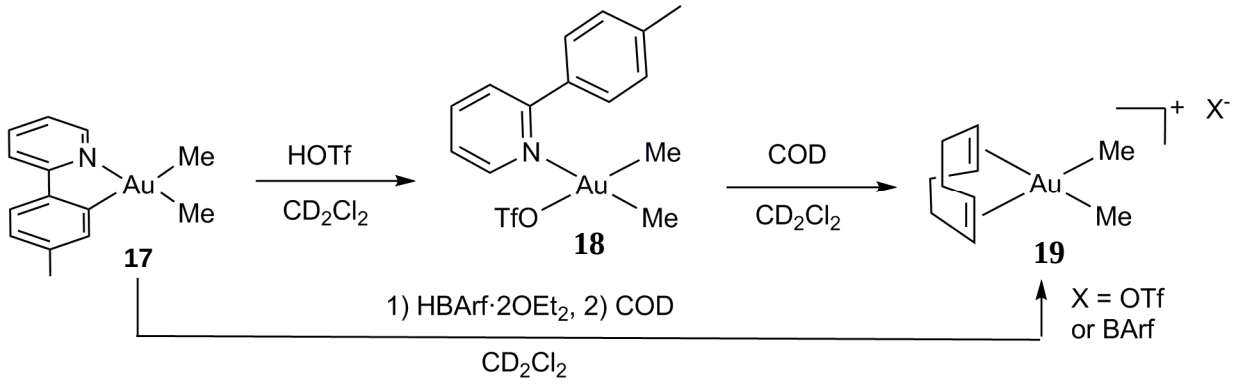

Figure 4.1. Protonation of (tpy)$AuMe_2$ **17** at low temperature followed by addition of cod to generate $[(cod)AuMe_2]^+[X]^-$ (**19**-X; X=OTf or BArf). BArf = tetrakis[3,5-bis(trifluoromethyl)phenyl]borate.

Addition of 1,5-cyclooctadiene (cod, 1 equiv) to the solution of **18** at –78 °C followed by slow warming to 0 °C resulted in the gradual consumption of cod with concomitant formation of the Au^{III} alkene complex $[(cod)AuMe_2]^+[OTf]^-$, (**19**-OTf; Figure 4.1) in 85% yield from **17** (NMR, internal standard). The byproduct is tolylpyridinium triflate, $tpyH_2OTf$, formed by reaction of HOTf with tpyH liberated from the Au center upon coordination of cod.

The ^1H NMR spectrum of **19**-OTf at 0 °C consists of a single Au–Me resonance at 1.71 ppm, a pair of multiplets for the CH_2 groups in the backbone of the bound cod at 2.75 and 2.99 ppm, and a broad singlet for the vinylic protons of the bound cod at 6.39 ppm, which is 0.8 ppm higher than the signal of free cod in dichloromethane-d_2 at 5.56 ppm. The Bochmann group reported that bound olefins in their system also appeared at higher chemical shift values compared to the free olefin.[13b] Although vinylic protons typically shift to lower δ values on binding to a metal center,[40] as seen in the Au^I complex $(HB\{3,5\text{-}(CF_3)_2pz\}_3)Au(C_2H_4)$,[31] there are also examples of shifts to higher δ values with especially electron deficient metals, such as Ag^I in $(HB\{3,5\text{-}(CF_3)_2tz\}_3)Ag\ (C_2H_4)$ (pz = pyrazolyl, tz = triazolyl).[41] The signal of the ethylene protons of this Ag complex appears 0.3 ppm higher than that of free ethylene. Notably, the ^{13}C resonance for the bound ethylene shifts to lower values by 13.6 ppm. In **19**-OTf the ^{13}C signal of the cod sp^2 carbon atoms is also shifted to a higher δ value, 134 ppm when compared to free cod at 129 ppm. Further support for the binding of cod to gold is a through-space NOE interaction (700 MHz, 233 K) between the vinylic protons of the bound cod and the Au–Me groups. The stability of **19**-OTf at ambient temperature in solution is somewhat limited. After 12 h at 25 °C, the concentration of **19**-OTf (initially ca. 14 mM) decreased by approximately 50% even with a cod concentration of 40 mM in dichloromethane-d_2. Attempts to obtain crystals from reaction mixtures containing **19**-OTf and excess HOTf invariably led to isolation of $[tpyH_2][OTf]$.

In an effort to isolate crystals of the Au^{III} alkene complex, the reaction was repeated using 0.9 equivalent of HOTf to suppress the formation of $tpyH_2OTf$ in the reaction mixture. However, the subsequent addition of as much as 50 equivalents of cod resulted in only approximately 30% yield of the desired **19**-OTf (NMR, internal standard). In addition, the reaction mixture contained **18** (ca. 20%) and a new species (ca. 20%) that was subsequently identified as $[(tpyH)_2AuMe_2]^+[OTf]^-$ (**20**-OTf, Figure 4.2) by comparison to an independently prepared and crystallographically characterized sample. Upon addition of tpyH (ca. 6 equiv) to the mixture above, the composition of the reaction mixture changed to <5% yield of **19**-OTf, approximately 20% of **18**, and approximately 60% of **17**-OTf. These observations suggest that **18**, **19**-OTf, **17**-OTf, free cod, and free tpyH are in equilibrium, that is, cod and tpyH compete for coordination sites at the Au^{III} moiety. Importantly, the ^1H NMR resonances of **19**-OTf remain unchanged regardless of whether the other species present in the reaction mixture are $tpyH_2OTf$ (resulting from excess acid) or **18** and **17**-OTf (less than 1 equiv of acid). From this observation we infer that **19**-OTf does not have an associated tpyH ligand in solution. All attempts to obtain crystals from reaction mixtures without excess HOTf resulted only in crystals of **17**-OTf.

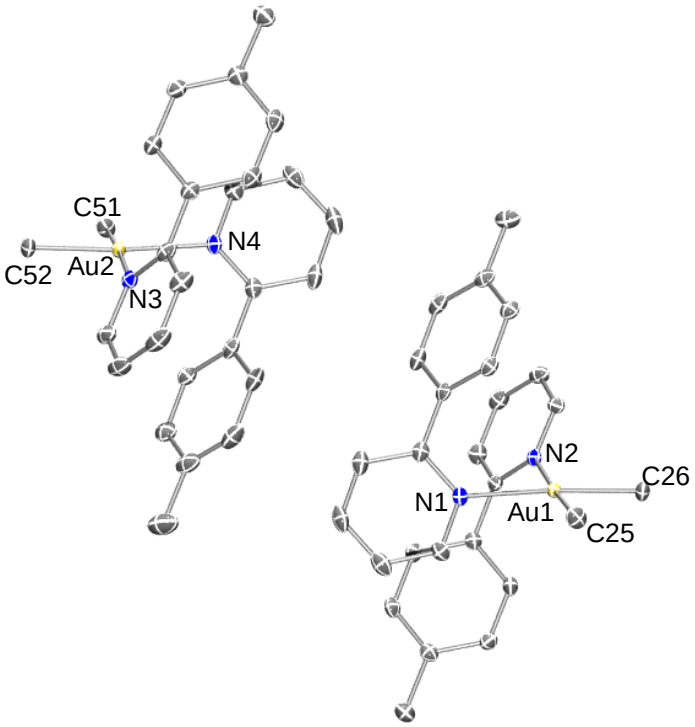

Figure 4.2. POV-Ray rendition of the ORTEP of (**17**-OTf) at the 50% probability level with hydrogen atoms, the triflate anion, and co-crystalized dichloromethane omitted for clarity.[42,43,44] Selected bond lengths (Å) and angles (deg) for (**17**-OTf): Au1−C26 = 2.035(2), Au1−C25 = 2.039(2), Au1−N1 = 2.1623(18), Au1−N2 = 2.1710(17), Au2−C51 = 2.035(2), Au2−C52 = 2.037(2), Au2−N3 = 2.1562(19), Au2−N4 = 2.1663(17).C26−Au1−C25 = 86.34(10), C25−Au1−N1 = 92.00(8), C26−Au1−N2 = 90.92(8), N1−Au1−N2 = 90.89(7), C51−Au2−C52 = 86.61(9), C52−Au2−N3 = 91.81(8), C51−Au2−N4 = 90.98(8), N3−Au2−N4 = 90.86(7).

When approximately one equivalent of $[(Et_2O)_2H]^+$ $[\{3,5\text{-}(CF_3)_2\text{-}C_6H_3\}_4B]^-$ (HBArf·2 OEt_2)[45] was used for the protonolysis of **17** in dichloromethane-d_2, followed by addition of 15 equivalents of cod, $[(cod)AuMe_2]^+[BArf]^-$ (**19**-BArf) was generated in approximately 70% yield (NMR, internal standard). The ^{1}H NMR chemical shifts for the Au–Me groups and the vinylic and CH_2 protons of bound cod in **19**-BArf appear within 0.2 ppm of the corresponding resonances in a spectrum of **19**-OTf. The solution containing **19**-BArf was layered with pentane and stored in a freezer at –35 °C, resulting in small crystalline demispheres suitable for X-ray diffraction. The structure of the cation of **19**-BArf is shown in Figure 4.3.

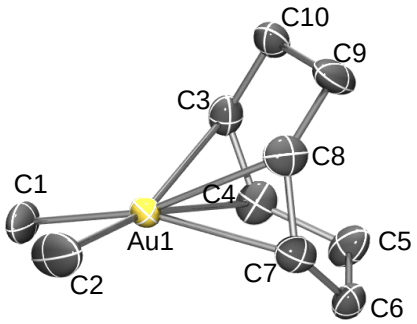

Figure 4.3. POV-Ray rendition of the ORTEP of **19**-BArf with 50% probability ellipsoids.[42,43,46] Hydrogen atoms and BArf anion are omitted for clarity. Selected bond lengths [Å] and angles [°]: Au1–C1 = 2.049(4), Au1–C2 = 2.05(4), Au1–C3 = 2.371(4), Au1–C4 = 2.415(4), Au1–C7 = 2.362(4), Au1–C8 = 2.406(4), C3–C4 = 1.348(5), C7–C(8) = 1.364(5), C3–Au1–C4 = 32.71(13), C7–Au1–C8 = 33.23(12), C7–Au1–C4 = 77.86(13), C3–Au1–C8 = 77.87(13), C1–Au1–C2 = 85.0(2).

Compound **19**-BArf crystallized in the monoclinic space group $P2_1/c$ with the Au cation sitting in a pocket formed by the aryl groups of several $BArf^-$ anions. The cation is nearly C2 symmetric (not crystallographically imposed). Interestingly, each cod C=C bond is asymmetrically bonded to Au such that one Au–C bond is significantly longer than the other (2.362(4) vs. 2.406(4) and 2.371(4) vs. 2.415(4) Å, respectively). The C=C bond lengths in **19**-BArf are 1.348(5) and 1.364(5) Å. Several cationic Au^I alkene complexes have been recently structurally characterized.[24-30,32] Their Au–C_{alkene} bond lengths are in the range of 2.098(5)[24]–2.37(1)[30] Å, and the C=C distances are in the range of 1.319[26]–1.409(4)[25] Å. It is noteworthy that the two long Au–C_{cod} distances in the cationic Au^{III} complex **19**-BArf are longer than the longest Au–C_{alkene} distances in the structurally characterized, cationic Au^I complexes.[24-30,32] Furthermore, the C=C distances in **19**-BArf are essentially in the middle of the range seen for these Au^I complexes, thus indicating some back-bonding from Au^{III} to the C=C bonds.

Summary

In summary, we have successfully characterized the first[13] Au^{III} alkene complex for which an X-ray structure could be obtained. This unambiguous demonstration of the existence of Au^{III} alkene complexes validates their inclusion in mechanistic proposals and will allow for further work to better understand mechanisms that potentially involve Au^{III} alkene complexes.

Experimental

General experimental methods

(tpy)$AuMe_2$[38] and $[(3,5\text{-}(CF_3)_2C_6H_3)_4B]^-[H(OEt_2)_2]^+ \cdot 4Et_2O$ (HBArf)[45,47] were prepared according to literature procedures. Dichloromethane-d_2, 1,2-dichloroethane and 1,5-cyclooctadiene were dried over CaH_2. Pentane was dried by passage through activated alumina and molecular sieves columns under a stream of argon. All procedures were carried out under a nitrogen atmosphere, using Schlenk techniques, vacuum manifold techniques, or in a nitrogen-filled glovebox. NMR spectra were recorded on Bruker Advance DRX500, AV500 or AV700 spectrometers operating at 500 or 700 MHz (^1H). ^1H NMR spectra are referenced to residual protiated solvent signals, ^{13}C NMR spectra are referenced to deuterated solvent signals, and ^{19}F spectra are referenced to neat trifluoroacetic acid as an external standard (−76.55 ppm). Chemical shifts for ^1H and ^{13}C are reported in parts per million (ppm) downfield from tetramethylsilane (0.00 ppm) and $CFCl_3$ is defined as 0.00 ppm in ^{19}F NMR. Coupling constants are reported in hertz (Hz). The following abbreviations are used: s (singlet), d (doublet), t (triplet), m (multiplet), br (broad).

In situ generation of (2-(*p*-tolyl)pyridine)AuMe$_2$(OTf) (18)

A screw top NMR tube with a teflon septum was charged with (tpy)AuMe$_2$ (**1)** (3-6 mg) inside a glovebox. Dichloromethane-d_2 (0.4-0.5 mL) and the internal standard, 1,2-dichloroethane (1 μL), were added. The solution was cooled to −78 °C and a dichloromethane-d_2 solution of triflic acid (0.1 M, 2.2 equiv.) was added. Compound **2** was typically observed in 85% yield by integration ^{1}H resonances relative to the internal standard. ^{1}H NMR (500 MHz, 233 K, dichloromethane-d_2): δ 8.72 (d, J = 3.6 Hz, 1H), 8.05 (t, J = 7.8 Hz, 1H), 7.72 (d, J = 7.8 Hz, 1H), 7.67 (d, J = 7.5 Hz, 2H), 7.62 (m, 1H), 7.37 (d, J = 7.8 Hz, 2H), 2.42 (s, 3H), 1.06 (s, 3H), 0.80 (s, 3H). ^{13}C NMR (176 MHz, 233 K, dichloromethane-d_2): δ 159.1, 149.3, 140.7, 140.4, 135.3, 129.8, 128.7, 127.4, 124.3, 21.3, 3.6, 3.3. (The CF_3 carbon of the triflate was not observed). ^{19}F NMR (470 MHz, 263 K, dichloromethane-d_2): δ −77.5.

In situ generation of [(1,5-cyclooctadiene)AuMe$_2$]$^+$[OTf]$^-$ (19-OTf)

To a solution of (tpyH)AuMe$_2$(OTf) (**18**; for preparation, see above) at −78 °C was added 1.2 equiv. of 1,5-cyclooctadiene. The NMR sample was warmed to 0 °C during 30 min. to give **19**-OTf in approximately 85% yield over two steps from **17**. ^{1}H NMR (500 MHz, 273 K, dichloromethane-d_2): δ 6.39 (br s, C=C*H*, 4H), 2.99 (m, CH_2, 4H), 2.75 (m, CH_2, 4H), 1.71 (s, Au−CH_3, 6H). ^{13}C NMR (126 MHz, 298 K, dichloromethane-d_2): δ 134.6, 29.1, 21.0. (The CF_3 carbon of the triflate was not observed). ^{19}F NMR (470 MHz, 263 K, dichloromethane-d_2): δ −77.9.

In situ generation of [(1,5-cyclooctadiene)AuMe$_2$]$^+$[BArf]$^-$ (19-BArf)

A screw top NMR tube with a teflon septum was charged with (tpy)AuMe$_2$ (**17**) (3.2 mg) inside a glovebox. Dichloromethane-d_2 (0.4-0.5 mL) and the internal standard, 1,2-dichloroethane (1

μL), were added. The solution was cooled to −78 °C and ca. 1 equiv. of HBArf·6OEt$_2$ in ~100 μL dichloromethane-d_2 was added. 1,5-Cyclooctadiene (15 equiv.) was then added giving **19**(BArf$^-$) in approximately 70% yield over two steps from 1. ^{1}H NMR (500 MHz, 273 K, dichloromethane-d_2): δ 6.29 (br s, C=C*H*, 4H), 2.99 (m, CH_2, 4H), 2.66 (m, CH_2, 4H), 1.68 (s, Au–CH_3, 6H). The solution was then layered with pentane and left in a –35 °C freezer yielding colourless demispheres suitable for X-ray crystallography (see below).

Independent generation of [(2-(*p*-tolyl)pyridine)$_2$AuMe$_2^+$][OTf$^-$] (20-OTf)

In a glovebox, a screw top NMR tube with a Teflon septum was charged with 5.4 mg of **17**. Dichloromethane-d_2 (0.4-0.5 mL) and the internal standard, 1,2-dichloroethane (1 μL), were added. The solution was cooled to −78 °C and a dichloromethane-d_2 solution of triflic acid (0.1 M, <1 equiv.) was added. The solution was warmed to −40 °C then cooled to −78 °C for the addition of 2.5 μL (2.0 equiv.) tolylpyridine giving **17**-OTf in approximately 60% yield (by NMR integration vs. internal standard). Crystals of **17**-OTf were obtained from a mixture of dichloromethane-d_2 and pentane at −35 °C. ^{1}H NMR (500 MHz, 278 K, dichloromethane-d_2): δ 7.88 (t, 7.7, 1H), 7.42 (d, J = 7.8 Hz, 1H), 7.25 (d, J = 7.6 Hz, 2H), 7.22 (d, J = 5.0 Hz, 1H), 7.14 (d, J = 7.0 Hz, 2H), 7.08 (t, J = 6.4 Hz, 1H). ^{13}C NMR (126 MHz, 298 K, dichloromethane-d_2): δ 158.8, 148.6, 141.4, 140.4, 135.5, 130.7, 128.2, 127.4, 125.2, 21.5, 4.7. (The CF_3 carbon of the triflate was not observed). ^{19}F NMR (470 MHz, 263 K, dichloromethane-d_2): δ −77.9.

Crystallographic characterization of 19-BArf

A colorless demisphere, measuring 0.15 x 0.10 x 0.07 mm^3, was mounted on a loop with oil. Data were collected at –173 °C on a Bruker APEX II single crystal X-ray diffractometer, Mo-radiation. Crystal-to-detector distance was 40 mm and exposure time was 10 s per frame for all sets. The scan width was 0.5°. Data collection was 100% complete to 25° in ϑ. A total of

166231 reflections were collected covering the indices, h = –15 to 15, k = –25 to 25, l = –26 to 26. 11088 reflections were symmetry independent and the R_{int} = 0.0785 indicated that the data were of average quality (0.07). Indexing and unit cell refinement indicated a primitive monoclinic lattice. The space group was found to be $P2_1/c$ (No.14). The data were integrated and scaled using SAINT, SADABS within the APEX2 software package by Bruker.[48] Solution by direct methods (SHELXS, SIR97[49,50]) produced a complete heavy atom phasing model consistent with the proposed structure. The structure was completed by difference Fourier synthesis with SHELXL97.[51,52] Scattering factors are from Waasmair and Kirfel.[53] Hydrogen atoms were placed in geometrically idealised positions and constrained to ride on their parent atoms with C–H distances in the range 0.95-1.00 Å. Isotropic thermal parameters U_{eq} were fixed such that they were 1.2 U_{eq} of their parent atom Ueq for CH's and 1.5U_{eq} of their parent atom U_{eq} in case of methyl groups. All non-hydrogen atoms were refined anisotropically by full-matrix least-squares. Structural parameters are reported in Table 4.1.

Table 4.1. Structural parameters for **19**-BArf

Parameter	**19-BArf**
Empirical formula	$C_{42}H_{30}AuBF_{24}$
Formula weight	1198.44
Temperature	100(2) K
Wavelength	0.71073 Å
Crystal system	Monoclinic
Space group	P 2_1/c
Unit cell dimensions	a = 11.3662(12) Å α = 90° b = 19.156(2) Å β = 98.279(6)° c = 19.703(2) Å γ = 90°
Volume	4245.2(8) $Å^3$
Z	4
Density (calculated)	1.875 Mg/m^3
Absorption coefficient	3.604 mm^{-1}
F(000)	2328
Crystal size	0.15 x 0.10 x 0.07 mm^3
Theta range for data collection	1.81 to 28.87°
Index ranges	$-15 \leq h \leq 15, -25 \leq k \leq 25, -26 \leq l \leq 26$
Reflections collected	166231
Independent reflections	11088 [R(int) = 0.0758]
Completeness to theta = 25.00°	100.0 %
Max. and min. transmission	0.7865 and 0.6140
Refinement method	Full-matrix least-squares on F^2
Data / restraints / parameters	11088 / 0 / 615
Goodness-of-fit on F^2	1.081
Final R indices [I>2sigma(I)]	R1 = 0.0316, wR2 = 0.0740
R indices (all data)	R1 = 0.0463, wR2 = 0.0857
Largest diff. peak and hole	2.197 and -1.968 e.$Å^{-3}$

Crystallographic characterization of 17-OTf

A colorless prism, measuring 0.18 x 0.13 x 0.10 mm^3 was mounted on a loop with oil. Data was collected at –173 °C on a Bruker APEX II single crystal X-ray diffractometer, Mo-radiation.

Crystal-to-detector distance was 40 mm and exposure time was 5 seconds per frame for all sets. The scan width was 0.5°. Data collection was 99.4% complete to 25° in ϑ. A total of 314146 reflections were collected covering the indices, h = –21 to 20, k = –17 to 17, l = –38 to 38. 14510 reflections were symmetry independent and the R_{int} = 0.0628 indicated that the data was of slightly better than average quality (0.07). Indexing and unit cell refinement indicated a primitive monoclinic lattice. The space group was found to be P 2_1/n (No.14). The data was integrated and scaled using SAINT, SADABS within the APEX2 software package by Bruker.[48] Solution by direct methods (SHELXS, SIR97[49,50])produced a complete heavy atom phasing model consistent with the proposed structure. The structure was completed by difference Fourier synthesis with SHELXL97.[7,8] Scattering factors are from Waasmaier and Kirfel.[53] Hydrogen atoms were placed in geometrically idealized positions and constrained to ride on their parent atoms with C–H distances in the range 0.95-1.00 Å. Isotropic thermal parameters U_{eq} were fixed such that they were 1.2U_{eq} of their parent atom U_{eq} for CH's and 1.5U_{eq} of their parent atom U_{eq} in case of methyl groups. All non-hydrogen atoms were refined anisotropically by full-matrix least-squares. Structural parameters are reported in Table 4.2.

Table 4.2. Structural parameters for **17**-OTf

Parameter	**17-OTf**
Empirical formula	$C_{55}H_{58}Au_2C_{l2}F_6N_4O_6S_2$
Formula weight	1514.01
Temperature	100(2) K
Wavelength	0.71073 Å
Crystal system	Monoclinic
Space group	P 2_1/n
Unit cell dimensions	a = 15.416(5) Å α = 90.000(5)° b = 12.851(5) Å β =103.443(5)° c = 28.979(5) Å γ = 90.000(5)°
Volume	5584(3) $Å^3$
Z	4
Density (calculated)	1.801 Mg/m^3
Absorption coefficient	5.492 mm^{-1}
F(000)	2968
Crystal size	0.18 x 0.13 x 0.10 mm^3
Theta range for data collection	1.68 to 29.73°
Index ranges	$–21 \leq h \leq 20, –17 \leq k \leq 17, –38 \leq l \leq 38$
Reflections collected	314146
Independent reflections	14510 [R(int) = 0.0628]
Completeness to theta = 25.00°	99.4 %
Max. and min. transmission	0.6096 and 0.4380
Refinement method	Full-matrix least-squares on F^2
Data / restraints / parameters	14510 / 0 / 702
Goodness-of-fit on F^2	1.031
Final R indices [I>2sigma(I)]	R1 = 0.0234, wR2 = 0.0393
R indices (all data)	R1 = 0.0389, wR2 = 0.0420
Largest diff. peak and hole	1.246 and –1.234 $e.Å^{–3}$

Coauthor contributions

Eirin Langseth performed the crystallizations of **19**-BArf and **17**-OTf and worked with Margaret Scheuermann to perform the NMR experiments described. David Balcells did the computational work associated with this project (not described here). Werner Kaminsky collected the crystallographic data and solved structures for **19**-BArf and **17**-OTf.

Notes to Chapter 4

(1) Hashmi, A. S. K. *Angew. Chem., Int. Ed.* **2010**, *49*, 5232.

(2) Hashmi, A. S. K. *Chem. Rev.* **2007**, *107*, 3180.

(3) Hashmi, A. S. K.; Hutchings, G. J. *Angew. Chem., Int. Ed.* **2006**, *45*, 7896.

(4) Rudolph, M.; Hashmi, A. S. K. *Chem. Soc. Rev.* **2012**, *41*, 2448.

(5) Arcadi, A. *Chem. Rev.* **2008**, *108*, 3266.

(6) Schmidbaur, H.; Schier, A. *Arabian J. Sci. Eng.* **2012**, *37*, 1187.

(7) Lo, V. K.-Y.; Kung, K. K.-Y.; Wong, M.-K.; Che, C.-M. *J. Organomet. Chem.* **2009**, *694*, 583.

(8) Li, Z.; Brouwer, C.; He, C. *Chem. Rev.* **2008**, *108*, 3239.

(9) Fürstner, A.; Davies, P. W. *Angew. Chem., Int. Ed.* **2007**, *46*, 3410.

(10) Shapiro, N. D.; Toste, F. D. *Synlett* **2010**, *2010*, 675.

(11) Nguyen, R.-V.; Yao, X.; Li, C.-J. *Org. Lett.* **2006**, *8*, 2397.

(12) Xiao, Y.-P.; Liu, X.-Y.; Che, C.-M. *J. Organomet. Chem.* **2009**, *694*, 494.

(13) The recent examples refer to the publication upon which this chapter is based (a) Langseth, E.; Scheuermann, M. L.; Balcells, D.; Kaminsky, W.; Goldberg, K. I.; Eisenstein, O.; Heyn, R. H.; Tilset, M. *Angew. Chem., Int. Ed.* **2013**, *52*, 1660–1663. and a report made nearly simultaneously (b) Savjani, N.; Roşca, D.-A.; Schormann, M.; Bochmann, M. *Angew. Chem., Int. Ed.* **2013**, *52*, 874–877.

(14) Schmidbaur, H.; Schier, A. *Organometallics* **2010**, *29*, 2.

(15) Norman, R. O. C.; Parr, W. J. E.; Thomas, C. B. *J. Chem. Soc., Perkin Trans. I.* **1976**, 811.

(16) Chalk, A. *J. Am. Chem. Soc.* **1964**, 4733.

(17) García-Mota, M.; Cabello, N.; Maseras, F.; Echavarren, A. M.; Pérez-Ramírez, J.; Lopez, N. *ChemPhysChem* **2008**, *9*, 1624.

(18) Kang, R.; Chen, H.; Shaik, S.; Yao, J. *J. Chem. Theory Comput.* **2011**, *7*, 4002.

(19) Norman, R. O. C.; Parr, W. J. E.; Thomas, C. B. *J. Chem. Soc., Perkin Trans. I.* **1976**, 1983.

(20) Brain, F. H.; Gibson, C. S.; Jarvis, J. A. J.; Phillips, R. F.; Powell, H. M.; Tyabji, A. *J. Chem. Soc.* **1952**, 3686.

(21) Monaghan, P. K.; Puddephatt, R. J. *Inorganica Chimica Acta* **1975**, *15*, 231.

(22) Armerr, B. B.; Schmidbaur, H. *Angew. Chem., Int. Ed.* **1970**, *9*, 101.

(23) Schmidbaur, H. *Angew. Chem., Int. Ed.* **1976**, *15*, 728.

(24) Cinellu, M. A.; Minghetti, G.; Stoccoro, S.; Zucca, A.; Manassero, M.; *Chem. Commun.* **2004**, 1618.

(25) Cinellu, M. A; Minghetti, G.; Cocco, F.; Stoccoro, S.; Zucca, A.; Manassero, M.; Arca, M. *Dalton Trans.* **2006**, 5703.

(26) Brown, T. J.; Dickens, M. G.; Widenhoefer, R. A. *Chem. Commun.* **2009**, 6451.

(27) Brown, T. J.; Dickens, M. G.; Widenhoefer, R. A. *J. Am. Chem. Soc.* **2009**, *131*, 6350.

(28) Hooper, T. N.; Green, M.; McGrady, J. E.; Patel, J. R.; Russell, C. A. *Chem. Commun.* **2009**, 3877.

(29) Brooner, R. E. M.; Widenhoefer, R. A. *Organometallics* **2011**, 3182.

(30) Brooner, R. E. M.; Widenhoefer, R. A. *Organometallics* **2012**, *31*, 768.

(31) Dias, H. V. R.; Wu, J. *Angew. Chem., Int. Ed.* **2007**, *46*, 7814.

(32) Dias, H. V. R.; Fianchini, M.; Cundari, T. R.; Campana, C. F. *Angew. Chem., Int. Ed.* **2008**, *47*, 556.

(33) Dias, H. V. R.; Lovely, C. J. *Chem. Rev.* **2008**, *108*, 3223.

(34) Dias, H. V. R.; Wu, J. *Eur. J. Inorg. Chem.* **2008**, *2008*, 509.

(35) M. A. Cinellu in Modern Gold Catalyzed Synthesis (Eds.: A. S. K. Hashmi, F.D. Toste), Wiley-VCH, Weinheim, 2012, pp. 175.

(36) Roşca, D.-A.; Smith, D. A; Hughes, D. L.; Bochmann, M. *Angew. Chem., Int. Ed.* **2012**, 10643.

(37) Egorova, O. A; Seo, H.; Kim, Y.; Moon, D.; Rhee, Y. M.; Ahn, K. H. *Angew. Chem., Int. Ed.* **2011**, *50*, 11446.

(38) Langseth, E.; Görbitz, C. H.; Heyn, R. H.; Tilset, M. *Organometallics* **2012**, *31*, 6567.

(39) Jawad, J. K.; Puddephatt, R. J.; Stalteri, M. A. *Inorg. Chem.* **1982**, *21*, 332.

(40) Crabtree, R. H. *The Organometallic Chemistry of the Transition Metals*, 5th ed; Wiley: Hoboken, 2005; pp127.

(41) Kou, X.; Dias, H. V. R. *Dalton Trans.* **2009**, 7529.

(42) Persistence of Vision Ray-Tracer (POV-Ray), available at http://www.povray.org/.

(43) ORTEP plots were created using Ortep-3 for Windows. See: Farrugia, L. J. *J. Appl. Crystallogr.* **1997**, *30*, 565.

(44) Full details on the structure of **17**-OTf (CCDC 910694) can be obtained free of charge from The Cambridge Crystallographic Data Centre via www.ccdc.cam.ac.uk/data_request/cif.

(45) Brookhart, M.; Grant, B.; Volpe, A. F. *Organometallics* **1992**, *11*, 3920. Differing from the description in this reference, the material used by us was found to have an additional 4 equiv. of Et2O associated.

(46) Full details on the structure of **19**-BArf (CCDC 910693) can be obtained free of charge from The Cambridge Crystallographic Data Centre via www.ccdc.cam.ac.uk/data_request/cif.

(47) Yakelis, N. A.; Bergman, R. G. *Organometallics* **2005**, *24*, 3579.

(48) Bruker (2007) APEX2 (Version 2.1-4), SAINT (version 7.34A), SADABS (version 2007/4), BrukerAXS Inc, Madison, Wisconsin, USA.

(49) Altomare, A.; Burla, M. C.; Camalli, M.; Cascarano, G. L.; Giacovazzo, C.; Guagliardi, A.; Moliterni, A. G.; Polidori, G.; Spagna, R. *J. Appl. Cryst.* **1999**, *32*, 115.

(50) Altomare, a.; Cascarano, G.; Giacovazzo, C.; Guagliardi, A. *J. Appl. Cryst.* **1993**, *26*, 343.

(51) G. M. Sheldrick, *SHELX97. Program for the Refinement of Crystal Structures*, University of Göttingen, Göttingen, Germany, **1997**.

(52) Mackay, S.; Edwards, C.; Henderson, A.; Gilmore, C.; Stewart, N.; Shankland, K.; Donald, A. *MaXus: a computer program for the solution and refinement of crystal structures from diffraction data.*, University of Glasgow, Scotland, **1997**.

(53) Waasmaier, D.; Kirfel, A. *Acta Crystallogr., Sect. A: Found. Crystallogr.* **1995**, *51*, 416.